Addressing voltage sag contribution of an optimally sized Industrial Hybrid Power System

Using a multi-objective sizing framework considering cost and CO2 emission

Max Deutman

TU Delft

Royal HaskoningDHV
Enhancing Society Together

Addressing voltage sag contribution of an optimally sized Industrial Hybrid Power System

Using a multi-objective sizing framework considering cost and CO2 emission

by

Max Deutman

in partial fulfilment of the requirements for the degree of

Master of Science
in Electrical Power Engineering

at the Delft University of Technology,
to be defended publicly on Monday September 11, 2023 at 09:00 AM

Student Number:	4592743
Project Duration:	Dec, 2022 - Sep, 2023
Faculty:	Electrical Engineering, Mathematics & Computer Science, Delft
Thesis Promotor:	Prof. Pavol Bauer
Supervisor:	Dr. Laura Ramírez Elizondo
Advisor:	Joel Alpízar Castillo MSc.
Committee Member:	Dr. Milos Cvetkovic
External Supervisor:	George Koolman MSc.

Cover: Mauro Torres V - Red and White Smokestacks of a Power Plant Under White Clouds

TU Delft

Royal HaskoningDHV
Enhancing Society Together

This Thesis is a collaboration with Delft University of Technology and Royal HaskoningDHV.

Preface

This thesis titled ”Addressing voltage sag contribution of an optimally sized Industrial Hybrid Power System” introduces a framework for sizing an industrial Hybrid Power System (HPS) to minimise Cost and CO2 emissions relative to connecting the industrial site directly to the grid with the help of a genetic algorithm, specifically NSGA-II. The framework utilises an Energy Management System (EMS) that is based on a rolling average principle which attempts to restrict the change in grid consumption from one time step to the next. The optimally sized configuration and its new grid consumption profile are analysed in the CIGRE MV Distribution Network to assess the effects of the new consumption profile on the bus voltages. The combination of a rolling average-based EMS and an optimal sizing with NSGA-II resulted in a 47% reduction of the CO2 emissions while not worsening the voltage behaviour in the system (with a focus on voltage sag introduced by large loads).

In the journey of research and exploration, there are moments that stand as pivotal milestones. This thesis represents such a moment for me as it marks the end of my Master Electrical Power Engineering. It’s a culmination of tireless efforts, invaluable guidance, and the pursuit of contributing to solving real-world problems.

As I look back on this journey, I am profoundly grateful for the support, mentorship, and encouragement provided by my supervisory team: Laura Ramírez Elizondo and Joel Alpízar Castillo for their support on the academic side of the thesis and George Koolman for his support in enabling me to perform this thesis at Royal HaskoningDHV in collaboration with DC Systems, Energy Conversion & Storage headed by Pavol Bauer.

The research done for this thesis has increased my understanding of real-world power systems, their challenges, and possible solutions to tackle these challenges.

I would like to express my sincere appreciation to all the individuals who have been part of this journey, providing insights, engaging in discussions, and offering unwavering support. The collaborative spirit within Royal HaskoningDHV, as well as the motivation derived from peers and mentors, has been a driving force throughout this research.

Last but certainly not least, I would like to thank my family and friends for their emotional, social, and financial support during my studies at TU Delft.

Max Deutman

Friday 8th September, 2023

Contents

1

Introduction

The Dutch industry plays a significant role in the nation's energy consumption, accounting for around a third of the total energy usage [1] and being heavily reliant on fossil fuels as can be seen in Figure 1.1[1], resulting in being responsible for a third of the total CO2 emissions in the Netherlands [2]. This heavy reliance on conventional energy sources raises environmental concerns and highlights the need for sustainable energy solutions. The transition to a more sustainable energy system is crucial to mitigate climate change, reduce greenhouse gas emissions, and ensure long-term energy security.

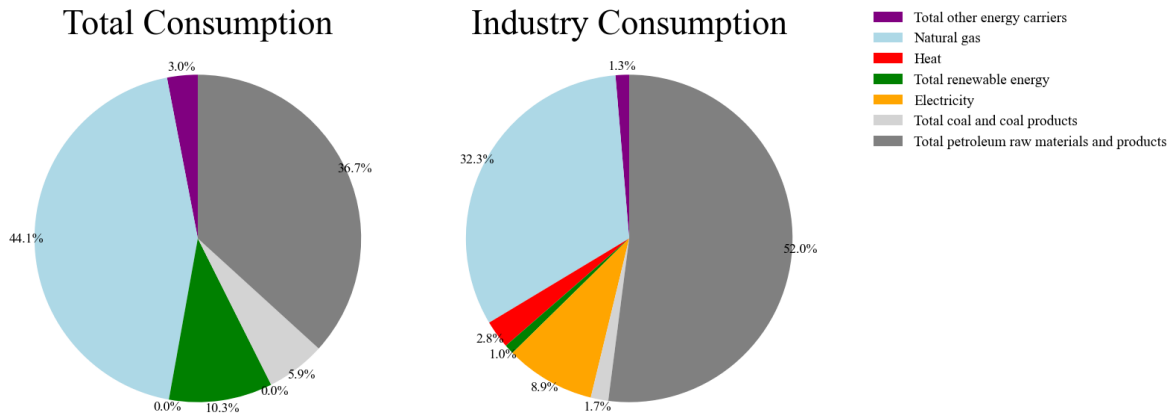

Figure 1.1: 2020 Total (including energy sector) and Industrial Sector Energy Consumption [3]

To address these challenges, the concept of Hybrid Power Systems (HPS) has emerged as a promising solution [4]. HPS combines different energy sources, including Renewable Energy Sources (RES), Energy Storage Systems (ESS), and supplementary generation capabilities, to achieve a more balanced and efficient energy supply. By integrating these diverse components, HPS offers the potential to optimise energy generation, enhance grid stability, and reduce both costs and environmental impact. HPSs are also particularly popular for remote energy applications where a diverse portfolio of energy-producing technologies is valued more highly than in grid-connected areas.

Optimal sizing of HPS components is a critical aspect of designing an efficient and cost-effective system. The size of each component, such as the PhotoVoltaic (PV) system, diesel generator, microturbine, Wind Turbine (WT), Battery Energy Storage System (BESS), etc. must be carefully determined to ensure optimal performance, considering factors such as energy demand, resource availability, grid capacity, and economic viability. With the changing landscape of emission regulations, this sizing can become extra difficult for fossil-fuel-based components, as emission penalties can be applied to these components.

[1]The heat consumption is not reported for the total energy consumption, the electricity usage is negative due to electricity being exported to other countries

The Dutch industry, heavily dependent on fossil fuel-based energy sources, faces the challenge of transitioning towards a more sustainable energy system. This is in part done by replacing existing processes with electrical counterparts, in other words: The electrification of industry. This electrification of industry poses an issue when the grid is in a congested state, as is the case in the Netherlands [5]. This is simply due to the fact that electrification replaces a fossil-fuel-based energy carrier with electricity, thus increasing the overall electricity demand. A solution for this issue is to bring in other sources of energy to the industrial site, in the form of HPSs. A first step into achieving a net-zero industry would thus be to investigate the introduction of HPSs for industrial loads.

The optimal sizing of HPS components for industrial applications poses a complex task. The sizing process involves finding the right balance between cost reduction and CO2 emission reduction, while ensuring grid stability. Industrial loads simplify and complicate this last issue simultaneously. It is not difficult to imagine industrial loads exhibiting constant behaviour or loads being predicted based on production quotas while also having very high power demands that incur huge costs if they are interrupted.

Moreover, the traditional approach to sizing energy components often overlooks the interconnected nature of the energy infrastructure. Individual sizing decisions are made without considering the potential impact on the overall energy system and voltage stability within an industrial bus system. Consequently, there is a need for a comprehensive multi-objective framework that incorporates cost, CO2 emissions, and voltage stability considerations to guide the sizing process of HPS components for industrial applications.

This master's thesis project aims to develop a comprehensive multi-objective framework for sizing an industrial Hybrid Power System that minimises cost and CO2 emissions while ensuring voltage stability within the industrial bus system. The research will be conducted in collaboration between Max Deutman and Royal HaskoningDHV, leveraging a multidisciplinary approach and real-world industry insights.

The methodology involves a thorough literature review on optimisation methods and Hybrid Power Systems for industrial applications. This review will establish a foundation of knowledge and identify the state-of-the-art techniques for HPS sizing. Based on the literature review, mathematical models for the PV, diesel, and BESS components will be developed and validated. These models will be integrated into an Energy Management System (EMS) to ensure the smooth operation and optimal control of the HPS.

A Genetic Algorithm optimisation approach will be employed to determine the optimal size of each component within the HPS. This approach will enable the exploration of the trade-off between cost and CO2 emissions, considering the specific constraints of the industrial load and grid capacity. The effectiveness of the optimised HPS configuration will be assessed by analysing its impact on voltage sag within an industrial bus system.

The main objective of this research is to optimally size a Hybrid Power System (PV-DSL-BAT) for an industrial load, minimising cost and CO2 emissions while ensuring voltage stability within the industrial bus system. To achieve this objective, the following research questions will be addressed:

1. Which equations and parameters can be utilised to implement models (PV, Diesel, or BESS) for the use in an Energy Management Systems designated to supply an industrial load?
2. What cost and emission savings can be achieved by sizing components to create a Hybrid Power System for an industrial load using a Genetic Algorithm, compared to directly supplying the load from the grid?
3. What effect does the optimal sizing of an individual node have on the voltage stability of an industrial distribution system?

By addressing these research questions, this thesis aims to contribute to the development of a comprehensive and practical framework for optimal Hybrid Power System sizing in industrial applications. The findings of this research will provide valuable insights for decision-making processes in achieving sustainable energy solutions for the Dutch industry.

2

Previous Literature

In order to gain an understanding of existing literature for the subject ”Addressing voltage sag contribution of an optimally sized Industrial Hybrid Power System - Using a multi-objective sizing framework considering cost and CO2 emission” it is convenient to divide the subject into smaller themes. The smaller themes that were identified for the literature research done in this paper are:

- (voltage) Influence of introducing PV, BESS, and/or Diesel Generators into an existing electrical infrastructure
- Sizing of (Industrial) Hybrid Power Systems
- Multi-objective optimisation techniques

2.1. Influence of PV, BESS, and/or Diesel Generators

In previous research and real-world data collected from completed projects, the addition of Distributed Generation (DG) to power systems has been analysed and conclusions can be drawn that DG is not a perfect solution. As mentioned in [6][7][8][9], DG with Renewable Energy Sources (RES), has benefits and downsides that are listed below in a summary:

Merits

- Reduced (transmission/distribution) system resources
- Increased reliability
- Decreased emissions
- Improve independence and adaptability

Demerits

- Low and/or variable resource availability
- Increased scheduling complexity
- Decreased power quality
- Possible impairment of protection systems

With this summary in mind, the voltage sag effects of an optimally sized HPS becomes a valuable research contribution. Firstly, voltage sag is a common power quality issue that can lead to disruptions in industrial processes and their surrounding electrical infrastructure. Sensitive equipment can be damaged and even black-outs can be caused by voltage instability [10]. Understanding the impact of an optimally sized HPS on voltage sag helps assess its effect on power quality and grid stability, especially with the integration of distributed generation sources like PV and BESS. Secondly, as industries strive for a sustainable energy transition, HPS configurations offer a promising solution. By studying their voltage sag effects, researchers contribute to the development of cleaner, more reliable, and resilient energy systems. This research ensures that the selected HPS configuration not only minimises cost and CO2 emissions but also maintains voltage within acceptable limits.

2.2. Sizing of (Industrial) Hybrid Power Systems

Throughout the design process of any new power system, careful considerations need to be made when sizing components. The optimal sizing of components in Hybrid Power Systems (HPS) is an important aspect of designing a stable and cost-effective system. To gain an understanding of how previous

Table 2.1: The optimisation methods used within other research articles.

	Optimization Method				
Source	***GA***	***PSO***	***HOMER***	***MILP***	***Other***
[11] [12] [13] [14] [15] [16] [17] [18] [19] [20] [21] [22] [23] [24] [25] [26] [27] [28] [29] [30] [31] [32]	X				
[33] [34] [35] [36]	X	X			
[37] [38]	X	X		X	
[39] [40] [41]	X	X	X		
[42]	X		X		
[43] [44] [45] [46] [47] [48]		X			
[49] [50] [51]			X		
[52] [53] [54] [55] [56] [57]				X	
[58] [59] [60] [61] [62] [63] [64] [65] [66] [67] [68] [69] [70] [71] [72] [73] [74] [75] [76] [77] [78] [79] [80]					X
Total:	32	15	7	9	23

Table 2.2: The objective functions used within other research articles.

	Objectives		
Source	***Cost***	***Emission***	***Other***
[54] [56] [79] [40] [35] [47] [55] [59] [71] [48] [15] [73] [57] [20] [69] [74] [12] [76] [75] [25] [36] [78] [39] [50] [26] [13] [28] [45] [51] [33] [16] [70] [31] [53] [24] [30] [64] [60] [77] [42] [17] [32] [29] [23] [41] [67] [63] [80] [14]	X		
[58] [19] [62] [61] [37] [65] [44] [46] [27] [11] [72] [38] [52] [43] [66]	X	X	
[49]	X		X
[18]		X	
[22] [21] [68] [34]			X
Total:	66	16	6

literature approached this process, 71 papers were examined and categorised. These categories can be seen in Table 2.1, Table 2.2, and Table 2.3. Previous literature has explored various approaches and methodologies for sizing components to achieve specific goals and objectives. In the context of industrial applications, the sizing process becomes even more complex due to the higher energy demands of industrial loads.

Previous literature used different optimisation techniques, such as Genetic Algorithms, Particle Swarm Optimisation, and Ant Colony Optimisation, to determine the optimal size of components (ranging from wind turbines to combined heat process systems) in HPS configurations. The objective functions used in these optimisation processes often consider factors such as system cost and sometimes CO2 emissions. Moreover, the optimisation process is usually subject to constraints to ensure that the HPS operates within the specified limits. Constraints may include limits on system capacity, voltage levels, or grid integration requirements.

When Table 2.1, Table 2.2, and Table 2.3 are examined. It becomes apparent that Genetic Algorithms are usually utilised to tackle the objective problem. When the papers are studied further, it also becomes clear that fewer papers deal with both cost and CO2 objective functions. The last examination that can be made is the type of power system that is used for the sizing. The research papers that were observed to focus on industrial loads always examined at least cost as an objective function. Adding CO2 to the objective function for this paper, while utilising the Genetic Algorithm to tackle this multi-objective problem for sizing already gives an interesting contribution to the available research specifying industrial loads.

Of the research papers that size components for industrial loads [14] [19] [49] [54] [56] [58] [62] [79], only [58], [19], and [62] appear to consider two objectives (cost and emissions). The research performed in [19] appears to be the only paper focusing on the sizing aspect of industrial loads with cost and emissions as objective functions, this paper is thus the most similar to the work that will be presented in this thesis and forms a solid base of knowledge for the work to be done. The scope of [62]

Table 2.3: The types of power systems used within other research articles.

Source	Type of power system			
	Residential	***Industrial***	***Stand-alone Microgrid***	***Other***
[77] [43] [11] [64] [70] [74] [75] [76] [78] [53] [42] [50] [47] [13] [16] [24] [25] [26] [30] [32]	X			
[56]	X	X		
[58] [62] [79] [54] [49] [14] [19]		X		
[59]	X		X	
[61] [66] [72] [52] [46] [27] [28] [67] [69] [71] [73] [51] [33] [45] [48] [12] [15] [17] [20] [23] [29] [31] [68] [21]			X	
[65] [37] [38] [44] [60] [63] [80] [55] [57] [39] [40] [41] [35] [36] [18] [34] [22]				X
Total:	22	9	25	17

includes emissions into its research, but only as an analysis step after the selected size of components has been added to the existing system, it does not include emissions into the objective functions. Investigated in [58], the use of a genetic algorithm (with both cost and emissions as objective functions) to optimise the Energy Management System (EMS) of an existing HPS. This does not translate directly to the work done in this thesis, but it already illuminates a research path that can be taken after optimal sizing: optimise the Energy Management System.

Innovative method for energy management: Modelling and optimal operation of energy systems
In this document, a comprehensive case study of a pharmaceutical industrial plant and its optimisation procedure is presented. The study delves into the various components of the power plant, including the characteristics of a natural gas internal combustion engine, steam boiler, hot water boiler, mechanical chiller, and absorption chillers. Additionally, it examines the energy flows and interconnections among these components, providing insight into the purpose and functionality of the installation. An essential aspect highlighted in the document is the significance of the electricity rate and the time scale in the economical optimisation of the power plant. By considering varying electricity rates and load demands, the optimisation process aims to achieve cost-effectiveness and minimise fuel consumption and pollutant emissions. It is important to note that this paper does not solely focus on the sizing of elements. Instead, it emphasises the broader challenge of optimising the Energy Management System (EMS) that governs the interactions and operations of the power plant components. While the optimal sizes of the components are determined, the document further explores the intricate task of optimising the EMS to enhance the overall efficiency and environmental performance of the power plant. The optimisation criteria discussed encompass minimising total cost, fuel consumption, and pollutant emissions. The results showcased in the document reveal that optimal management of the power plant components can lead to substantial gains in terms of cost-effectiveness, fuel consumption reduction, and emission mitigation. Overall, this case study serves as a comprehensive exploration of energy management in industrial applications. It demonstrates the importance of integrating component sizing and EMS optimisation to achieve sustainable and efficient energy solutions. By dynamically coordinating the operation of various components based on electricity rates and load demands, the EMS plays a pivotal role in optimising the overall performance of the pharmaceutical industrial plant.

Optimal sizing of an industrial microgrid considering socio-organisational aspects
This document discusses the concept of industrial symbiosis and its application in eco-industrial parks for achieving sustainable development. It focuses on the power system of an industrial park located in the region of Ghent, highlighting the integration of renewable energy sources and the use of microgrids. The document explores the optimal sizing of collective energy systems, considering factors such as renewable generation, storage control, and demand response. It also discusses the economic and environmental evaluation of these systems. The paper utilises a genetic algorithm for optimisation

in combination with hourly historical data over the course of 1 year to observe seasonal and daily meteorological patterns. The system parameters (implemented using MATLAB) considered for sizing the installation include installed solar power, installed wind power, installed combined heat and power (CHP), battery storage capacity, and maximum battery power. The objective functions considered in this paper for the sizing are the minimisation of the levelized cost of electricity and the reduction of CO2 emissions.

Optimization of Distributed Energy Resources in an Industrial Microgrid
This research paper introduces a comprehensive model for an industrial microgrid with integrated distributed energy resources. The context of this study revolves around an existing manufacturing facility situated in Ireland. The core objective of this model is to meticulously compute both the cost and emissions associated with the utilisation of a diverse array of resources aimed at fulfilling the electricity demand of the facility.

The paper is composed of multiple elements including load forecasting, analysis of pricing and emissions, utilisation of wind power, management of demand response, and the integration of energy storage systems. Collectively, these components weave a robust framework capable of assessing the economic benefits of harnessing DERs and their potential to reduce the facility's reliance on the conventional power grid.

The results stemming from the model are marked by their accuracy in forecasting the facility's load demand. Indicators such as a Mean Absolute Percentage Error (MAPE) of 4.1% underline the model's reliability in predicting energy consumption patterns. However, it's worth noting that the specific implementation of sizing components within the model is not explicitly addressed, it rather showcases the potential economic benefits achievable through the strategic deployment of DERs.

Optimal sizing of battery storage systems for industrial applications when uncertainties exist
The objective of the paper is to propose a new method for sizing a battery energy storage system (BESS) in the presence of uncertainties. The paper aims to address the problem of determining the optimal size of a BESS installed in an industrial facility to reduce the facility's electricity bill. The main focus is on considering the uncertainties involved in the electricity bill cost coefficients and the profile of the facility's load demand. The paper formulates the optimisation problem for calculating the total costs of the BESS. The problem takes into account the investment costs, maintenance costs, and benefits derived from the installation of the BESS. The objective is to minimise the total costs incurred for energy. The optimisation problem is solved using a constrained optimisation model that considers the daily optimal operation of the battery. The paper applies decision theory to choose the best size for the BESS. Three different decision theory approaches are used: (i) minimising the expected cost, (ii) minimising the regret felt by the decision maker (DM), and (iii) a combination of (i) and (ii). The expected cost and regret are calculated for each alternative and future scenario. The best sizing alternative is chosen based on the minimum expected cost or the minimum regret, depending on the approach used. The proposed procedure is applied to an actual industrial facility to demonstrate its practicality. The uncertainties in the sizing of the BESS are represented by different future scenarios, each characterised by assigned probabilities.

Hybrid-Microgrid Planning, Sizing and Optimization for an Industrial Demand in Pakistan
This paper aims to analyse the sizing and optimisation of a hybrid microgrid system to meet the electricity demand of an industrial load in Faisalabad city, Pakistan. The objective of the study is to determine the optimal sizing and configuration of the hybrid microgrid system that can meet the industrial electricity demand reliably and sustainably. The paper uses the HOMER software for optimisation, which employs an enumeration method to simulate all possible system configurations. The optimisation variables include the size of the PV array, number of wind turbines, size of each generator, number of batteries, size of the converter, and dispatch strategy. The optimisation is based on the Net Present Cost (NPC), which is a measure of the life cycle cost of the system. The paper also considers various constraints and control parameters, such as the minimum renewable energy requirement, maximum annual capacity shortage, operating reserve from PV output, simulation time step, and set point state of charge. These constraints and parameters help in designing a cost-effective and reliable hybrid microgrid system.

Holistic Approach for the Optimization of Industrial Hybrid Energy Hubs with MILP
This paper presents a holistic approach for optimising Energy Hubs in industrial applications using Mixed Integer Linear Programming (MILP). The objective is to achieve optimal production and energy scheduling while considering different scenarios within an industrial process. The paper proposes a modular modelling approach with five generic modules: converter, storage, input, output, and connection. The optimisation problem is formulated as a MILP problem with linear constraints and a linear objective function. The approach allows for the integration of different energy carriers and networks into the modelling and optimisation of industrial plants. The objective function in the optimisation problem includes real costs, penalties, or rewards on decision variables to shift the optimisation towards a desired goal. By using a MILP problem formulation, the optimisation can be solved with state-of-the-art solvers and results in a global optimum.

Optimal techno-economic sizing of a multi-generation microgrid system with reduced dependency on grid for critical health-care, educational and industrial facilities
This document focuses on the optimal sizing and configuration of a multi-generation microgrid system. It addresses the challenges of energy security and power supply quality by integrating renewable energy sources and energy storage technologies. The paper presents a generalised model for techno-economic optimisation and applies it to different types of facilities such as healthcare, educational, and industrial facilities. The goal is to minimise the lifetime cost of energy supply while reducing dependency on the grid. It generalised model considers the configuration of battery energy storage systems, solar PV systems, biomass, and diesel generators. The paper highlights the economic benefits of operating the battery system alongside different distributed generators, compared to existing utility pricing models. The results of the case studies show that the optimal asset configuration with renewable energy sources can provide cost-effective solutions with a minimal carbon footprint.

The economic value of combined PV-battery systems for an industrial load under different price scenarios
This document discusses the economic value of combined PV and BESS for industrial loads in the Netherlands. It highlights the need for energy storage systems in a future renewable-based power system and the challenges faced in integrating them. The document presents a basis for the valuation of BESS for industrial sites and provides insights into the energy system modelling and simulation. Energy storage systems are crucial for maintaining the stability of the electricity grid in the face of increasing deployment of variable renewable energy sources. The original grid design was not based on decentralised and variable generation, leading to challenges in integrating Energy storage systems. The simulation of different configurations of PV and battery systems provides insights into self-consumption, self-sufficiency, and the potential economic benefits for industrial loads.

2.3. Multi-Objective Optimisation Techniques

Multi-objective optimisation techniques play a crucial role in addressing the complex trade-offs that arise in designing Hybrid Power Systems. The simultaneous consideration of multiple objectives, such as cost and CO2 emissions, allows decision-makers to identify a range of Pareto-optimal solutions that offer different trade-offs between these objectives. In the case of this thesis, Cost and CO2 emissions. Identified techniques to tackle these multi-objective problems are most prominently: Genetic Algorithms (GA), Particle Swarm Optimisation (PSO), HOMER, and Mixed Integer Linear Programming (MILP)

While PSO and HOMER have shown promise in certain optimisation tasks, they may not be inherently suited for multi-objective optimisation [81], requiring weights to be added to multiple objectives effectively turning it into a mono-objective optimisation problem. Additionally, HOMER, often considered a black box model [50], may lack transparency in its optimisation process, making it challenging to understand and verify the obtained results. Furthermore, in literature when HOMER is used for optimisations, GA is used as a verification technique with similar results [42].

Genetic Algorithms (GA) have demonstrated their effectiveness and suitability for multi-objective optimisation tasks [82] making it an ideal choice for tackling the intricate trade-offs in designing HPS components. The transparent nature of GA also allows for better insight into the optimisation process and easier validation of results. Even when a comparison is made between PSO, HOMER, and GA with a mono-objective optimisation, the results are similar [40].

As a result, in this research, we have opted to utilise Genetic Algorithms as our primary multi-objective optimisation technique. Subsequently, the GA will be expanded with elitism and nondomination into the Nondominated Sorting Genetic Algorithm II (NSGA-II) [36]. Key differences between GA and NSGA-II (and the reason for utilising it) [36] is the use of nondominated sorting, elitism, and crowding distance sorting in NSGA-II. Nondominated sorting divides the population into multiple fronts based on their dominance relationship, allowing NSGA-II to maintain a diverse set of solutions that are close to the Pareto-optimal front. Elitism keeps the best individuals from each generation preserved in the next generation. This helps to maintain the best solutions over generations and prevents the loss of valuable information. Crowding distance helps to maintain diversity by assigning a fitness value based on the density of solutions in a particular region of the objective space. It encourages the exploration of different regions and prevents the convergence of a single solution.

Overall, NSGA-II performs better than regular GA in multi-objective optimisation problems. It provides a more diverse set of solutions that cover a wider range of trade-offs between conflicting objectives. This makes it a powerful tool for decision-making in complex problems. Leveraging the power of NSGA-II effective sizing of HPS components, considering Cost and CO2 emissions, is attempted through the comparison of a diverse range of optimal solutions on the Pareto front.

3
Methodology

For the work completed in this Thesis, three main subjects were adhered to: Modelling, Sizing, and Analysing. For the modelling of the PV-DSL-BAT and grid components, Mosaik [83] will be used as co-simulation software in combination with a custom EMS and industrial load profiles [84]. The sizing will be done with a Genetic Algorithm to tackle the multi-objective problem: Total Cost of the System and CO2 emissions in one year of operation. The analysis of the bus voltages will be performed on the CIGRE MV Distribution Network [85] with PandaPower [86] to perform unbalanced load flow calculations. A comparison will be made of the system before and after the optimal sizing has taken place. These three subjects combine towards reaching the research objective: "Optimally size a Hybrid Power System (composed of a PV system, Diesel Generator, and Battery Energy Storage System; PV-DSL-BAT) to minimise cost and CO2 emissions for an industrial load and analyse the effect of this optimally sized profile on voltage sag in an industrial bus system."

3.1. Modelling

In this work, mathematical models will be created in Python for the use in co-simulation software Mosaik. These models will replicate behaviours of Grid connection, PV, Diesel Generator, and BESS systems in response to an industrial load profile. An EMS will also be created to route the power exchange between these components. The necessary behaviours of the created models in this work are limited to the exchange of power within certain thresholds/limits and to keep track of the exchanged energy and used resources. The exchanged energy and used resources will be used to calculate the objective functions, cost and CO2 emissions, of the system through the Levelized Cost of Energy (LCOE) and CO2 emission factors. The LCOE and CO2 emission factors are multiplied by the energy and resources used in one year of simulation to calculate the average cost and CO2 emission for a full year of operation.

For the CO2 emissions considered in this thesis, the scope 1 and 2 emissions are addressed. These are defined by the World Economic Forum [87] as:

- Scope 1: These are "direct" emissions – those that a company causes by operating the things that it owns or controls. These can be a result of running machinery to make products, driving vehicles, or just heating buildings and powering computers.
- Scope 2: These are "indirect" emissions created by the production of the energy that an organisation buys. Installing solar panels or sourcing renewable energy rather than using electricity generated using fossil fuels would cut a company's Scope 2 emissions.

In this thesis, these scope definitions translate to the direct release of CO2 through the burning of diesel in the diesel generator (Scope 1) and the purchasing of electricity from the grid (Scope 2).

3.1.1. Mosaik

Before the models are created, it is necessary to become familiar with the co-simulation software Mosaik. This ensures that the models are created in a manner compatible with Mosaik.

MOSAIK [83] is a co-simulation framework that focuses on providing high usability and flexibility. MOSAIK is closely linked to the same approach used for multi-agent systems (MAS), which allows

for modelling components and their interactions in different domains. MAS-type solutions are especially beneficial for complex Cyber-Physical Energy Systems (CPES)[1], similar to the energy system(s) modelled in this work.

MOSAIK has been applied in various CPES test cases, including the evaluation of optimisation strategies for dynamic virtual power plants, market-based re-dispatch solutions, congestion management in distribution systems, and large-scale roll-out of CPES solutions. It has also been used in hardware-related projects focused on microgrid testing and improving laboratory and co-simulation platforms for CPES testing.

The MOSAIK system architecture follows a modular approach, with the core framework serving as the central component. The framework does not contain simulation models itself but interfaces with a growing ecosystem of simulators. Users can interact with MOSAIK through two APIs: the component API for establishing an interface between MOSAIK and a new simulator, and the scenario API for setting up executable co-simulation scenarios.

The scheduling algorithm used by MOSAIK is a flexible discrete-time simulation. It employs a data flow graph to indicate the data dependencies between simulators in the co-simulation. The graph is automatically established at the beginning of the co-simulation process based on the connections defined by the user. Each simulator has predecessors that provide data and successors that require data. The simulation process for each simulator progresses in steps until the end of the co-simulation is reached.

The simulation process for each individual simulator in MOSAIK is structured in steps that indicate its temporal progression, represented visually in Figure 3.1. The step size is measured in integers to ensure comparability between different simulators. The simulation process iterates for each simulator, performing a step each time until the end of the co-simulation is reached. The data exchange between simulators is conducted asynchronously to improve performance.

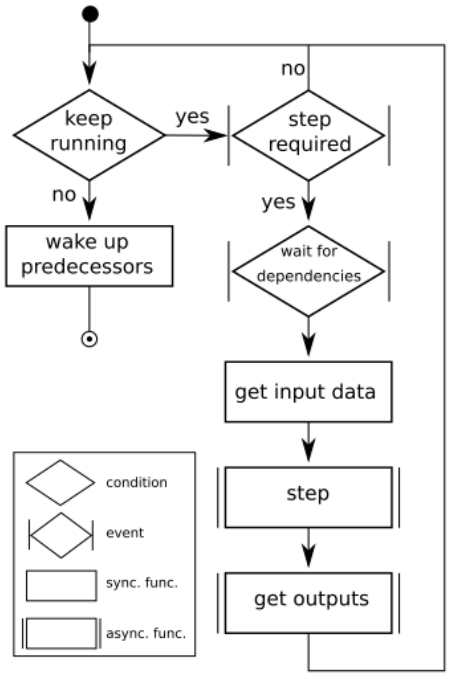

Figure 3.1: Simulation process for an individual simulator [83]

The data exchange between a simulator and MOSAIK is divided into three stages. First, the input data required by the simulator is read from MOSAIK's internal buffer and put into the simulator's input buffer. The data requirement is specified via the data flow graph. The actual exchange of data between simulators is managed via the discrete event simulation framework Simpy, which allows for efficient management of the timing of asynchronous simulation processes.

Levelized Cost Of Energy

In this thesis, the LCOE is utilised to calculate the objective function, while it can also provide a comparison with LCOE values available in existing literature to benchmark the calculated values. The LCOE calculation offers additional insights into the long-term economic viability of HPS configurations, supporting the selection of sustainable energy solutions that align with industrial load demands and environmental objectives.

The LCOE calculates a value for the price per generated kWh. The calculation includes the investment expenditures, operations and maintenance expenditures, fuel expenditures, electricity generated, discount rate, and the lifetime of the system. These parameters, summarised in Table 3.1, are used in the LCOE function given by Equation 3.1 [88] with the following assumptions:

- The investment expenditures only consider the initial capital investments and installation costs.

[1] A Cyber-Physical Energy System is a complex system that combines physical energy systems, such as electric power grids and distributed energy resources, with the digital world of information and communication infrastructure. CPES also takes into account human behaviour, economic factors, and environmental considerations.

- The discount rate is taken as the Weighted Average Cost of Capital (WACC) and has a value of 1.15% [89].
- The lifetime of the system is set to 10 years. This is based on the shortest lifetime between PV (25 years [29]), BESS (20 years [90]), and, even though it is not directly modelled, the BESS inverter (10 years)[2].

$$\text{LCOE} = \frac{\sum_{t=1}^{n} \frac{I_t + M_t + F_t}{(1+r)^t}}{\sum_{t=1}^{n} \frac{E_t}{(1+r)^t}} \tag{3.1}$$

Table 3.1: Parameters for LCOE calculation

Parameter	Symbol
Investment expenditures in the year t	I_t
Operations and maintenance expenditures in the year t	M_t
Fuel expenditures in the year t	F_t
Electricity generation in year t	E_t
Discount rate	r
Lifetime of the system	n

3.1.2. Grid

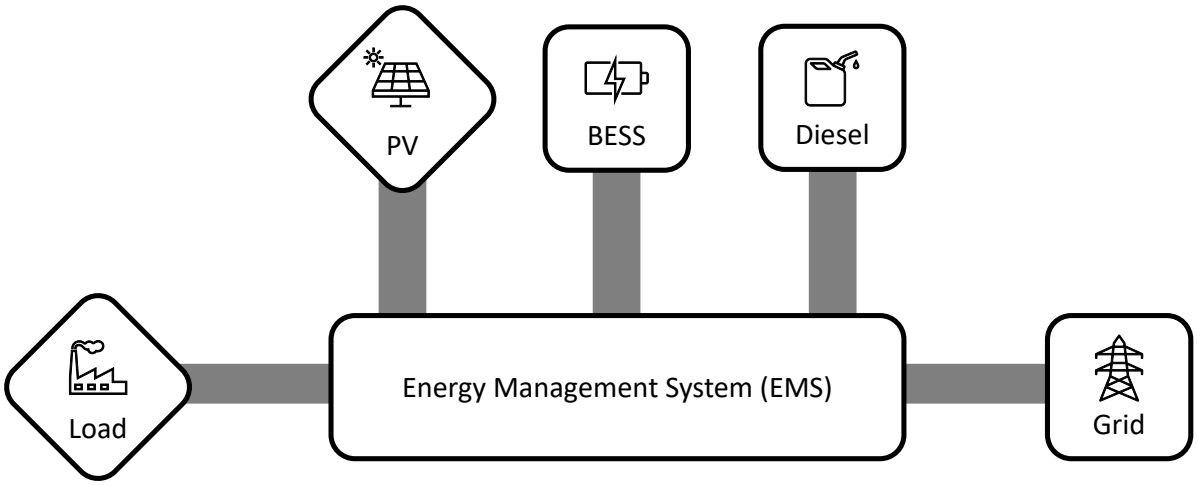

Figure 3.2: Simplified diagram of the models created in Mosaik

The grid connection, depicted as one of the model blocks in Figure 3.2[3], which will only consist of an upper power limit, the contracted capacity. The assumption is made that the Grid model can also accept power being supplied into it with the same magnitude limit. Per kWh that is supplied by the grid, a cost and CO2 metric is calculated based on data summarised in 3.2. The grid model keeps track of the maximum injected power in a time step ($O_{\text{G}-kW}$) and the total energy injected by the grid ($O_{\text{G}-kWh}$). Together with the maximum power, total kWh, and the parameters in 3.2 the cost and CO2 emission of the grid is calculated according to 3.2 and 3.3 respectively. The Python code for the grid model can be found in A.1.

$$\begin{aligned} F(Cost_{\text{Grid}}) = O_{\text{G}-kW}(t_{\text{end}}) * C_{\text{G}-TP} * 12 + \\ O_{\text{G}-kWh}(t_{\text{end}}) * (C_{\text{G}-TE} + C_{\text{G}-E}) + \\ I_{\text{G}-kW} * (C_{\text{G}-C} + C_{\text{G}-T} + C_{\text{G}-TC}) * 12 \end{aligned} \tag{3.2}$$

[2]The Diesel Generator is not mentioned in years but rather in operating hours, namely 7000 [29]. A maximum operating lifetime of 10 years is also mentioned for grid-supporting and off-grid applications [91]

[3]The squares indicate models that are controlled by the EMS during a timestep. The diamonds indicate data sets, these provide values to the EMS during a timestep

Table 3.2: 2022 Grid connection parameters for cost and CO2 calculation

Parameter [unit]	Amount	Symbol
Grid Model Input Contracted Capacity [kW]	$-$	$I_{\mathsf{G}-kW}$
Grid Model Output Maximum Power up until current time step [kW]	$-$	$O_{\mathsf{G}-kW}$
Grid Model Output total kWh injected up until current time step [kWh]	$-$	$O_{\mathsf{G}-kWh}$
Average Market Price [€/kWh] [92]	0.24124	$C_{\mathsf{G}-P}$
Grid CO2 Emission Factor 2022 [kg/kWh] [93]	0.526	E_{G}
Grid Connection Fixed Rate [€/Month] [94]	$12.65 - 709.00$	$C_{\mathsf{G}-CF}$
Grid Transport Fixed Rate [€/Month] [94]	$36.75 - 230.00$	$C_{\mathsf{G}-TF}$
Grid Transport kWh Rate [€/kWh] [94]	$0.00 - 0.0107$	$C_{\mathsf{G}-TE}$
Grid Transport Contract Rate [€/kW/Month] [94]	$1.21 - 1.94$	$C_{\mathsf{G}-TC}$
Grid Transport Maximum kW Rate [€/kW_{max}/Month] [94]	$1.73 - 2.70$	$C_{\mathsf{G}-TP}$

$$F(CO2_{\mathsf{Grid}}) = O_{\mathsf{G}-kW}(t_{\mathsf{end}}) * E_{\mathsf{G}} \tag{3.3}$$

3.1.3. PV

The PV model used for the simulation is in the form of a power profile that is created beforehand according to a specific location and the chosen scale of PV installation. This scalable PV profile is generated with PVGIS [95][96] based on the installed capacity (kWp) and a chosen location. In the case of this thesis, the location is set in Pernis, Netherlands $[51.889, 4.388]$ (an industrial site best known for its petrochemical industry) to mimic the industrial setting in which the simulation, optimisation, and analysis should take place. Based on the selected location, a yearly profile is generated using PVGIS. This tool, developed by the Joint Research Centre, uses horizon information, solar radiation databases, terrain elevation, temperatures, and numerous other models and/or calculations to provide an hourly PV output power profile. The most recent dataset available in PVGIS is from the year 2020 (a leap year), which will be used in this thesis. PVGIS includes a system loss component (equal to 14%) and calculates the slope and azimuth of the PV system that gives the highest energy output for the whole year for the given location.

The PV model will provide the EMS with a PV power value for each timestep. The EMS will keep track of the utilised PV power and potential curtailment. This curtailment will be used to determine the netto PV energy usage from the total PV injected power. The netto PV energy consists of all usage, including injection into the grid. No direct monetary compensation for injected PV power into the grid will be given, as the Netherlands is removing its net metering construction [97]. The netto PV energy will be used for the calculation of the total cost, including the calculation of the LCOE. The Cost and CO2 emission of the PV system are then calculated according to 3.4 and 3.5 respectively.

$$F(Cost_{\mathsf{PV}}) = max(1, O_{\mathsf{PV}-kWh}(t_{\mathsf{end}})) * LCOE_{\mathsf{PV}} \tag{3.4}$$

$$F(CO2_{\mathsf{PV}}) = 0 \tag{3.5}$$

Validation

The PVGIS system has already validated its outputs with measurements from the European Solar Test Installation (ESTI) [100]. The performance of PVGIS can be evaluated based on the deviation of

[4] the 2021 USD prices are converted to 2022 Euro prices with [98] [99]

Table 3.3: 2022 PV parameters for cost calculation

Parameter [unit]	Amount	Symbol
PV Output netto kWh generated [kWh]	$-$	$O_{\mathsf{PV}-kWh}$
PV Investment Cost [€/kWp] [88] [4]	950.85	$C_{\mathsf{PV}-I}$
PV Operating and Maintenance Cost [€/kWp/year] [88] [4]	16.93	$C_{\mathsf{PV}-OM}$
PV Levelized Cost Of Energy [€/kWh]	$-$	$LCOE_{\mathsf{PV}}$

its energy production calculations from real data. A comparison of the energy production for a roof-mounted photovoltaic installation of 9.6 kWp in the area of Athens and a 105.6 kWp open field array in Asopos, Lakonia is evaluated in [101]. PVGIS achieved an annual energy production deviation of -2.0% and $+3.0\%$ from the measurements. This indicates that PVGIS estimates the energy production of photovoltaic systems with a relatively high level of accuracy. In Cabauw, Netherlands a comparison of the global horizontal irradiance measured and calculated by PVGIS achieved a Root Mean Square Deviation (RMSD)[5] of 86.9 W/M^2. As this thesis is focused on industrial loads these error margins are considered acceptable, particularly when realising that the deviation in the Netherlands is in the order of watts while the system for industrial application will be in the order of kilowatts.

The validation that needs to be done for this thesis encompasses the sizing aspect, where the validation needs to be made that the dataset of 1 kWp solar installation multiplied by a scalar gives the same results as the $scalar$ kWp solar installation. This involved generating multiple datasets from PVGIS, each corresponding to different installed PV capacity values: 1 kWp, 2 kWp, 5 kWp, 10 kWp, 50 kWp, 100 kWp, 500 kWp.

The 1 kWp dataset was scaled with the corresponding integer values (i.e. $2, 3, 5, 10, 50, 100, 500$) to create simulated profiles for each installed capacity. By comparing the simulated profiles to the PVGIS datasets for the same capacities, the validation aimed to assess the accuracy and scalability of the PVGIS outputs.

Two figures were created to assess the scalability of PVGIS datasets Figure 3.4 and Figure 3.3. Figure 3.4 shows the different datasets created by PVGIS and Figure 3.3 shows these PV profiles divided by the 1 kWp dataset. It can be observed from the figure that these profiles are an exact match with the integer scales of the 1 kWp dataset. This ensures that for the sizing done in this thesis, the integer scaling of the 1 kWp dataset can be used as opposed to configuring a setup that downloads new datasets for each new size. This also shows that PVGIS scales the data with the installed peak power linearly.

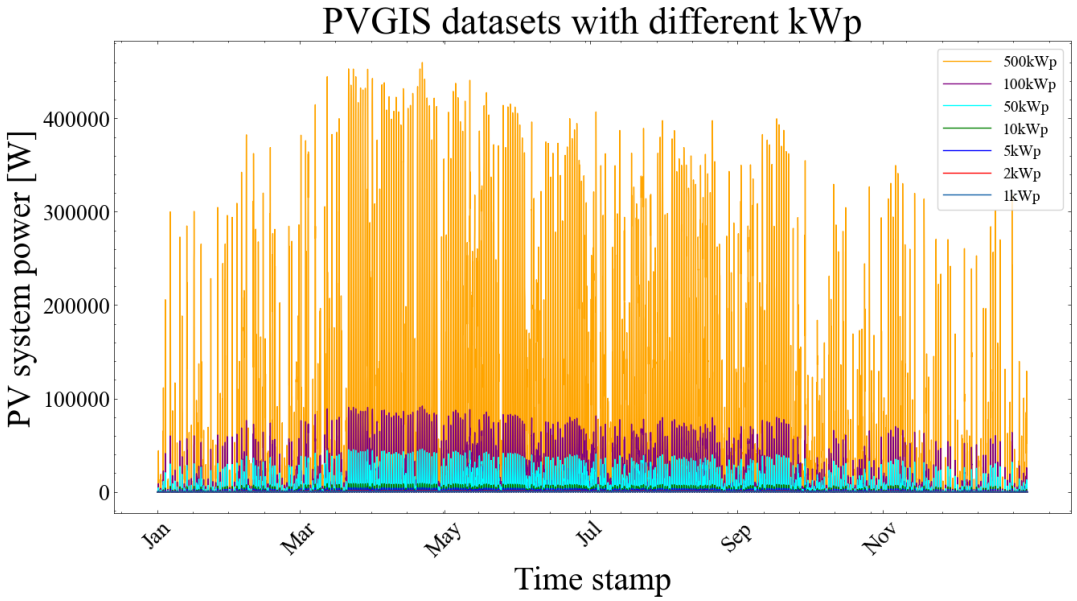

Figure 3.3: PVGIS PV Profiles for 1 kWp, 2 kWp, 5 kWp, 10 kWp, 50 kWp, 100 kWp, 500 kWp installed capacity at $[51.889, 4.388]$

[5]This is similar to the Root Mean Square Error (RMSE) listed in Equation 3.8

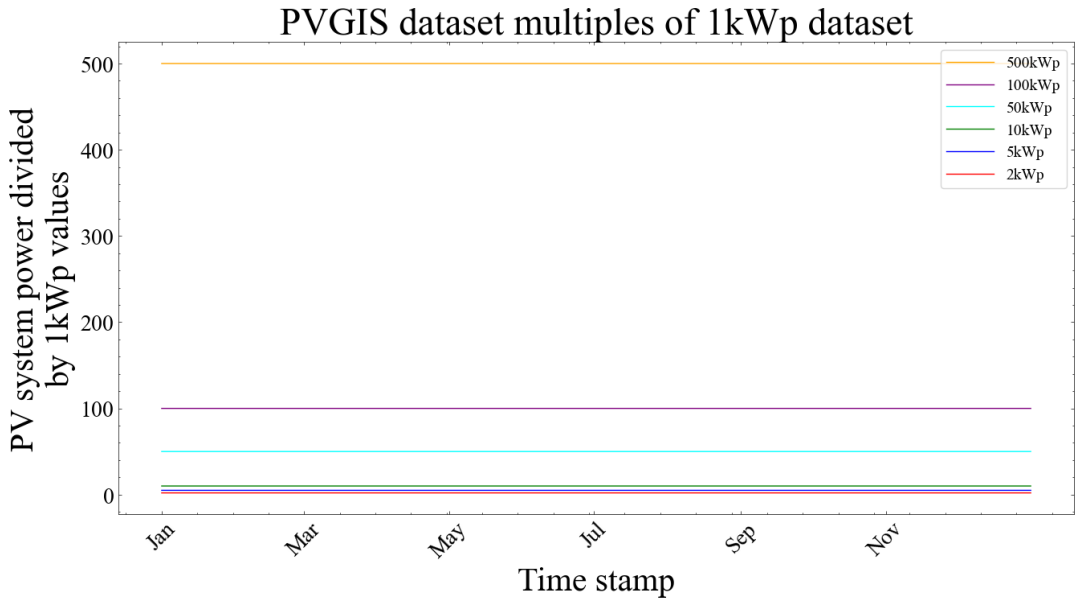

Figure 3.4

3.1.4. Diesel Generator

Within an HPS, it is advisable to incorporate dispatchable energy sources to increase power production during the intermittency of renewable energy sources. For this thesis, a model is created with the help of diesel generator datasets. This process can be repeated for different types of dispatchable generators, but for this thesis diesel generator data is used as it is probably the most popular type of generator and the choice for industrial applications [102].

To model the cost and CO2 characteristics of a diesel generator, datasets from a diesel generator manufacturer will be used in combination with the parameters mentioned in literature. The generator will work similarly to the grid in the sense that it will provide power below a certain upper limit, but will also use a threshold value. This threshold indicates that diesel generators are not suited to be operated at low power outputs relative to their maximum capacity [29].

The dataset used provides the output power and the corresponding fuel consumption for different sizes of generators. For each of these generators, a fuel consumption for different power output percentages (25%, 50%, 75%, 100%) is also given. These power outputs, together with the corresponding fuel consumption are plotted in a scatter plot Figure 3.5. For these scatter points a trend line is added through linear regression that solves Equation 3.6 [103], where X is the vector containing the power of the generators and y is the vector containing the corresponding fuel consumption. The resulting trendline and thus the equation used to calculate the fuel usage per time step can be seen in Equation 3.7. With this model (trend line), the Root Mean Square Error (RMSE) is calculated with Equation 3.8 to indicate the error of the model to the actual data points.

$$\min_{w} ||Xw - y||_2^2 \tag{3.6}$$

$$O_{\mathsf{D}-L}(t) = \begin{cases} O_{\mathsf{D}-L}(t-1) + (0.0513 * P(t) + 1.562), & \text{if } P(t) > 0 \\ O_{\mathsf{D}-L}(t-1), & \text{otherwise} \end{cases} \tag{3.7}$$

$$RMSE = \sqrt{\sum_{i=1}^{n} \frac{(\hat{y}_i - y_i)^2}{n}} \tag{3.8}$$

To calculate the costs and CO2 emissions of the diesel generator that has supplied a certain amount of kWh, formulas 3.9 and 3.10 are used. Herein 3.9 uses the total energy injected by the diesel generator ($O_{\mathsf{D}-kWh}$) and the Levelized Cost Of Energy (LCOE) to calculate the average cost of the diesel generator over one year of simulation. The cost function of the diesel generator includes a minimum

Table 3.4: 2022 Diesel Generator parameters for cost and CO2 calculation

Parameter [unit]	Amount	Symbol
Diesel Generator Model Output total kWh injected [kWh]	–	$O_{\text{D}-kWh}$
Diesel Generator Model Output total litres consumed [L]	–	$O_{\text{D}-L}$
Average Diesel Price [€/L] [104]	2.09	$C_{\text{D}-P}$
Diesel CO2 Emission Factor [6] [kg/L] [93]	3.473	E_{D}
Diesel Generator Investment Cost [€/kW] [Appendix B]	450	$C_{\text{D}-I}$
Diesel Generator Operating and Maintenance Cost [€/kW/year] [Appendix B]	10	$C_{\text{D}-OM}$
Diesel Generator Levelized Cost Of Energy [€/kWh]	–	$LCOE_{\text{Diesel}}$

of 1 kWh to ensure the costs of the installed diesel generator are always taken into account, even if the diesel generator does not provide any power throughout the simulation. The total CO2 emissions for one year of operation of the diesel generator are calculated through the consumed litres of diesel ($O_{\text{D}-kWh}$), which the diesel generator model keeps track of. The Python code for the Diesel Generator model can be found in A.2.

$$F(Cost_{\text{Diesel}}) = max(1, O_{\text{D}-kWh}(t_{\text{end}})) * LCOE_{\text{Diesel}} \tag{3.9}$$

$$F(CO2_{\text{Diesel}}) = O_{\text{D}-L}(t_{\text{end}}) * E_{\text{D}} \tag{3.10}$$

Validation

The validation of our model (trend line) is the RMSE (Equation 3.8) of all the actual data sheet values to all the values predicted by the linear regression line. This RMSE value of 2.43 gives the error indication of the model over the complete range of 0 to 3600 kVA[7]. When the RMSE is calculated for lower ranges of generators the RMSE is lower. The larger diesel generators introduce more volatility in the fuel consumption values. The RMSE for lower power ranges can be seen in Appendix C, showcasing that the RMSE value of 2.43 is an upper limit.

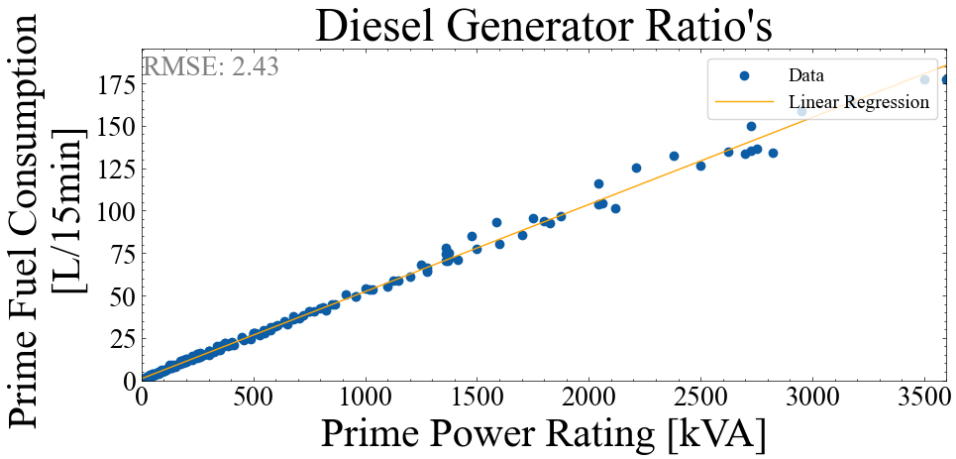

Figure 3.5: Linear Regression line used as the model for Diesel Generator

3.1.5. Battery Energy Storage System

Battery Energy Storage Systems are well suited for renewable energy storage and backup power applications [105], which increase the sustainability of the electricity grid and its operational reliability. Within BESSs, Li-Ion stands out as the new dominating technology for stationary applications, where previously this title was held by Lead-Acid technologies [106]. Within Li-Ion technologies, NMC (Nickel Manganese Cobalt) and LFP (Lithium Iron Phosphate) are two of the main technologies used for grid

[6] The Well-To-Wheel (WTW) Emission Factor
[7] Larger diesel generators exist, but the data sheets examined did not readily provide fuel efficiencies

Table 3.5: BESS model parameters for Equation 3.11, Equation 3.12, and Equation 3.13

Parameter [unit]	Source	Value
η_{charge} [%]	subsection 3.1.5 - Validation	0.9
$\eta_{\text{discharge}}$ [%]	subsection 3.1.5 - Validation	0.998
σ_{self} [%/day]	[110] [108] [111]	0.1

applications. Even though literature sometimes suggests that LFP dominates grid-connected uses while NMC dominates Electric Vehicle applications [107]. A comparison of these technologies' performance in [105] and [108] shows that they are both suited for usage in stationary applications (e.g. grid frequency regulation, forecast accuracy improvement, power gradient reduction, and uninterruptible power supply). In this thesis, the NMC technology is chosen, as the verification of battery models based on [109] utilises NMC Li-Ion technology for stationary applications.

The BESS model for this thesis is based on elementary energy and power equations where the energy in a time step is increased or decreased by a certain amount. These equations are split into three parts: charging Equation 3.11, discharging Equation 3.12, and idling (self-discharge) Equation 3.13. Some models of Battery systems use the round trip efficiency instead of separate charge and discharge efficiencies, but this can be calculated simply by multiplying charge and discharge efficiencies together $\eta_{\text{roundtrip}} = \eta_{\text{charge}} * \eta_{\text{discharge}}$ [90]. The values used for η_{charge}, $\eta_{\text{discharge}}$, and σ_{self} and their sources are given in Table 3.5.

For the BESS in this thesis, the State Of Charge (SOC) will be limited between 20% and 90% [112] by the Energy Management System (EMS) described in subsection 3.1.6. The capacity [kWh] and power rating [kW] ratio of the BESS will be set to a fixed value, which will be elaborated in subsection 3.1.5 - Validation.

To calculate the cost function associated with the discharged kWh of the BESS, a specific LCOE for storage applications is used, namely the Levelized Cost Of Storage (LCOS) 3.14 [113]. This is similar to the LCOE 3.1, except the electricity generated E_t is equal to the discharged energy and the fuel expenditure F_t is equal to the cost of electricity[8].

Similarly to the other models, the BESS Cost and CO2 functions are calculated using Equation 3.15, Equation 3.15, and Table 3.6. The Python code for the BESS model can be found in A.3.

$$E(t) = E(t-1) + P(t)\eta_{\text{charge}}\Delta t \tag{3.11}$$

$$E(t) = E(t-1) + \frac{P(t)\Delta t}{\eta_{\text{discharge}}} \tag{3.12}$$

$$E(t) = E(t-1) - \sigma_{\text{self}}\Delta t \tag{3.13}$$

$$\text{LCOS} = \frac{\sum_{t=1}^{n} \frac{I_t + M_t + F_t}{(1+r)^t}}{\sum_{t=1}^{n} \frac{E_t}{(1+r)^t}} \tag{3.14}$$

$$F(Cost_{\text{BESS}}) = max(1, O_{\text{B}-kWh}(t_{\text{end}})) * LCOS_{\text{BESS}} \tag{3.15}$$

$$F(CO2_{\text{BESS}}) = 0 \tag{3.16}$$

Validation

The validation process for the BESS system will be done to extract correct values for η_{charge} and $\eta_{\text{discharge}}$ that gives the BESS system real-world behaviour including any possible inverters. This involves comparing the SOC of the BESS model at the end of a defined power profile, with the SOC measurements obtained from an actual BESS with an inverter that is described in [109].

The real-world BESS system from which η_{charge} and $\eta_{\text{discharge}}$ values will be extracted is shown in Figure 3.7 and its details are summarised in Table 3.7. Here the BESS model energy-to-power ratio

[8]The cost of electricity generated by either the grid, diesel generator, or PV is taken into account in these models themselves and not additionally in the LCOS formula

Table 3.6: 2022 BESS parameters for cost calculation

Parameter [unit]	Amount	Symbol
BESS Output kWh injected [kWh]	–	$O_{\text{B}-kWh}$
BESS Investment Cost [€/kWh] [114]	142.65	$C_{\text{B}-I}$
BESS Operating and Maintenance Cost [€/kW/year] [113] [4]	10	$C_{\text{B}-OM}$
BESS Levelized Cost Of Storage [€/kWh]	–	$LCOS_{\text{BESS}}$

Table 3.7: [109] BESS system specifications

Parameter [unit]	Amount
Technology	Li-Ion NMC
Design capacity [kWh]	571.9
Nominal power [kW]	250
Energy-to-Power Ratio [h]	2.28

is also set to a value of 2.28 similar to its real-world counterpart. This value is within the bounds of energy-to-power ratios of 0.17 to 8 found in literature [115][113][55].

A predetermined power profile (given in Figure 3.6 [109]) is run through the real-world test setup, and also through the proposed BESS model. The η_{charge} and $\eta_{\text{discharge}}$ parameters of the proposed BESS model are then adjusted until both the real-world and model BESS achieve similar SOC readings at the end of the predetermined power profile.

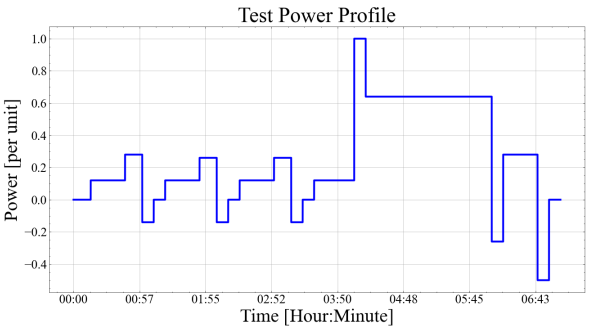

Figure 3.6: [109] Power Profile for test setup in Figure 3.7

The starting SOC for the real-world and model BESS systems is 92.8% and the end SOC for the real-world model is 15.75%. Tuning the η_{charge} and $\eta_{\text{discharge}}$ to values of 0.9 and 0.998 respectively resulted in an end SOC for the model of 15.74% and whose SOC progression can be seen in Figure 3.8. The blue star indicates the ”perfect” value of 15.75%. The downside of this method of tuning is that only the end SOC of the real-world BESS system is known and thus the model parameters are only tuned to mimic this end SOC. Herein it is thus not possible to complete an RMSE calculation of all the SOC points to check if the RMSE is smaller than 2.00%, a threshold mentioned in [116].

The values of 0.9 and 0.998 for the η_{charge} and $\eta_{\text{discharge}}$ and thus a value of $\eta_{\text{roundtrip}} = \eta_{\text{charge}} * \eta_{\text{discharge}} = 0.8982$ are supported by values used in other literature. [30] [117] mention $\eta_{\text{discharge}}$ values of (nearly) 100%, [90] [117] [111] mention $\eta_{\text{roundtrip}}$ values of 90%, and [45] [118]mention a η_{charge} value of 90%.

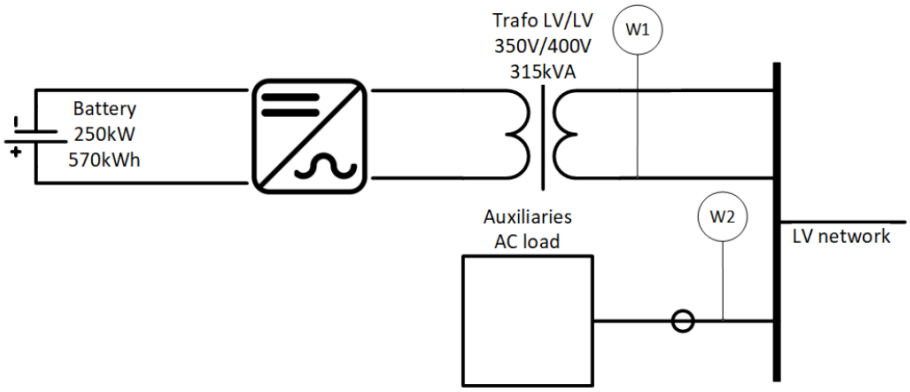

Figure 3.7: Li-Ion NMC BESS setup used in [109]

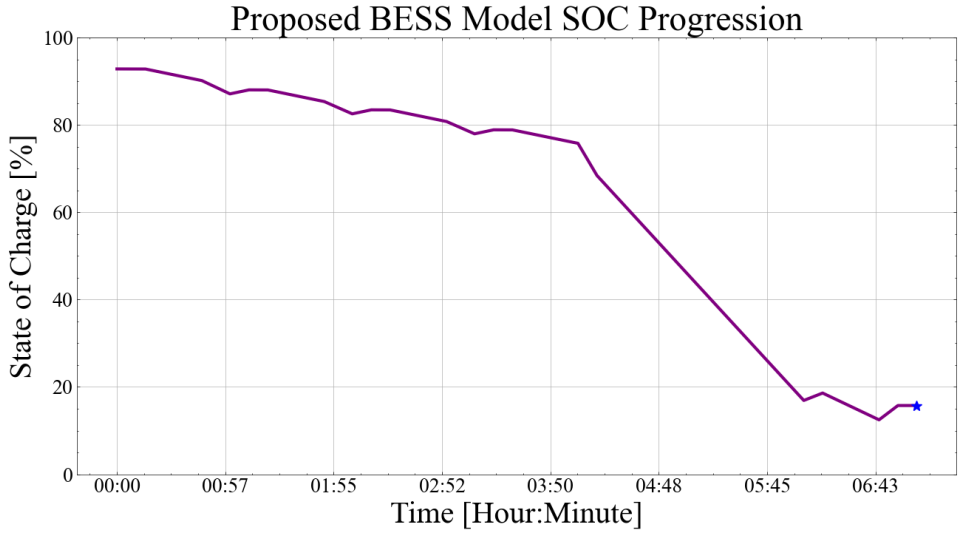

Figure 3.8: SOC progression of the proposed BESS model reacting to the power profile in Figure 3.6

3.1.6. Energy Management System

With the models for the grid, PV, diesel generator, and BESS system, an EMS can be created to schedule power to and from components in order to supply the industrial load. This EMS will be based on an elementary method, namely a rolling average in combination with a priority list.

Firstly the load profile is chosen at random out of a dataset. The choice is made randomly to mimic the behaviour of an industrial site that sets out to optimally size components for itself without consulting all of its ”neighbours”. Industrial sites usually have their management structure and can make decisions autonomously (within regulations) regarding their bottom line, Costs. The dataset ”Load profile data of 50 industrial plants in Germany for one year” [84] contains 20 load profiles for the year 2016 and 30 load profiles for the year 2017 in increments of 15 minutes (which will be the increments used throughout this EMS). The dataset for the year 2016 is chosen because it is a leap year and thus has the same amount of data points as the PVGIS dataset mentioned in subsection 3.1.3.

Within this total dataset of 20 load profiles, the load profile that will be used in the EMS and thus will also be sized and analysed in section 3.2 and section 3.3 is ”LG 1”, which was randomly chosen with [119]. The ”LG 1” profile can be seen in Figure 3.9.

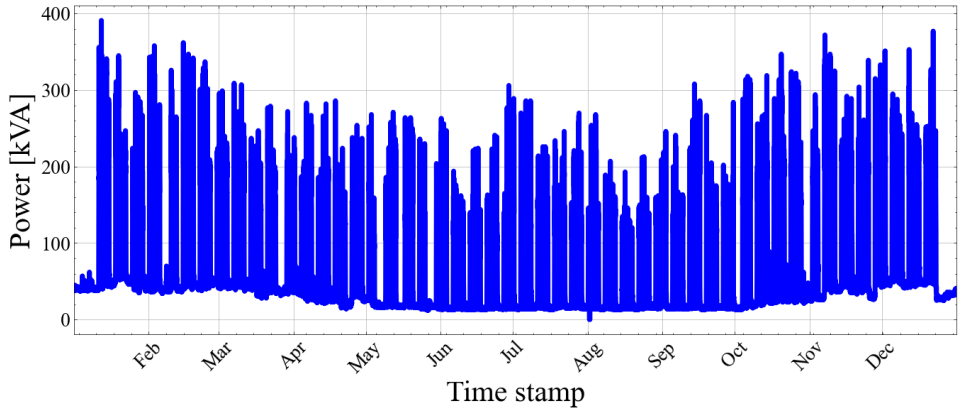

Figure 3.9: ”LG 1” [84] load profile in 2016

For the EMS power scheduling Apparent power is considered. The assumption is made that industrial sites perform power factor compensation themselves for their equipment and/or processes if necessary, but the grid point connection has a power factor of 0.85 [120] [121]. The PV, BESS, and Diesel generators are all assumed to be able to supply (and extract) at least up to 0.85 power factor

[122] [123] [124]. Their power scheduling will be according to the apparent power of the load profile. When power is supplied or extracted by the components, the assumption is made that the active and reactive power are increased/lowered in the same ratio as the 0.85 power factor. After the sizing for example, the new apparent power profile of the grid usage will be different, but the ratios of active and reactive power will stay the same.

The EMS can be seen depicted as a flowchart in Figure 3.10 and an illustration of the workings of the EMS can be seen in Figure 3.11. The steps of the EMS depicted in the flowchart and the accompanying example are segmented below:

1. (3.11a) A Rolling Average (RA) is created between the $Load$ and PV profiles (a 6 hour rolling average in the example Figure 3.11a).
2. (3.11b) Bounds (RA_{lower} and RA_{upper}) are added to the Rolling Average, which can be static or proportional. The bounds seen in Figure 3.11b are a static percentage (25% in this example) of the grid capacity. The proportional bound would be a percentage of the rolling average. The static bound is chosen for the explanation of the EMS as it is easier to understand.
3. (3.11c) The Grid usage is set within the bounds to as close as possible to the load profile, also ensuring the Grid usage stays within its own capacity limit $\text{Grid}_{\text{limit}}$.
4. (3.11d) The PV is used to supply power to the load and grid within the rolling average bounds. The "PV Usage" is not an actual model output, but rather a variable in the EMS where the energy used by the PV profile is recorded so the EMS does not request this energy from another model (BESS or diesel generator) as well. The "shortage" after the Grid and PV ($ShGPV$) is calculated also for this reason, to dispatch power to other components if the Grid and PV are insufficient.
5. (3.11e) The BESS system is used to supply or extract power between the current power combination and the load profile ($ShGPV$). During the night the BESS discharges with a power equal to the last SOC during the day (PV $\neq 0$) minus the SOC lower bound, divided by 18 hours[9], also shown in Equation 3.17. This will let the BESS system provide a small power benefit to the grid usage during the night.
6. (3.11f) The Diesel generator is used to supply power (within its rater power limit $\text{Diesel}_{\text{limit}}$ where the current power combination ("shortage after Grid, PV, and BESS $ShGPVB$) is still below the load profile. The diesel generator model has a lower threshold and will thus not turn on for small power demands (30% of diesel generator rating).
7. (3.11g) The PV is once again used to minimise curtailment with the grid usage staying within the rolling average bounds.
8. (3.11h) In the final step, if the power combination is not satisfactory to supply the load demand ("shortage after Grid, PV, BESS, and Diesel $ShGPVBD$), the grid is allowed to exit the Rolling Average bound to supply the load. If the final power combination does not match the Load profile, the Power Not Supplied is recorded. The curtailed PV power is also recorded during this step.

$$P_{\text{night}} = \frac{SOC_{\text{PV}\neq 0}[\text{end}] - SOC_{\text{lower-bound}}}{h_{\text{night}}} \tag{3.17}$$

This EMS will be used in combination with the sizing mentioned in section 3.2 and the analysis mentioned in section 3.3. The EMS will be used to determine the grid usage profile (with sized components) that will be entered into PandaPower for analysis with the CIGRE MV Distribution Network.

[9] 18 hours is the largest time span between PV generation in the PVGIS dataset

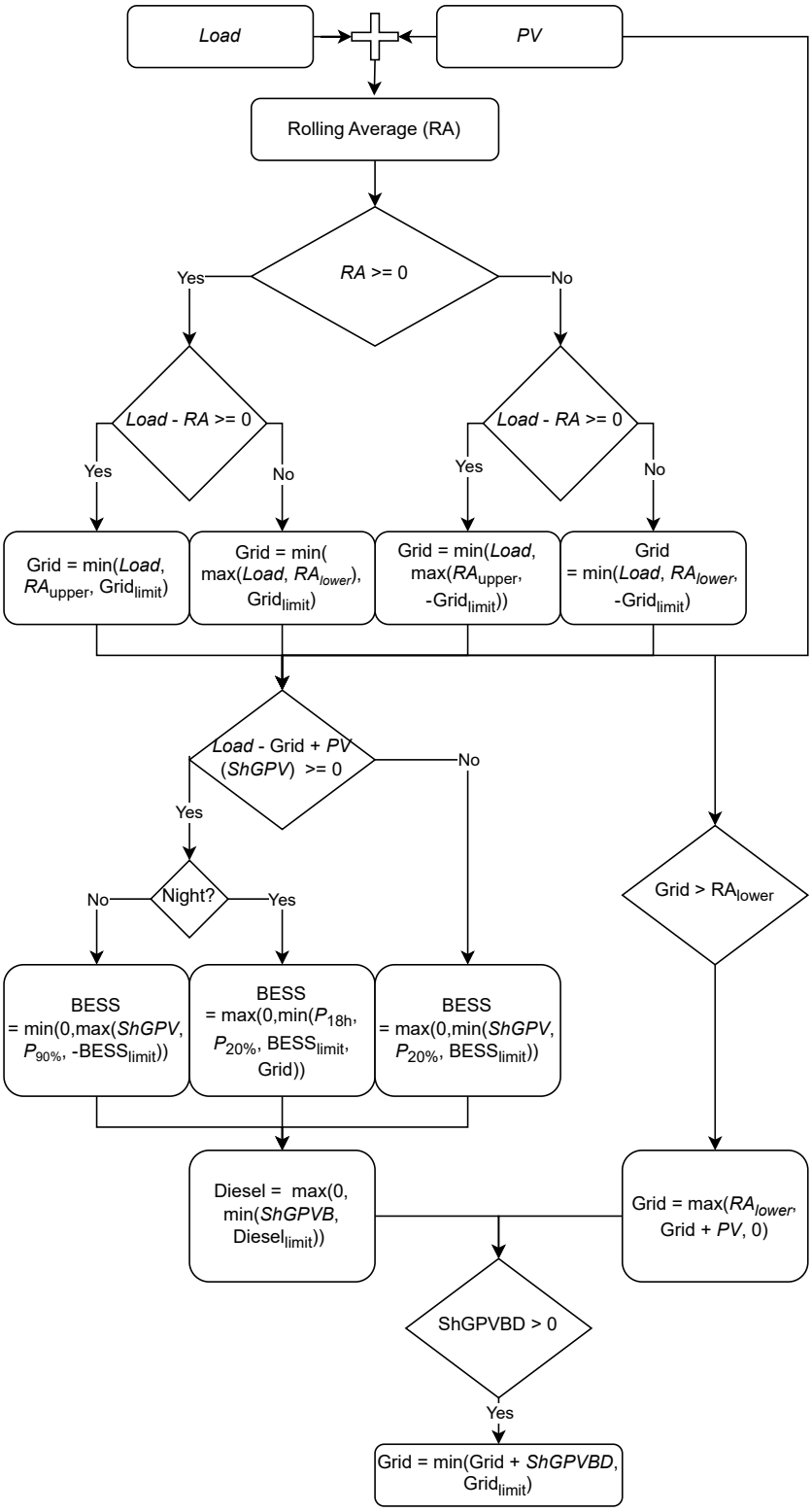

Figure 3.10: Energy Management System explained in steps 1 - 8

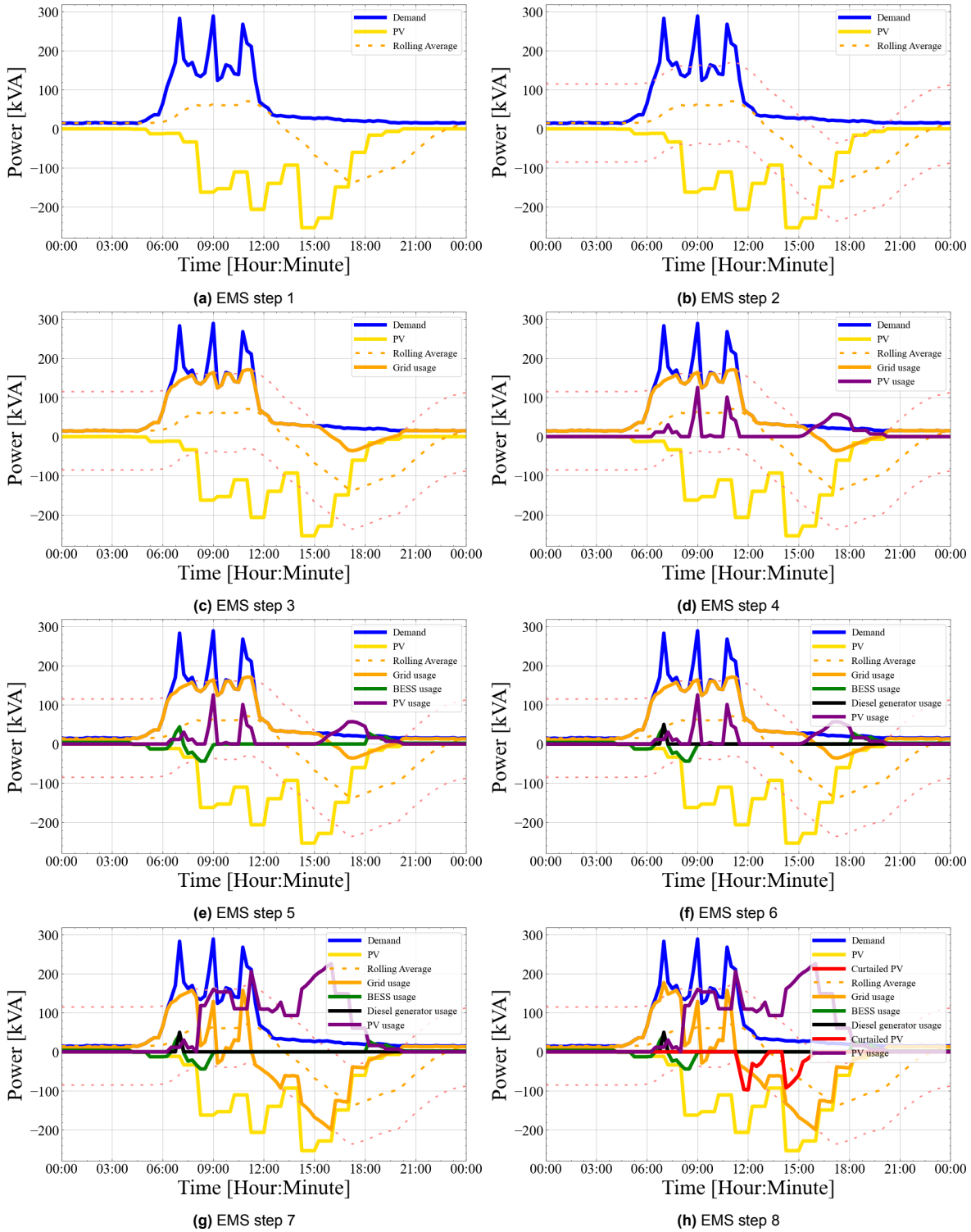

(a) EMS step 1 **(b)** EMS step 2

(c) EMS step 3 **(d)** EMS step 4

(e) EMS step 5 **(f)** EMS step 6

(g) EMS step 7 **(h)** EMS step 8

Figure 3.11: Explanation of the EMS (with a a 6 hour rolling average and a static bound of 25% in this example), timestamp of 01 July 00:00 to 02 July 00:00

3.2. Sizing

With the models created in section 3.1, the optimal size of each component can be determined. This optimal size will be determined through a Genetic Algorithm (GA), a multi-objective optimisation algorithm. To determine when a component is sized correctly, objective functions need to be made, which will be explained in subsection 3.2.1. For the sizing, four different scenarios will be examined. These scenarios are different in terms of parameters relating to the Energy Management System (EMS). As explained in subsection 3.1.6, the EMS is based on a rolling average and a static or dynamic bound around this rolling average. Because these two parameters could affect the sizing, four scenarios are proposed, as seen in Table 3.8. In this table, the Rolling Average Hours determines the number of time steps that are taken into the average. A 12 hour rolling average will have $12 * 4$ 15-minute time steps in the average. The static or dynamic component of the rolling average bound, as seen in Figure 3.11b, determines if the bound around the rolling average is a fixed interval (static) or based on a percentage of the current grid-usage (dynamic). The static bounds are calculated with respect to the grid capacity. The percentage bound is the percentage of either the grid capacity (static) or the current grid-usage (dynamic) that surrounds the rolling average line.

3.2.1. Objective Functions

The objective functions created for Cost and CO2 emissions give a value to a certain combination of component sizes which will help identify better or worse performance. This will create a Pareto front from which an optimal solution will be chosen that has the shortest Euclidean distance to $(0, 0)$ (a solution that has no Costs or CO2 emissions).

For the Cost Objective function, each component (PV, BESS, Diesel Generator) will be evaluated based on LCOE/LCOS and the Grid connection will be evaluated on yearly cost and cost of energy (we assume the grid connection is already installed). The cost formulas for each component have already been explained in Equation 3.2, Equation 3.4, Equation 3.9, and Equation 3.15. These can then be combined into the total Cost function by simply summing them into Equation 3.18. Additionally, a hefty Energy Not Supplied (ENS) [kWh] penalty is added to ensure the solutions given always supply the load profile. The ENS is rounded up the the nearest integer.

$$\begin{aligned} F(Cost) = (F(Cost_{\text{Grid}}) + F(Cost_{\text{PV}}) + F(Cost_{\text{BESS}}) + \\ F(Cost_{\text{Diesel}}) + round(ENS)) * (1 + 10 * round(ENS)) \end{aligned} \tag{3.18}$$

The CO2 Emissions Objective function evaluates the environmental performance of the HPS configuration, considering the total CO2 emissions resulting from grid usage and the consumption of diesel by the diesel generator. The total CO2 emission objective function can be created by again summing the sub-functions and adding a penalty function for Energy Not Supplied. The individual CO2 cost functions for the grid and diesel generator were explained in Equation 3.3 and Equation 3.10 and combined into Equation 3.19.

$$F(CO2) = (F(CO2_{\text{Grid}}) + F(CO2_{\text{Diesel}}) + round(ENS)) * (1 + 10 * round(ENS)) \tag{3.19}$$

These two objective functions are both normalised to aid the interpretation of the results. The base scenario, with which the objective functions are normalised, is when no PV-DSL-BAT components have been added and the load profile is sent directly to the grid. For the chosen load profile ”LG 1”, the maximum power is 391 kVA and this will be chosen as the grid capacity connection for calculating the base objective functions. The base scenario parameters and resulting Cost and CO2 function are summarised in Table 3.9. These values give a starting point from which differently sized HPSs can

Table 3.8: Four EMS scenarios that will be sized

Scenario	Rolling Average Hours	Static or Dynamic bound	Percentage bound
1	12	Static	100%
2	12	Dynamic	100%
3	6	Static	50%
4	6	Dynamic	50%

Table 3.9: Base scenario parameters

Parameter [unit]	Amount
Grid capacity [kVa]	391
PV capacity [kWp]	0
Diesel generator capacity [kVa]	0
BESS capacity [kWh]	0
$F(Cost_{\text{Base}})$ [1000×€]	559
$F(CO2_{\text{Base}})$ [tonne]	306

be compared. Together with the EMS created in subsection 3.1.6, the load profile can be seen in Figure 3.12. The line thickness of the 'Grid usage' is smaller than the 'Demand' line to be able to see both lines, they follow each other perfectly.

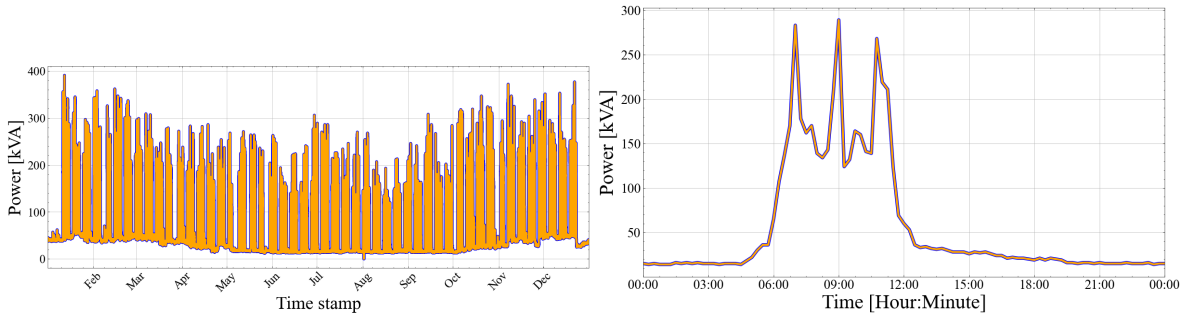

(a) Yearly power profile of base HPS

(b) Power profile of base HPS, 01 July 00:00 to 02 July 00:00

Figure 3.12

3.2.2. Pseudo Pareto Front

With the definition of the objective functions and the base scenario, the sizing can be commenced. However, it is advisable to have a prediction before the sizing commences to make sense of possible outcomes. This will be done with a "pseudo" Pareto front, where the size of one component is changed and the effect is observed in the Cost and CO2 function values. This is not a multi-objective optimisation but a sequential optimisation, where the resulting optimum for a variable in one optimisation is used to optimise another variable. For this "Pseudo" Pareto front, the grid capacity is sized first, then the PV system, then the diesel generator, and finally the BESS; all from 0 to 1000 in steps of 100. This is done to create a large spread of solutions as a starting point.

An example (scenario 3) of the "pseudo" Pareto fronts can be seen in Figure 3.13. Here the fronts can be seen when the sizing is done sequentially: First, the grid is sized to 391 kVA (with grid capacity below 391 kVA, there is ENS and thus a very high penalty), then the PV is sized to 300 kWp, and the Diesel and BESS systems appear to only worsen the Cost function while not improving the CO2 function. This gives an estimate for the optimal size of the HPS, with a grid capacity near 391 kVA and a PV system in the neighbourhood of 300 kWp. Because this is a sequential optimisation with only a small test population, this estimate needs to be taken with a fair amount of scepticism. Only after the optimisation with GA has been completed, does it become clear if the estimate with sequential optimisation provides meaning.

3.2.3. Genetic Algorithm

With the first steps taken towards an optimal combination of grid capacity, PV, Diesel, and BESS with a sequential optimisation, the optimisation can be extended with Genetic Algorithm (GA) optimisation. In chapter 2 the suitability of GA for this type of optimisation was explained, specifically Nondominated Sorting Genetic Algorithm (NSGA-II) [36]. NSGA-II incorporates nondominated sorting, elitism, and crowding distance to improve on the standard implementation of GA. These additions to GA and the overall workflow of NSGA-II is presented below, as well as the initialisation of the algorithm.

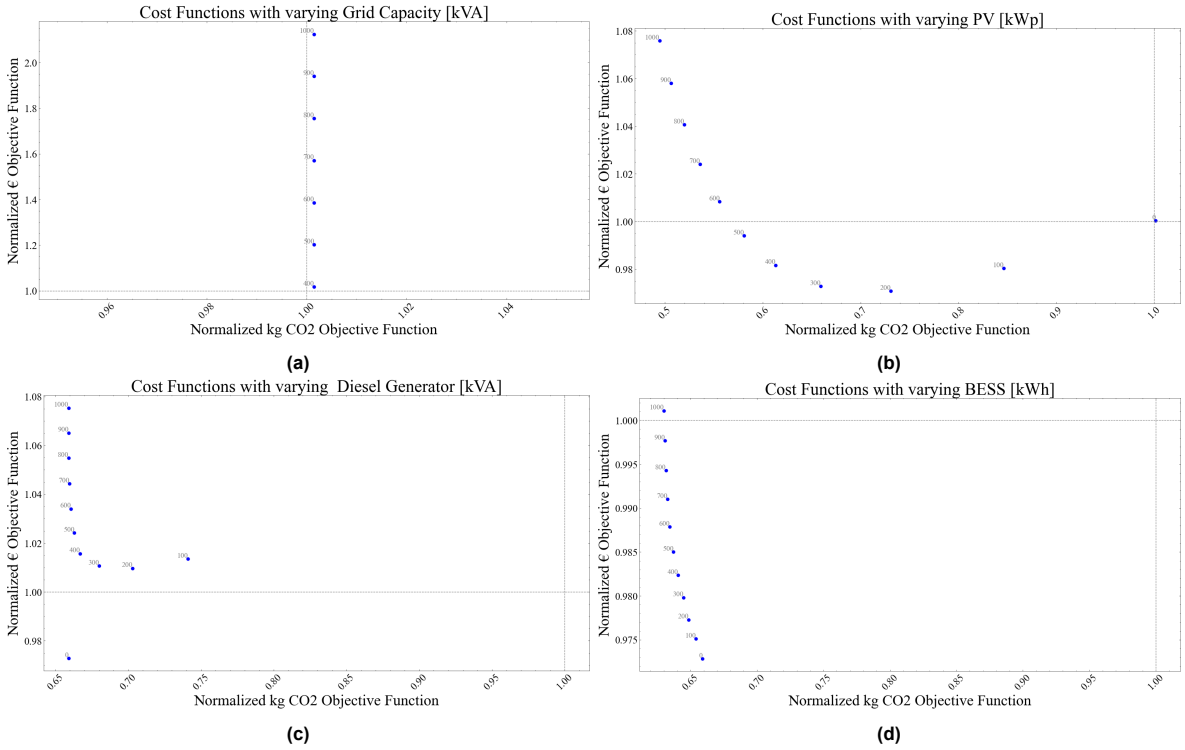

Figure 3.13: "Pseudo" Pareto front created for scenario 2: a 12 hour rolling average and a dynamic boundary of 100%

NSGA-II

The overall workflow of the NSGA-II algorithm can be seen in Figure 3.14. And comprises of the following steps:

1. The population is initialised, for this thesis the initialisation is based on [12].
2. The population is ranked with nondominated sorting and crowding distance with an elitist approach. The parent and offspring are regarded as unique individuals and are sorted together, this can result in a new generation consisting of only parents, only offspring, or anything in between.
3. M top-ranking individuals are chosen to be the parents of the new generation.
4. Mutation and Crossover occurs inside the Genetic Operator to create N offspring.
5. The new generation of size $M+N$ is ranked with nondominated sorting and crowding distance.
6. Steps 2 - 5 are repeated until a termination criterion is reached, a maximum number of generations.

The sorting step 2, which includes nondominated sorting and crowding distance, is illustrated in Figure 3.15

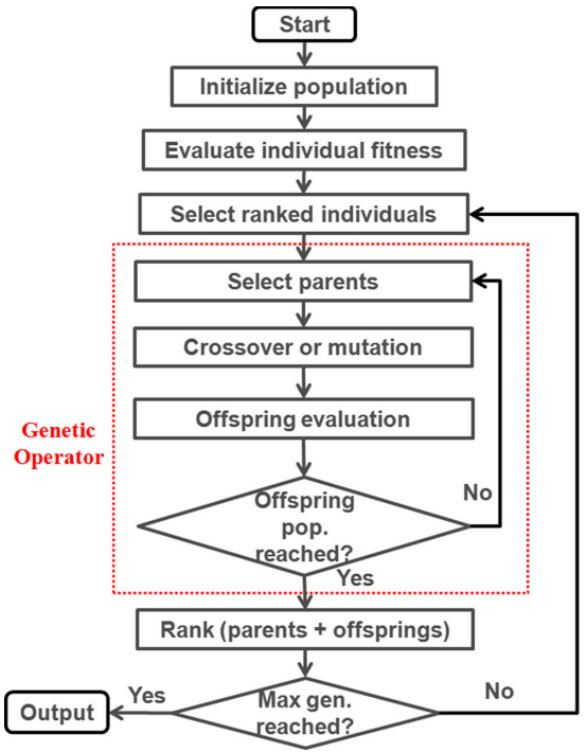

Figure 3.14: NSGA-II algorithm flowchart [125]

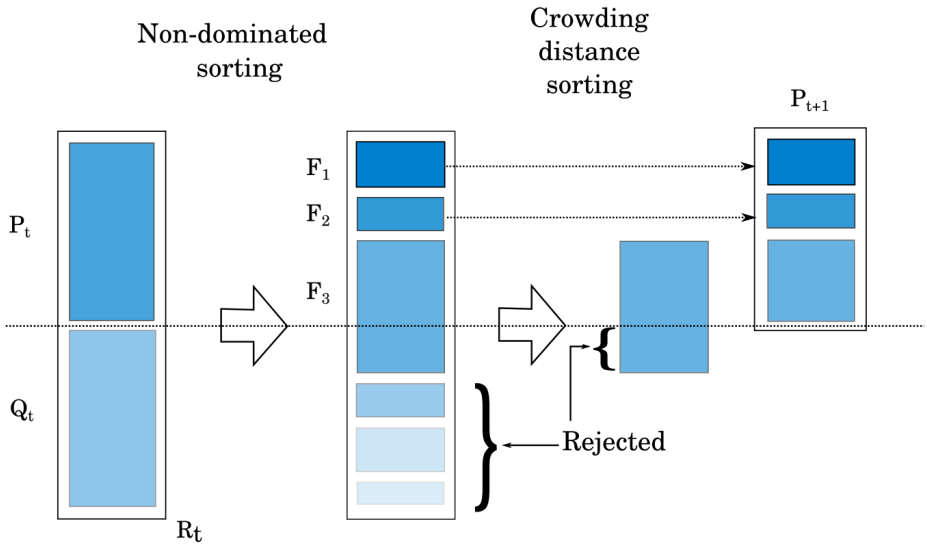

Figure 3.15: Illustration of selection in NSGA-II with nondomination and crowding distance sorting [126]

Nondominated Sorting

Nondominated sorting is a method of ranking individuals and creating nondominated fronts by examining how many solutions dominate another solution. A solution dominates another if it is better performing in at least one objective function while not being worse than another. A nondominated individual cannot be improved in one objective function without sacrificing performance in another objective. In this sorting approach, each solution is assigned two entities: domination count (the number of solutions that dominate this solution) and a set of solutions that it dominates. The solutions in the first nondominated front have a domination count of zero. Then, for each solution, the domination count of each member in its set is reduced by one. If the domination count of a member becomes zero, it is placed in a separate list, which represents a new nondominated front. This process is repeated until all fronts are identified. This process becomes apparent if it is examined visually, an example of nondomination can be seen in Figure 3.16a.

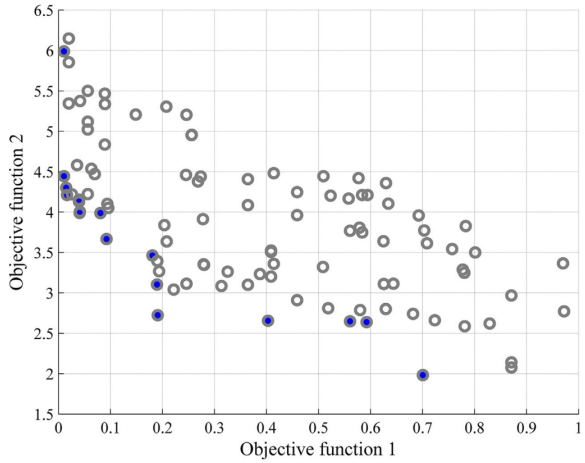

(a) Illustration of dominated and nondominated (blue) individuals [36]

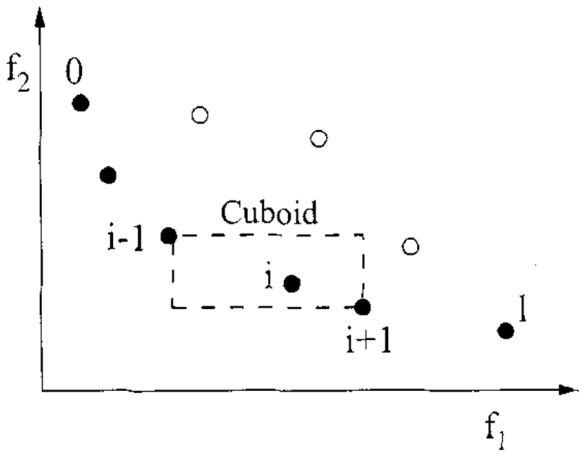

(b) Illustration of crowding distance sorting [127]

Crowding Distance

When the nondominated fronts are identified, the combination of the best nondominated fronts may contain more individuals than the parent population. When this occurs crowding distance sorting is utilised to reduce the total solution set to M individuals. Crowding distance uses the Manhattan distance

normalised to the difference between the worst and best-performing solution per objective function. This can better be illustrated with the crowding distance loop expanded in Equation 3.20, the Crowding distance assignment for all solutions in a nondominated set $\mathcal{I}$ [127]. The crowding distance of all solutions is first set to zero. Then for each objective (Cost and CO2), the solutions are sorted based on their value for that objective function. The crowding distances of the worst and best solution of the objective function are set to infinity to ensure that they are always considered for the next population. For every other solution between the worst and best-performing solution, the distances are increased by the difference in distance between the solution behind and in front of it, normalised to the difference between the value of the worst and best solution. $\mathcal{I}[i].m$ refers to the mth objective function value of the ith individual in the set $\mathcal{I}$ and f_m^{max} and f_m^{min} are the maximum and minimum values of the mth objective function [127].

$$
\begin{aligned}
&l = |\mathcal{I}| && \text{number of solutions in } \mathcal{I}\\
&\text{for each } i, \text{ set } \mathcal{I}[i]_{\mathrm{D}istance} = 0 && \text{initialise distance}\\
&\text{for each objective } m\\
&\quad \mathcal{I} = \text{sort}(\mathcal{I}, m) && \text{sort using each objective value}\\
&\quad \mathcal{I}[1]_{\mathrm{D}istance} = \mathcal{I}[l]_{\mathrm{D}istance} = \text{inf} && \text{so that boundary points are always selected}\\
&\quad \text{for } i = 2 \text{ to } (l-1) && \text{for all other points}\\
&\quad\quad \mathcal{I}[i]_{\mathrm{D}istance} = \mathcal{I}[i]_{\mathrm{D}istance} + (\mathcal{I}[i+1].m - \mathcal{I}[i-1].m)/(f_m^{max} - f_m^{min})
\end{aligned}
\tag{3.20}
$$

Genetic Operator

Based on [127] [18] the NSGA-II algorithm will incorporate Simulated Binary Crossover and polynomial mutation [128] for the genetic operator. An implementation of this combination can also be observed in [129].

Simulated Binary Crossover (SBX) creates two children ($x_i^{(1,t+1)}$ and $x_i^{(2,t+1)}$) from two parent solutions ($x_i^{(1,t)}$ and $x_i^{(2,t)}$) with the help of a random number $u_i \in [0,1]$, a crossover index η_c, Equation 3.21, and Equation 3.22 [130].

$$
\beta_{qi} = \begin{cases} (2u_i)^{\frac{1}{\eta_c+1}}, & u_i \leq 0.5 \\ \left(\frac{1}{2(1-u_i)}\right)^{\frac{1}{\eta_c+1}}, & \text{otherwise} \end{cases}
\tag{3.21}
$$

$$
\begin{aligned}
x_i^{(1,t+1)} &= 0.5\left[(1+\beta_{qi})\, x_i^{(1,t)} + (1-\beta_{qi})\, x_i^{(2,t)}\right] \\
x_i^{(2,t+1)} &= 0.5\left[(1-\beta_{qi})\, x_i^{(1,t)} + (1+\beta_{qi})\, x_i^{(2,t)}\right].
\end{aligned}
\tag{3.22}
$$

Polynomial Mutation is designed for variables with a predefined minimum x_i^U and maximum value x_i^L (which is the case in this thesis, as will be illustrated later). The newly created offspring with SBX $x_i^{(1,t+1)}$ is mutated to $y_i^{(1,t+1)}$. This is done through Equation 3.23, Equation 3.24, ur_i (a pseudo random number) $0 \leq r_i < 1$, and a parameter η_m that determines the mutation range [131][130].

$$
y_i^{(1,t+1)} = x_i^{(1,t+1)} + \left(x_i^U - x_i^L\right)\bar{\delta}_i
\tag{3.23}
$$

$$
\bar{\delta}_i = \begin{cases} (2r_i)^{\frac{1}{1+\eta_m}} - 1, & r_i < 0.5 \\ (1-(2(1-r_i))^{\frac{1}{1+\eta_m}}, & r_i \geq 0.5 \end{cases}
\tag{3.24}
$$

Initialisation

The initialisation of the algorithm is based on parameters found in [12] [132] [18]. The parameters chosen for the optimisation are summarised in Table 3.10. The population is set by first calculating the maximum number of solutions and taking 0.003% of this value. For the sizing in this thesis, four variables (Grid, PV, Diesel, BESS) are considered to have a minimum and maximum value.

For the grid connection, based on [94], the minimum capacity is chosen to be 50 kVA and the maximum at 2000 kVA. The sizing of the grid is then chosen to be done in steps of 25, giving a total of 78 different grid capacity possibilities.

Table 3.10: Parameters for the NSGA-II algorithm

Parameter	Value
Population	395
Number of offspring	99
Crossover rate	0.9
Mutation rate	0.01

For the PV system, an attempt to limit this based on real-world data [133] was made. But the difference between the maximum power of the load evaluated in this thesis 391 kVA and the real-world PV system 26200 kWp is too large. This would result in a PV system that is always generating towards the grid, instead of mainly being used for the load. We therefore limit the size of the PV system to 10 times the maximum power of the load 3910 kVA. With sizing steps of 100, this results in 39 different PV installation possibilities. For the diesel generator, the maximum value was set to the largest generator found in the dataset [134], 3600 kVA. With sizing steps of 100, this results in 36 different diesel generator possibilities. Finally, for the BESS, the sizing was limited again by real-world counterparts found in [135] to 48000 kWh. This is however a search area that would make the optimisation take days, it is halved to 24000 (Enough to supply the maximum load of "LG 1" for 2.5 days). With sizing steps of 200, 96 different BESS possibilities can be examined. This gives a total of 10513152 possibilities. Multiplied by 0.003% gives a starting population of 395. With the same population to offspring ratio in [132], the number of offspring is calculated to be 99. The crossover and mutation rates are set to 0.9 and 0.01 as presented in [12].

With these parameters, the sizing can be mathematically expressed as Equation 3.25

$$
\begin{aligned}
\min F(m)(x_{\text{Grid}}, x_{\text{PV}}, x_{\text{Diesel}}, x_{\text{BESS}}) \quad & m = Cost, CO2 \\
\text{s.t.} \quad & 50 \leq x_{\text{Grid}} \leq 2000 \\
& 0 \leq x_{\text{PV}} \leq 3910 \\
& 0 \leq x_{\text{Diesel}} \leq 3600 \\
& 0 \leq x_{\text{BESS}} \leq 24000 \\
& x_{\text{Grid}} \in \mathbb{N} \mid x_{\text{Grid}} = 25g,\ g \in \mathbb{N} \\
& x_{\text{PV}} \in \mathbb{N} \mid x_{\text{PV}} = 100i,\ i \in \mathbb{N} \\
& x_{\text{Diesel}} \in \mathbb{N} \mid x_{\text{Diesel}} = 100j,\ j \in \mathbb{N} \\
& x_{\text{BESS}} \in \mathbb{N} \mid x_{\text{BESS}} = 200k,\ k \in \mathbb{N}
\end{aligned}
\tag{3.25}
$$

This minimisation equation takes the previously mentioned constraints and displays them in a universal language. The objective functions are Cost and CO2, which are calculated by running a year-long power profile with a combination (within certain limits) of variables: Grid, PV, Diesel, and BESS. This minimisation is done until 15 generations of solutions are reached.

3.3. Analysing

In this section, the methodology for the voltage analysis on the CIGRE Medium Voltage (MV) Distribution system before and after the optimal sizing of the Hybrid Power System (HPS) is presented. The main objective is to evaluate the impact of the optimally sized HPS on the voltage behaviour of the network. For industrial applications, the IEEE recommends performing a balanced steady-state load flow analysis [136]. A tool that can achieve such an analysis on the CIGRE MV distribution system is PandaPower [86].

PandaPower presents a model for the CIGRE MV Distribution system for which load profiles can be entered into each load element so that a load flow analysis can be performed over the course of a whole year. The load profiles of German industries [84] will be distributed across the load elements of the CIGRE MV Distribution network. This is done to assess the capabilities of the elements in the CIGRE MV Distribution network (Lines, Transformer, etc.) and ensure they are at least capable of enduring the load profiles of the German Industry.

Because there are more load profiles than loads/busses, a randomizer is used to assign certain load profiles to the load elements. The resulting allocation can be seen in Table 3.11[10]. With this allocation of load profiles to load elements, it becomes clear which busses will be interesting to examine: the busses surrounding bus 11 which has been allocated load profile $LG1$ (the optimally sized profile).

The PandaPower equivalent of the CIGRE MV distribution network can be seen in Figure 3.19b. The interconnection between elements is the same, except that PandaPower displays switch ”S2” at the bottom of the topology.

The last step before a load flow can be performed is to calculate the reactive and active power profiles from the apparent power load profiles. This is necessary to ensure the load flow analysis calculates bus voltages correctly. The active and reactive power profiles will be calculated using a power factor of 0.85 [120] [121]. The active power P is calculated using Equation 3.26 and the reactive power Q is calculated through Equation 3.27 using the power factor pf and the apparent power S. From the apparent power profiles provided in [84], two profiles for the active and reactive power are created.

$$|P| = S * pf \tag{3.26}$$

$$|Q| = \sqrt{(S^2 - P^2)} \tag{3.27}$$

The CIGRE MV distribution network contains 14 loads that are connected through a series of busses, lines, and switches. In the ordinary scenario, all the switches are in the open position. This essentially creates two separated feeders for the grid connection, which might cause the line loading of the left feeder (in Figure 3.19: Feeder 1) to jump to values outside its limits. The first load flow that is thus performed is a load flow with all the switches open, to make sure that the scenario before introducing optimal HPS sizing does not already exhibit critical behaviour. This examination can be seen in Figure 3.17. Line ”line1_2” is overloaded ($> 100\%$) with switch ”S1” in the open position during some time intervals. Even though some cables could potentially handle short duration of overloading, this is not a scenario that is ideal to use as a comparison basis. Thus, the base scenario, from which the comparison of load flow analysis for the CIGRE MV Distribution system without and with optimally sized HPS will be made, will have the switch ”S1” closed. This relieves the overloading of the lines as can be seen in Figure 3.18.

An added layer of complexity in the analysis arises from the potential injection of power from the optimally sized HPS into adjacent nodes(feed-in). This intriguing scenario comes into play when the sizing of components, encompassing the Grid, PV, Diesel Generator, and BESS leads to the PV generation surpassing the actual load profile in a given time step. This overabundance of PV generation triggers a situation where the surplus power can potentially be injected back into the grid. The way the EMS is defined in subsection 3.1.6, this is technically allowed.

While this surplus PV power injection doesn’t translate into direct monetary compensation for the Cost objective function (due to the feed-in tariffs set to zero [97]), it might still hold significant merit. The deliberation around this revolves around the prospect that a larger PV system could indeed be the optimal solution, even when the excess power injection doesn’t yield direct financial returns. This perspective underscores the intricate considerations and nuanced decision-making inherent in optimising HPS components.

[10] This allocation was done at the same time as the random allocation of the loads to busses that are mentioned in section 3.3

To delve deeper into this scenario, an additional layer of analysis is added. This involves imposing a limitation on the grid-usage profile, effectively curbing any surplus power injection from the PV system into the grid. In essence, this secondary analysis aims to simulate a scenario where the industrial load is not permitted to inject power back into the grid.

This extra analysis also alleviates one of the negative effects of distributed generation, volatility. As mentioned earlier, renewable generation is very intermittent and could cause unwanted voltage deviations. A feed-in restriction is thus a simple way to overcome this negative effect, while still witnessing the effects of optimally sized components for the industrial profile $LG1$.

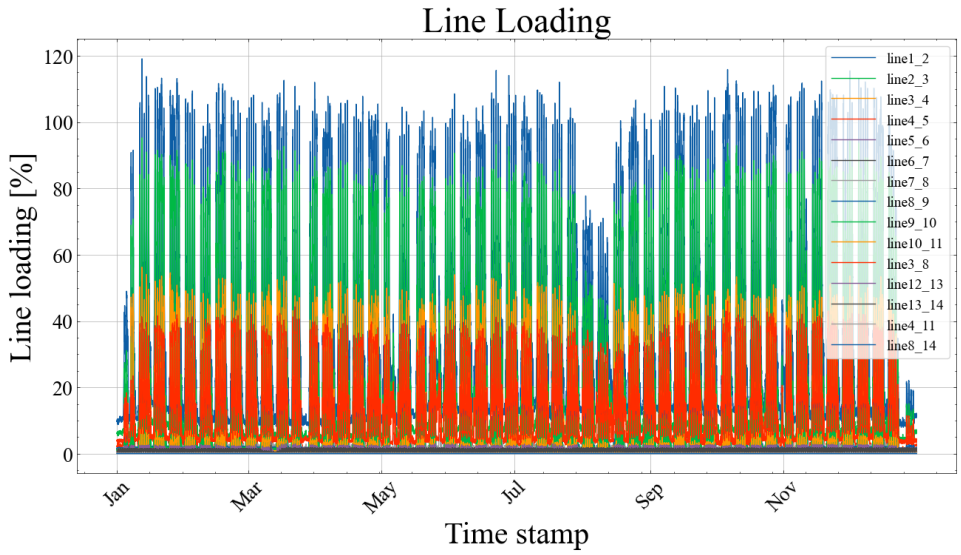

Figure 3.17: Line loading of CIGRE MV network with all switches in open position

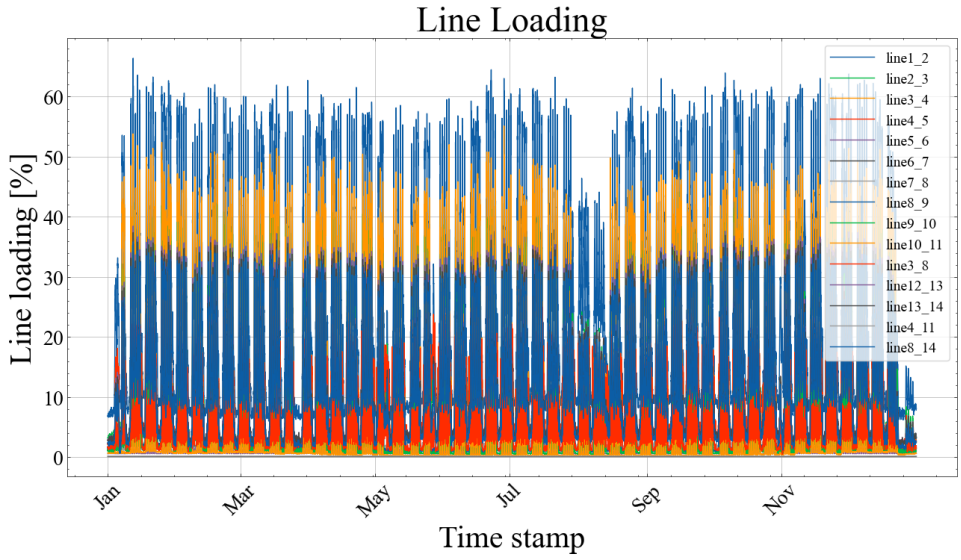

Figure 3.18: Line loading of CIGRE MV network with all switches in open position except S1

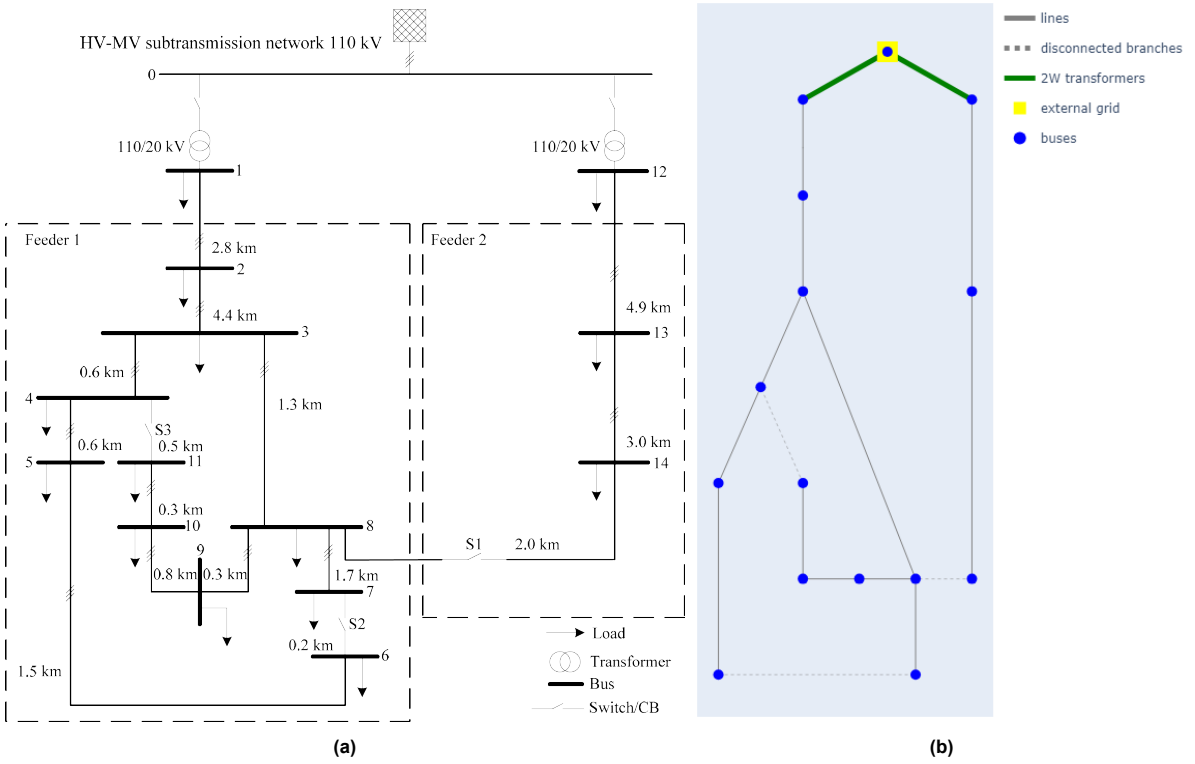

Figure 3.19: The CIGRE MV Distribution network and its counterpart in PandaPower

Table 3.11: Random load profile assignment to busses in CIGRE MV distribution network [119]

CIGRE MV Bus #	**1**	**2**	**3**	**4**	**5**	**6**	**7**	**8**	**9**	**10**	**11**	**12**	**13**	**14**
Load Profile #	3	20	17	7	8	5	14	9	12	18	1	2	16	10

4

Results

In this chapter, the results obtained from the multi-objective optimisation process with NSGA-II are presented. They are presented in the form of four Pareto fronts, one for each EMS scenario. The Pareto fronts represent the trade-off between the two objective functions: Cost and CO2 emissions. The optimal solution within the four Pareto fronts will be taken as the solution with the smallest Euclidean distance from the origin. With this optimal solution, the analysis mentioned in section 3.3 will be performed on the CIGRE MV Distribution Network. The analysis will showcase the workings of the CIGRE network in a base case scenario without an optimally sized Hybrid Power System (HPS). The analysis will then elaborate on the differences in voltage behaviour when the optimally sized HPS is implemented.

4.1. Sizing

Before the optimisation was conducted with the Genetic Algorithm NSGA-II, a ”Pseudo” Pareto front was created with sequential optimisation. An optimisation that consisted of starting from a Power System with a Grid connection that is sized to an optimal value (the maximum power requested by the load in a year), Sizing a PV connection to supplement this grid connection, Sizing a BESS, and finally sizing a Diesel Generator. The sequential optimisation resulted in similar results for all four EMS scenarios, which can be viewed in Appendix D. The results all favoured a grid connection equal to the maximum value of the load profile[1], a PV system of 300 kVA, and no diesel generator or BESS system. This is not a good way to approach an optimisation, because the components are all optimised separately and the amount of different combinations is very limited. This sequential optimisation is helpful in gaining an expectation of where an optimisation with NSGA-II will lead.

For the actual optimisation with the NSGA-II algorithm and its initialisation presented in subsection 3.2.3 - Initialisation the Pareto fronts (or rather the nondominated front in the last generation of solutions) for each scenario can be seen in Figure 4.1. The four different EMS scenarios (described in Table 3.8) result in different Pareto fronts with the two dynamic fronts (scenario 2 and 4) showing more environmentally favourable solutions, shown by there lower CO2 objective functions. This can be explained by the dynamic bound that is utilised in EMS scenarios 2 and 4. The dynamic bound restricts the Grid usage to a smaller allowable window, which lowers the Grid Scope 2 CO2 emissions.

A single optimisation of a scenario took anywhere between 24 and 76 hours. This is partly due to the rather long simulation time within Mosaik, here a full year of simulation can sometimes take minutes, depending on how many components the EMS needs to schedule. These few minutes result in a singular output value of the Cost and CO2 objective functions for the given combination of Grid, PV, Diesel, and BESS. The NSGA-II algorithm will need to perform this workflow for 15 generations of solutions based on 395 parents and 99 offspring, this results in a long simulation time.

[1] Because the grid is sized first in the sequential optimisation, the most economical value is equal to the maximum power value of the load profile. If the grid capacity is lower than the maximum power value, the Energy Not Supplied penalty will severely worsen the Cost and CO2 objective functions. On the other hand, a grid capacity larger than the maximum power value is unnecessary. It will only increase the Cost objective function.

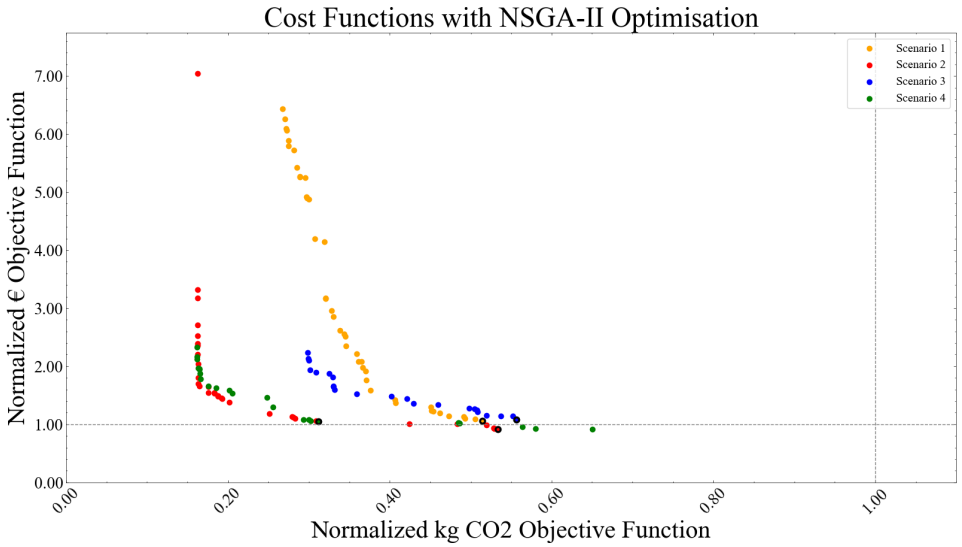

Figure 4.1: Pareto fronts created for scenarios 1, 2, 3, and 4 described in Table 3.8

Table 4.1: Optimal HPS configurations for the four EMS scenarios described in Table 3.8

Scenario	**1**	**2**	**3**	**4**
€ Objective Function	1.055	**0.913**	1.080	1.045
CO2 Objective Function	0.514	**0.533**	0.556	0.312
Euclidean distance to (0,0)	1.174	**1.058**	1.214	1.090
Sized Grid Capacity [kVA]	375	**325**	425	300
Sized PV Capacity [kWp]	800	**500**	600	1400
Sized Diesel Generator [kVA]	100	**100**	0	100
Sized BESS [kWh]	1000	**1200**	200	2600

From the NSGA-II optimisation for each scenario, a last nondominated front is extracted (the solutions). These will be evaluated as the optimal Pareto fronts of solutions and for each scenario, these Pareto fronts can be seen in Figure 4.1. The final singular solutions chosen from each scenario to be analysed, are the solutions with the shortest Euclidean distance to the origin and are marked within the figure.

Besides the objective function values of the optimal solutions, the combination of component sizes and the new grid-usage profile is important for the voltage analysis that needs to be performed. For each of the optimal solutions presented in Figure 4.1, the corresponding HPS configurations can be found in Table 4.1. From these four optimal configurations, the configuration of scenario 2 is taken because of its shortest Euclidean distance to the origin in the Pareto plot with CO2 and Cost in its axes. This is the configuration that will be analysed with PandaPower. The other solutions within the Pareto fronts and their corresponding combination of components can be examined in Appendix E.

The solution chosen for the evaluation with PandaPower is different from the estimate made from the ”Pseudo” Pareto fronts. The estimate consisted of a grid connection equal to 391 kWh and a PV capacity of 300 kWp with no Diesel or BESS components. The optimal HPS configuration presented by the NSGA-II algorithm consists of a similar grid and PV capacities, but an additional 100 kVA Diesel Generator and a 1200 kWh BESS, equivalent to 12 Tesla Model X cars [137].

4.2. Analysis

With the optimal PV-DSL-BAT HPS configuration (Table 4.1) provided by the NSGA-II optimisation, the analysis of this HPS on the CIGRE MV Distribution Network can be performed. Firstly the new resulting power profile for the optimal configuration can be seen in Figure 4.2. Comparing the figure to Figure 3.12, it becomes clear that the combination of components lowered the grid-usage profile, sometimes even below zero. These feed-in moments will be removed for the final analysis as mentioned in

section 3.3. This is to ensure the voltage behaviour within the CIGRE MV Distribution Network does not worsen when the HPS is implemented.

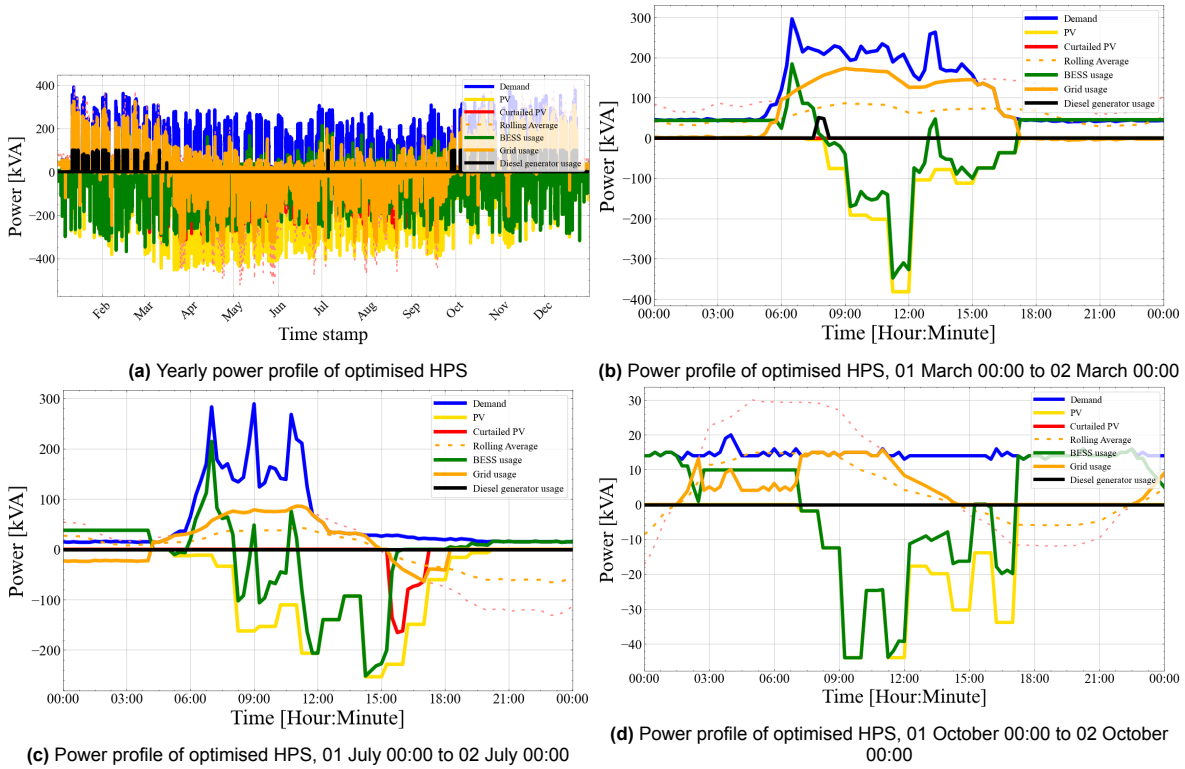

(a) Yearly power profile of optimised HPS

(b) Power profile of optimised HPS, 01 March 00:00 to 02 March 00:00

(c) Power profile of optimised HPS, 01 July 00:00 to 02 July 00:00

(d) Power profile of optimised HPS, 01 October 00:00 to 02 October 00:00

Figure 4.2

With the new power profile (namely the Grid usage), a load flow analysis is performed on the CIGRE MV Distribution Network. The voltages of the buses are plotted in Figure 4.3, without and with optimal HPS components added to bus 11 or the ”LG 1” profile.

From an initial examination of the two voltage graphs (Figure 4.3a and Figure 4.3b) before and after sizing, there appears to be little difference except for a few peaks above $1.03p.u.$ that were not present before and are thus viewed as a worsening of the voltage behaviour in the CIGRE MV Distribution network. These peaks are introduced because of PV power being sent into the network. These peaks disappear when PV feed-in is not allowed and PV power is thus curtailed, this can be seen in Figure 4.3c. In the case of this thesis, these observations can be viewed as positive, as a PV-DSL-BAT Hybrid Power System achieves similar performance to the base case scenario while improving the Cost and CO2 emissions in one year.

The new optimal power profiles allocated by the EMS to the different components also show an interesting behaviour in the BESS. The BESS is (dis)charging at very low power ratings, this indicates the BESS is being used to alleviate minor deviations within the rolling average EMS. The low power ratings are also in part due to the BESS energy-to-power ratio of 2.28. Increasing this ratio would result in a lower nominal power of the BESS, and thus result in higher power ratings being issued by the EMS to the BESS. A negative effect of utilising low power ratios in BESSs is the (in)efficiency of inverters at low power ratings [29]. This results in the BESS charge level being depleted more during discharging or increased less during charging. If Figure 4.4a is examined, it shows that the SOC of the BESS is not near the lower bound during most of the year, indicating possible leeway in terms of handling lower efficiencies provided by the inverter.

No feed-in

As shown in Figure 4.3c, the thorough analysis of the voltage behaviour in the CIGRE MV Distribution Network will be done with a restriction: no feed-in is allowed from the HPS (load 11) into the distribution network. This restriction can be implemented because the power that the EMS dispatches to the grid (feed-in) originates from PV power, and can thus be curtailed. The curtailment of the PV results

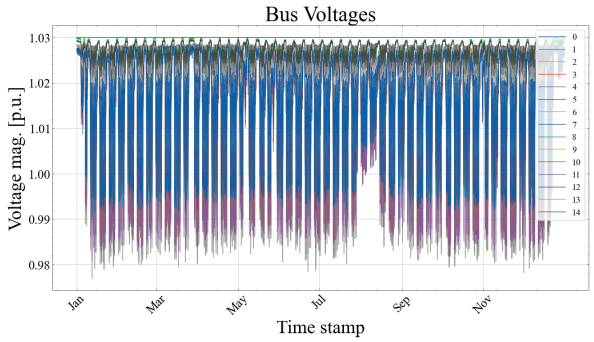

(a) Bus Voltages of CIGRE MV Distribution Network without HPS components

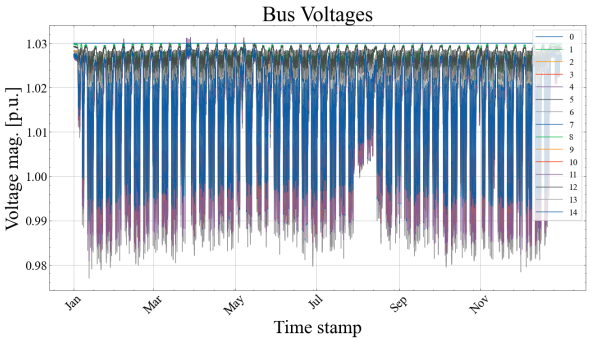

(b) Bus Voltages of CIGRE MV Distribution Network with optimal HPS components installed at bus 11

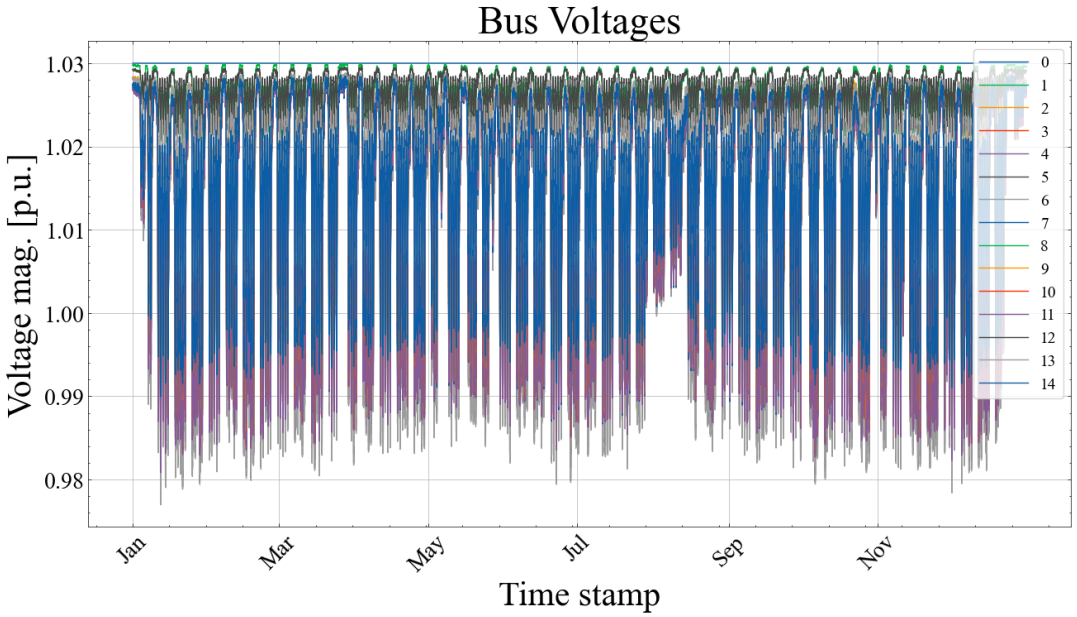

(c) Bus Voltages of CIGRE MV Distribution Network with optimal HPS components installed at bus 11 and no feed-in to the grid allowed

Figure 4.3

in 135949 kWh not being fed into the grid. By comparison, the PV system (with feed-in disabled) contributes 287409 kWh to the HPS. This curtailment has an effect on the LCOE of the PV system, but because the Cost objective function is calculated with the netto PV production and then afterwards multiplied by the netto PV production, it does not change the Cost of the PV system in one year[2].

In order to more thoroughly assess the changes in voltage behaviour when feed-in is disallowed (this is chosen because feed-in introduces voltage behaviour that was not present before sizing), the voltages of bus 10, 9, and 8 (and the lines connected to them) are examined separately alongside bus 11 and can be seen in Figure 4.6. The time frames of March 1^{st}, July 1^{st}, and October 1^{st} were chosen to be spread out evenly across the year. Figures for the active power, reactive power, line loading, and bus voltages of busses 10, 9, 8, and 11 can also be found in Appendix F.

In Figure 4.6 a clear sag in voltage can be observed when the voltages are plotted for a day, especially in Figure 4.6b and Figure 4.6c. This voltage sag is due to a large load in the system, namely load 8, which can be seen in Figure 4.7. The effect of introducing the optimally sized components at bus 11 shows a small positive effect in combating this voltage sag. The voltage sag does not get worse when bus 11 has PV-DSL-BAT elements added to it. When Figure 4.8 is examined, the voltage is seen to rise during its lowest point slightly. This can be explained by examining the Equation 4.1 for voltage

[2]This has been confirmed by altering the EMS not to allow feed-in. The LCOE of the PV system with feed-in was 0.13 with a netto PV production of 450 MWh and the LCOE of the PV system without feed-in was 0.19 with a netto PV production of 315 MWh

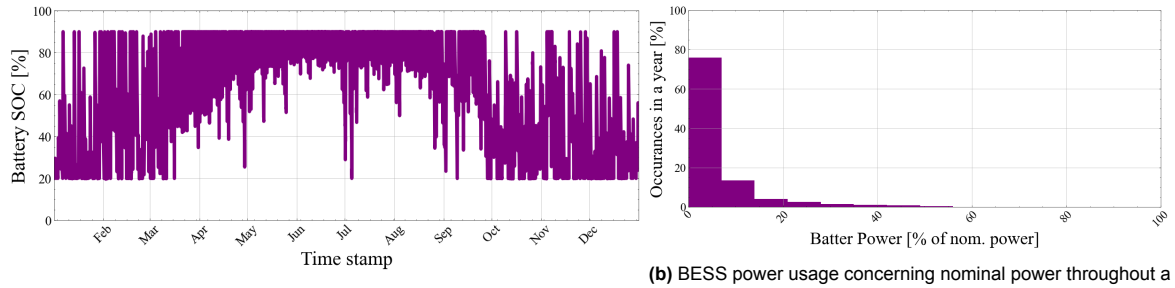

(a) BESS SOC through a full year of simulation

(b) BESS power usage concerning nominal power throughout a full year of simulation

Figure 4.4

drop derived from Figure 4.5.

Within transmission systems, the equation can be simplified to showcase the voltage drop being largely dependent on the reactive power [138]. However, in this thesis, the CIGRE MV Distribution system is considered and this simplification does not hold. With an R/X ratio of 2.3 [139] (which does signify $R << X$), the Equation 4.1 cannot be simplified for the CIGRE MV Distribution system. The effects of both active and reactive power must be considered when assessing the contribution of load 8 to the sag in voltage seen in Figure 4.6.

$$\Delta u = \frac{RP_2 + XQ_2}{V_2} \tag{4.1}$$

The new grid-usage profile, consequent to the optimally sized HPS components and the EMS, at bus 11 results in a decreased voltage sag. This is because the HPS demands both less reactive and less active power from the distribution network. Equation 4.1 explains how this reduced demand of power alleviates, albeit minor, the voltage sag as a result of the significant loading at bus 8. This can be seen in Figure 4.8. Here the voltages of all the busses are plotted before and after introducing the HPS, the absolute differences between are also plotted. These difference all show an upward contribution of the voltage.

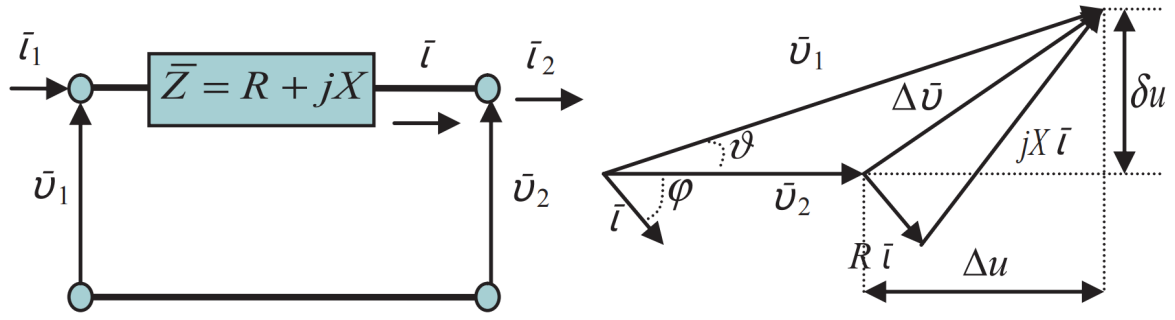

(a) Short line model one-line diagram [138]

(b) Short line model phasor diagram [138]

Figure 4.5

This conclusion is rather elementary, but it still poses a good result for the current study case. Less grid usage is simply better for the voltage level of the grid. When the EMS with rolling average is utilised in combination with a diverse power portfolio (PV, Diesel, BESS) Cost and CO2 decreases can be achieved without compromising the current situation. The importance of the rolling average EMS is not directly measured, but it can be inferred that an EMS not utilising a rolling average could result in a very choppy grid-usage profile, possibly worsening the voltage behaviour.

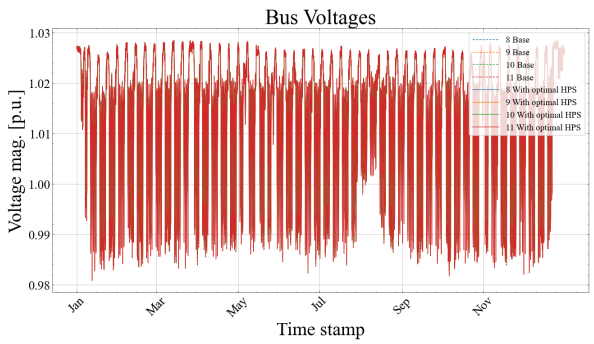

(a) Bus 8, 9, 10, 11 voltages before and after sizing

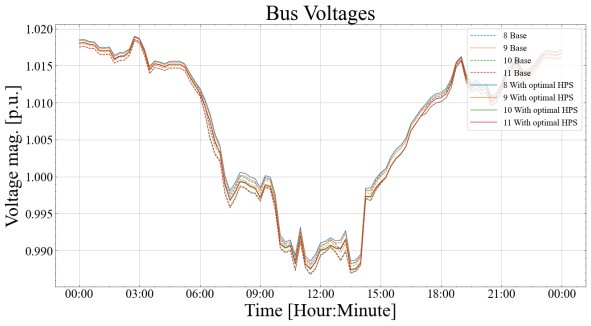

(b) Bus 8, 9, 10, 11 voltages before and after sizing, 01 March 00:00 to 02 March 00:00

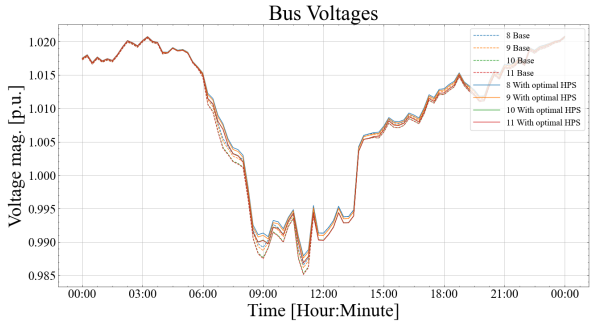

(c) Bus 8, 9, 10, 11 voltages before and after sizing, 01 July 00:00 to 02 July 00:00

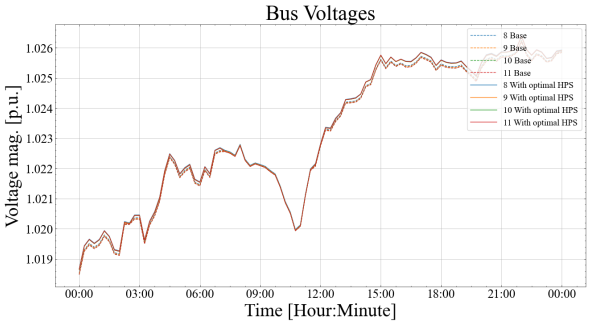

(d) Bus 8, 9, 10, 11 voltages before and after sizing, 01 October 00:00 to 02 October 00:00

Figure 4.6

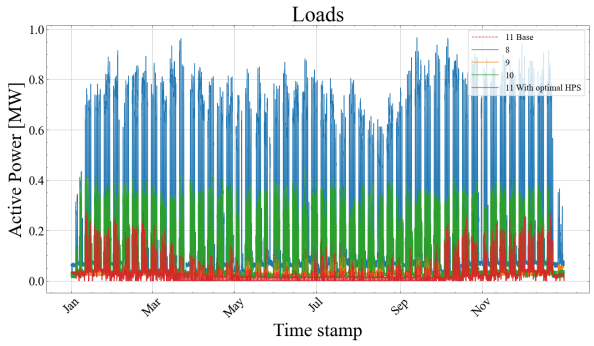

(a) Loads for bus 8, 9, 10, and 11 (with and without sizing)

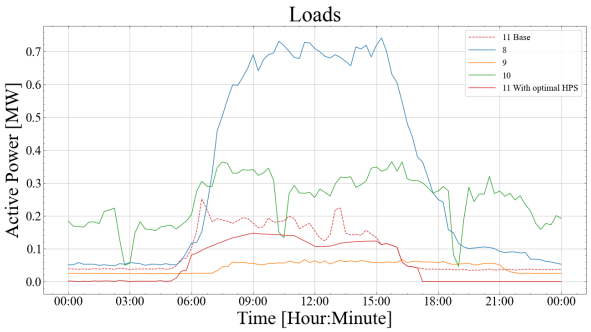

(b) Loads for bus 8, 9, 10, and 11 (with and without sizing), 01 March 00:00 to 02 March 00:00

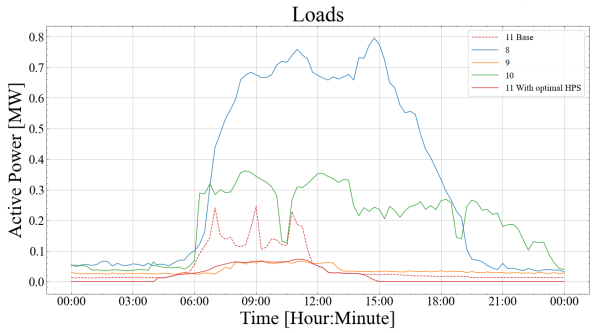

(c) Loads for bus 8, 9, 10, and 11 (with and without sizing), 01 July 00:00 to 02 July 00:00

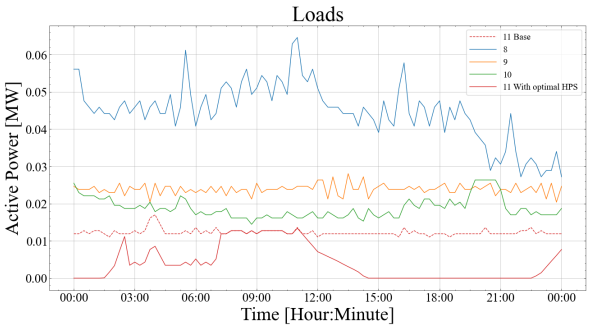

(d) Loads for bus 8, 9, 10, and 11 (with and without sizing), 01 October 00:00 to 02 October 00:00

Figure 4.7

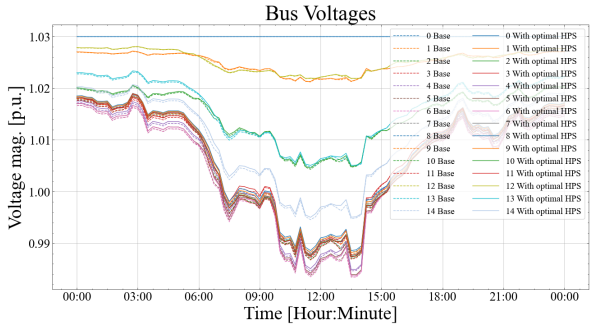

(a) Bus voltages before and after sizing, 01 March 00:00 to 02 March 00:00

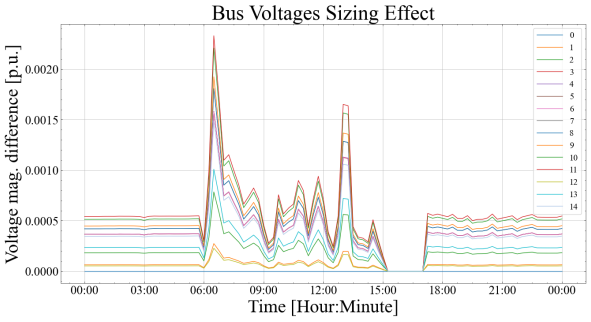

(b) Bus voltage deviation after sizing, 01 March 00:00 to 02 March 00:00

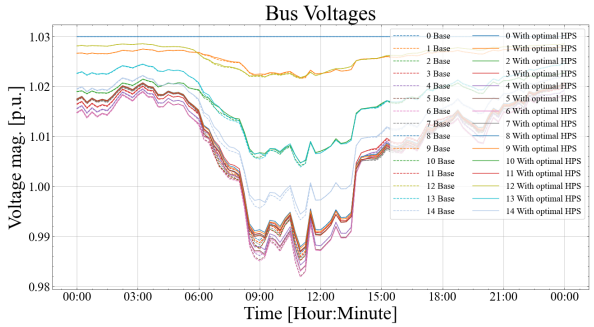

(c) Bus voltages before and after sizing, 01 July 00:00 to 02 July 00:00

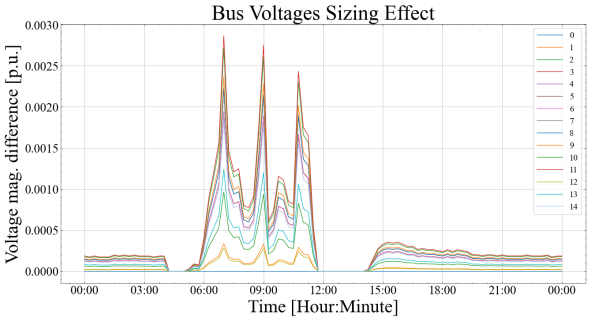

(d) Bus voltage deviation after sizing, 01 July 00:00 to 02 July 00:00

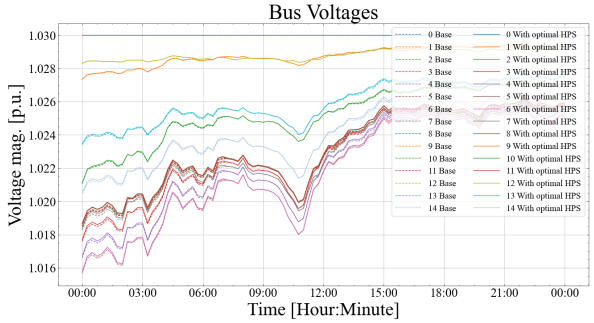

(e) Bus voltages before and after sizing, 01 October 00:00 to 02 October 00:00

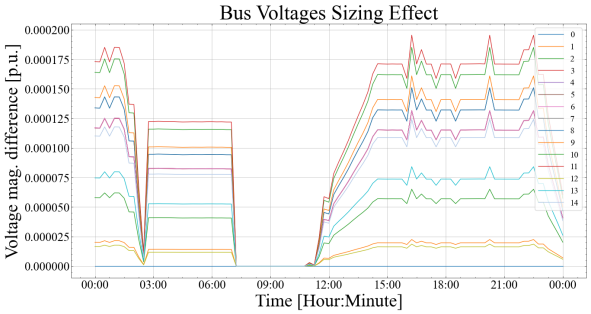

(f) Bus voltage deviation after sizing, 01 October 00:00 to 02 October 00:00

Figure 4.8

5

Conclusion and Discussion

This thesis addressed the topic of ”Addressing voltage sag contribution of an optimally sized Industrial Hybrid Power System - Using a multi-objective sizing framework considering cost and CO2 emission.”

The objective of this research was to optimally size a Hybrid Power System (PV-DSL-BAT) for an industrial load, minimising cost and CO2 emissions and assess the effects of this sizing on the voltage sag within an appropriate industrial system (MV distribution system). After this sizing was completed, the voltage within the CIGRE MV Distribution system was analysed through a balanced load flow study. The load flow was performed on the CIGRE MV Distribution system with loads sourced from a dataset of industrial loads and once more on the same system, but with one of the load profiles being altered as a result of the sizing (the grid-usage profile changes when PV, Diesel, and BESS power sources are added). The resulting analysis briefly showed the negative (albeit small) effect of grid feed-in from an industrial load that was not there before. Further analysis showed the sizing of load ”LG 1” (which was randomly selected from the available profiles) did not have a negative effect on the voltage sag introduced by a large load in the system. It had a little positive effect on the voltage sag, but more importantly, it didn’t appear to have a negative impact.

With the chapters written in this thesis, the corresponding research questions answered along the way were:

1. Which equations and parameters can be utilised to implement models (PV, Diesel, or BESS) for the use in an Energy Management Systems designated to supply an industrial load?
2. What cost and emission savings can be achieved by sizing components to create a Hybrid Power System for an industrial load using a Genetic Algorithm, compared to directly supplying the load from the grid?
3. What effect does the optimal sizing of an individual node have on the voltage stability of an industrial distribution system?

The work presented in this thesis contributed to the research of optimally sizing Hybrid Power Systems for Industrial applications with the proven method of multi-objective optimisation through a genetic algorithm. The combination of Cost and CO2 as objective functions results in a feasible Hybrid Power System (HPS) that is less dependent on the grid connection, resulting in the utilisation of components that improve the cost-effectiveness and released emissions of an industrial site. The key component of this thesis, that allowed the addition of optimally sized components to the HPS without worsening the voltage behaviour of surrounding nodes in a Medium Voltage distribution system, is the Energy Management System (EMS) based on a rolling average principle. This elementary EMS showcased the feasibility of combining PV, BESS, and Diesel Generator systems with an industrial load, without worsening any existing voltage behaviour. An inference that could benefit the decision-making for implementing similar Hybrid Power Systems that could lower the carbon footprint of the Dutch industry.

Which equations and parameters can be utilised to implement models (PV, Diesel, or BESS) for the use in an Energy Management Systems designated to supply an industrial load?

The first research question was answered in the validation sections of the models in chapter 3. The validation sections listed the error margins of the models, giving a basis from which the significance of

the results can be assessed.

The grid model did not have an error margin in terms of power output, as it was modelled as purely an upper limit. The error margins for the Cost and CO2 functions are also not addressed as all the parameters are based on available sources.

The PV model, or rather the dataset that is scaled beforehand, has an acceptable error margin as mentioned in subsection 3.1.3. The deviation in the order of watts for the Netherlands gives reassurance for the data that is provided for larger installations (in the 100s of kilowatts)

The diesel generator model also exhibits acceptable levels of error for the application in this thesis. These error levels are further decreased when lower values of diesel generators are considered (which is the case for the optimal size determined by the NSGA-II algorithm).

The BESS model has an error limit of 0.01% when the power profile (mentioned in [109]) is used. Unfortunately, this error margin is only for this specific power profile and the last SOC measurement. It does not consider the error across the whole test profile, and no other test profiles are used for validation. However, because the calculated values of η_{charge} and $\eta_{\text{discharge}}$ are similar to values found in the literature, the BESS model can be used with the confidence introduced by these literature values.

What cost and emission savings can be achieved by sizing components to create a Hybrid Power System for an industrial load using a Genetic Algorithm, compared to directly supplying the load from the grid?

The research objective was to optimally size a Hybrid Power System (HPS) for an industrial load, composed of PV, Diesel Generator, and Battery Energy Storage System (BESS), to minimise cost and CO2 emissions while adhering to grid capacity limitations.

Through a literature review, insights into possible sizing algorithms for use in industrial loads were gained. The most promising solution for a multi-objective optimisation was determined to be the Genetic Algorithm, particularly the Nondominated Sorting Genetic Algorithm II (NSGA-II). The addition of nondominated sorting, elitism, and crowding distance sorting results in an algorithm that is capable of generating Pareto fronts from which an optimal solution can be chosen. The manner of choosing the optimal solution was based on a technique taught in elementary school, the Pythagorean theorem (or otherwise the Euclidean distance).

With the initialisation of the algorithm supported by parameters and formulas found in literature and a fair amount of simulation time, the Pareto fronts for four different EMS scenarios were given. The optimal solution provided significant CO2 savings almost, 47%, while also reducing the Cost by a little less than 9%. Herein lies the additional benefit of multi-objective optimisation. It is apparently easier to lower the emissions, but doing this in a cost-effective way presents challenges.

What effect does the optimal sizing of an individual node have on the voltage stability of an industrial distribution system?

The voltage sag analysis of the optimally sized HPS was conducted to evaluate its impact on power quality and grid stability. The CIGRE MV Distribution network provided a solid basis from which balanced load flow analyses could be performed on a configuration of industrial loads (without and with one of these loads optimally sized). After removing a negative effect of the sizing (feed-in), the voltage behaviour of the system was almost unchanged, with even slight positive effects in voltage sag caused by the largest load in the network.

This analysis provided essential validation of the optimal sizing of a Hybrid Power System controlled by a rolling average EMS. This insight could provide decision-makers with more options to tackle the emissions produced in the Netherlands.

5.1. Discussion and Recommendations

While the research presented in this thesis answers several important research questions and provides valuable insights that could potentially lead to a reduction in emissions in the Netherlands, there are some shortcomings that can be improved on and areas identified for further research.

One of the shortcomings of the research is the limited validation of the BESS model used in the study. Although the validation sections provide error margins for the PV and diesel generator, the validation for the BESS model is not comprehensive enough to assess the accuracy and reliability across different scenarios. Further validation using a wider range of test profiles and real-world data would enhance the credibility of the research findings.

The paper focuses on Cost and CO2 emissions related to the grid usage of an industrial site, neglecting other important sources of emissions, namely the industrial processes. Identifying and incorporating electrification as a means to reduce CO2 (with a certain cost) could provide even more valuable insights into the possibility of fully electrifying the Dutch industry.

The research does not explicitly address the implementation of the sized components in terms of size. While the economic benefits of optimal sizing are showcased, the practical aspects of implementing the recommended sizes are not discussed. Investigating the feasibility and challenges of implementing the optimal sizes in real-world industrial sites would be a valuable addition to the research to increase the grasp on feasibility.

The random allocation of load profiles to busses in the CIGRE MV Distribution network does mimic the real-world behaviour of a diverse landscape of industrial sites and the scenario that a single site decides to invest in Cost and CO2 saving measures. The effect of sizing the largest load profile in the system could be a better stress test of the distribution system.

To address the aforementioned shortcomings and further enhance the research, the following extra steps could be considered:
The Lio-Ion NMC BESS that was used for the validation of the BESS model in this thesis can be cycled with other load profiles, and probably already has. using a wider range of test data benefits the BESS model's accuracy in terms of charge and discharge parameters. Another bold step that could be taken is to separately model the inverter of the BESS. As the inverter exhibits power efficiency characteristics of its own. This would provide a more accurate implementation of a BESS model.

Electrification could be incorporated in a rather simple way by researching available technologies and noting their electricity usage and the process they replace. The replaced process (that was first operated by a fossil fuel-based counterpart) has a certain emission. The extra electricity demand of the electrified process can be added to the EMS, and the reduced emission could be subtracted from the CO2 objective function (and the costs added to the Cost objective function)

The practical aspects of implementing the recommended component sizes in real-world industrial applications can be investigated. This could for example be done with the physical size of components. Datasheets can provide a certain footprint for a given power/energy output. These footprints can then be fit into satellite images of existing industrial sites to examine crudely if the sized components would fit.

The NSGA-II algorithm can be run for the largest load in the CIGRE MV Distribution system with the same allocation as Table 3.11. Because of the larger load profile and thus larger consideration for maximum PV, the total number of solutions would increase, and thus also the starting population and number of offspring. This would require a longer simulation time than is currently available for the remaining time in the thesis period.

Extra Research
In addition to the suggested steps that could be readily implemented, further research could be conducted in the following areas:

Optimal Energy Management System. As briefly mentioned in [58], the Energy Management System is a research topic of its own. The Energy Management System can also be controlled by a Genetic Algorithm for example, instead of using a rolling average and a priority list. For each time step, the EMS (based on a genetic algorithm) could calculate the optimal dispatch strategy. Other implementations of EMSs could also benefit the sizing of the components, but this would have to be researched and implemented.

The research done in this thesis could also be extended to the optimisation of other power system configurations. Extending the research to optimise Hybrid Power Systems for microgrid applications, where the system operates in isolation or in conjunction with the main grid could provide additional insights into the self-sufficiency provided by the PV-DSL-BAT components. Another power system configuration that could provide additional security and energy efficiency is the interconnection of loads in a Virtual Power Plant. The optimal sizing of one load, with allowable feed-in, could benefit other loads if the dispatch between them is controlled to limit deviation in supply and demand.

By addressing these suggestions and conducting further research in these areas, the knowledge and understanding of optimal Hybrid Power Systems in industrial energy management can be significantly advanced, leading to more sustainable and efficient energy solutions for the industry.

In conclusion, this research contributes to the advancement of Hybrid Power Systems for industrial applications. The multi-objective optimisation approach allows for the identification of cost-effective and environmentally friendly HPS configurations. The voltage sag analysis validates the system's power quality, ensuring its reliable and stable operation. By continually improving HPS models and exploring innovative EMS solutions, the industrial sector can embrace sustainable energy practices, reduce carbon emissions, and foster a more resilient energy future.

References

[1] [Online]. Available: https://www.energieinnederland.nl/cijfers/2021.

[2] C. B. voor de Statistiek, *Welke sectoren stoten broeikasgassen uit?* 2023. [Online]. Available: https://www.cbs.nl/nl-nl/dossier/dossier-broeikasgassen/welke-sectoren-stoten-broeikasgassen-uit-.

[3] C. B. voor de Statistiek, *Energieverbruik*, 2023. [Online]. Available: https://www.cbs.nl/energieverbruik.

[4] S. Rehman, "Hybrid power systems – Sizes, efficiencies, and economics," *Energy Exploration & Exploitation*, vol. 39, no. 1, pp. 3–43, 2021, ISSN: 0144-5987. DOI: 10.1177/0144598720965022. [Online]. Available: http://journals.sagepub.com/doi/10.1177/0144598720965022.

[5] [Online]. Available: https://capaciteitskaart.netbeheernederland.nl/.

[6] S. E. Razavi, E. Rahimi, M. S. Javadi, *et al.*, "Impact of distributed generation on protection and voltage regulation of distribution systems: A review," *Renewable and Sustainable Energy Reviews*, vol. 105, no. May 2018, pp. 157–167, 2019, ISSN: 18790690. DOI: 10.1016/j.rser.2019.01.050.

[7] K. H. Ahmed and A. A. Aboushady, *Distributed generation systems*. 2017, pp. 239–282, ISBN: 9781785611230. DOI: 10.1049/pbpo092e_ch7.

[8] Y. A. Elshrief, D. H. Helmi, A. D. Asham, and B. A. Abozalam, "Merits and Demerits of the Distributed Generations Connected to the Utility Grid," *Menoufia Journal of Electronic Engineering Research*, vol. 28, no. 1, pp. 259–262, 2019, ISSN: 1687-1189. DOI: 10.21608/mjeer.2019.70907. [Online]. Available: http://mjeer.journals.ekb.eg/article_70907.html.

[9] S. Samal, P. K. Hota, and P. K. Barik, "Performance Improvement of a Distributed Generation System Using Unified Power Quality Conditioner," *Technology and Economics of Smart Grids and Sustainable Energy*, vol. 5, no. 1, 2020, ISSN: 21994706. DOI: 10.1007/s40866-020-00095-3.

[10] H. S. Salama and I. Vokony, "Voltage stability indices–A comparison and a review," *Computers and Electrical Engineering*, vol. 98, no. November 2020, 2022, ISSN: 00457906. DOI: 10.1016/j.compeleceng.2022.107743.

[11] U. Akram, M. Khalid, and S. Shafiq, "Optimal sizing of a wind/solar/battery hybrid grid-connected microgrid system," *IET Renewable Power Generation*, vol. 12, no. 1, pp. 72–80, 2018, ISSN: 17521424. DOI: 10.1049/iet-rpg.2017.0010. [Online]. Available: https://onlinelibrary.wiley.com/doi/10.1049/iet-rpg.2017.0010.

[12] J. L. Bernal-Agustín and R. Dufo-López, "Efficient design of hybrid renewable energy systems using evolutionary algorithms," *Energy Conversion and Management*, vol. 50, no. 3, pp. 479–489, 2009, ISSN: 01968904. DOI: 10.1016/j.enconman.2008.11.007.

[13] B. O. Bilal, V. Sambou, P. A. Ndiaye, C. M. F. Kebe, and M. Ndongo, "Multi-objective design of PV-wind-batteries hybrid systems by minimizing the annualized cost system and the loss of power supply probability (LPSP)," in *2013 IEEE International Conference on Industrial Technology (ICIT)*, IEEE, 2013, pp. 861–868, ISBN: 978-1-4673-4569-9. DOI: 10.1109/ICIT.2013.6505784. [Online]. Available: http://ieeexplore.ieee.org/document/6505784/.

[14] G. Carpinelli, A. R. di Fazio, S. Khormali, and F. Mottola, "Optimal sizing of battery storage systems for industrial applications when uncertainties exist," *Energies*, vol. 7, no. 1, pp. 130–149, 2014, ISSN: 19961073. DOI: 10.3390/en7010130. [Online]. Available: http://www.mdpi.com/1996-1073/7/1/130.

[15] J. Carroquino, C. Escriche-Martínez, L. Valiño, and R. Dufo-López, "Comparison of economic performance of lead-acid and li-ion batteries in standalone photovoltaic energy systems," *Applied Sciences (Switzerland)*, vol. 11, no. 8, 2021, ISSN: 20763417. DOI: 10.3390/app11083587.

[16] C. Chen, S. Duan, T. Cai, B. Liu, and G. Hu, "Optimal Allocation and Economic Analysis of Energy Storage System in Microgrids," *IEEE Transactions on Power Electronics*, vol. 26, no. 10, pp. 2762–2773, 2011, ISSN: 0885-8993. DOI: 10.1109/TPEL.2011.2116808. [Online]. Available: http://ieeexplore.ieee.org/document/5715890/.

[17] X. Darning, K. Longyun, C. Liuchen, and C. Binggang, "Optimal sizing of standalone hybrid wind/PV power systems using genetic algorithms," in *Canadian Conference on Electrical and Computer Engineering*, vol. 2005, IEEE, 2005, pp. 1722–1725, ISBN: 0-7803-8885-2. DOI: 10.1109/CCECE.2005.1557315. [Online]. Available: http://ieeexplore.ieee.org/document/1557315/.

[18] K. Deb, K. Sindhya, and T. Okabe, "Self-adaptive simulated binary crossover for real-parameter optimization," in *Proceedings of GECCO 2007: Genetic and Evolutionary Computation Conference*, New York, NY, USA: ACM, 2007, pp. 1187–1194, ISBN: 1595936971. DOI: 10.1145/1276958.1277190. [Online]. Available: https://dl.acm.org/doi/10.1145/1276958.1277190.

[19] S. De Clercq, B. Zwaenepoel, and L. Vandevelde, "Optimal sizing of an industrial microgrid considering socio-organisational aspects," *IET Generation, Transmission and Distribution*, vol. 12, no. 14, pp. 3442–3451, 2018, ISSN: 17518687. DOI: 10.1049/iet-gtd.2017.1545. [Online]. Available: https://onlinelibrary.wiley.com/doi/10.1049/iet-gtd.2017.1545.

[20] R. Dufo-López and J. L. Bernal-Agustín, "Design and control strategies of PV-diesel systems using genetic algorithms," *Solar Energy*, vol. 79, no. 1, pp. 33–46, 2005, ISSN: 0038092X. DOI: 10.1016/j.solener.2004.10.004.

[21] R. Dufo-López and J. L. Bernal-Agustín, "Multi-objective design of PV–wind–diesel–hydrogen–battery systems," *Renewable Energy*, vol. 33, no. 12, pp. 2559–2572, 2008, ISSN: 09601481. DOI: 10.1016/j.renene.2008.02.027. [Online]. Available: https://linkinghub.elsevier.com/retrieve/pii/S0960148108000724.

[22] J. P. Fossati, A. Galarza, A. Martín-Villate, and L. Fontán, "A method for optimal sizing energy storage systems for microgrids," *Renewable Energy*, vol. 77, pp. 539–549, 2015, ISSN: 18790682. DOI: 10.1016/j.renene.2014.12.039.

[23] Y. E. García-Vera, R. Dufo-López, and J. L. Bernal-Agustín, "Optimization of isolated hybrid microgrids with renewable energy based on different battery models and technologies," *Energies*, vol. 13, no. 3, p. 581, 2020, ISSN: 19961073. DOI: 10.3390/en13030581. [Online]. Available: https://www.mdpi.com/1996-1073/13/3/581.

[24] A. González, J. R. Riba, A. Rius, and R. Puig, "Optimal sizing of a hybrid grid-connected photovoltaic and wind power system," *Applied Energy*, vol. 154, pp. 752–762, 2015, ISSN: 03062619. DOI: 10.1016/j.apenergy.2015.04.105. [Online]. Available: https://linkinghub.elsevier.com/retrieve/pii/S0306261915005681.

[25] M. S. Ismail, M. Moghavvemi, and T. M. Mahlia, "Genetic algorithm based optimization on modeling and design of hybrid renewable energy systems," *Energy Conversion and Management*, vol. 85, pp. 120–130, 2014, ISSN: 01968904. DOI: 10.1016/j.enconman.2014.05.064. [Online]. Available: http://dx.doi.org/10.1016/j.enconman.2014.05.064.

[26] E. Koutroulis, D. Kolokotsa, A. Potirakis, and K. Kalaitzakis, "Methodology for optimal sizing of stand-alone photovoltaic/wind-generator systems using genetic algorithms," *Solar Energy*, vol. 80, no. 9, pp. 1072–1088, 2006, ISSN: 0038092X. DOI: 10.1016/j.solener.2005.11.002. [Online]. Available: https://linkinghub.elsevier.com/retrieve/pii/S0038092X05003713.

[27] P. Li, R. X. Li, Y. Cao, D. Y. Li, and G. Xie, "Multiobjective sizing optimization for island microgrids using a triangular aggregation model and the levy-harmony algorithm," *IEEE Transactions on Industrial Informatics*, vol. 14, no. 8, pp. 3495–3505, 2018, ISSN: 15513203. DOI: 10.1109/TII.2017.2778079. [Online]. Available: https://ieeexplore.ieee.org/document/8122057/.

[28] A. Maheri, "Multi-objective design optimisation of standalone hybrid wind-PV-diesel systems under uncertainties," *Renewable Energy*, vol. 66, pp. 650–661, 2014, ISSN: 09601481. DOI: 10.1016/j.renene.2014.01.009. [Online]. Available: https://linkinghub.elsevier.com/retrieve/pii/S096014811400038X.

[29] R. Dufo-López, J. L. Bernal-Agustín, and J. Contreras, "Optimization of control strategies for stand-alone renewable energy systems with hydrogen storage," *Renewable Energy*, vol. 32, pp. 1102–1126, 7 Jun. 2007, ISSN: 09601481. DOI: 10.1016/j.renene.2006.04.013. [Online]. Available: https://linkinghub.elsevier.com/retrieve/pii/S096014810600108X.

[30] S. Tito, T. Lie, and T. Anderson, "Optimal sizing of a wind-photovoltaic-battery hybrid renewable energy system considering socio-demographic factors," *Solar Energy*, vol. 136, pp. 525–532, 2016, ISSN: 0038092X. DOI: 10.1016/j.solener.2016.07.036. [Online]. Available: http://dx.doi.org/10.1016/j.solener.2016.07.036https://linkinghub.elsevier.com/retrieve/pii/S0038092X16302948.

[31] H. Yang, W. Zhou, L. Lu, and Z. Fang, "Optimal sizing method for stand-alone hybrid solar-wind system with LPSP technology by using genetic algorithm," *Solar Energy*, vol. 82, no. 4, pp. 354–367, 2008, ISSN: 0038092X. DOI: 10.1016/j.solener.2007.08.005. [Online]. Available: https://linkinghub.elsevier.com/retrieve/pii/S0038092X07001831.

[32] B. Zhao, X. Zhang, P. Li, K. Wang, M. Xue, and C. Wang, *Optimal sizing, operating strategy and operational experience of a stand-alone microgrid on Dongfushan Island*, 2014. DOI: 10.1016/j.apenergy.2013.09.015. [Online]. Available: https://linkinghub.elsevier.com/retrieve/pii/S0306261913007629.

[33] M. Fadaee and M. Radzi, "Multi-objective optimization of a stand-alone hybrid renewable energy system by using evolutionary algorithms: A review," *Renewable and Sustainable Energy Reviews*, vol. 16, no. 5, pp. 3364–3369, 2012, ISSN: 13640321. DOI: 10.1016/j.rser.2012.02.071. [Online]. Available: http://dx.doi.org/10.1016/j.rser.2012.02.071https://linkinghub.elsevier.com/retrieve/pii/S1364032112001669.

[34] A. H. Fathima and K Palanisamy, *Optimization in microgrids with hybrid energy systems - A review*, 2015. DOI: 10.1016/j.rser.2015.01.059. [Online]. Available: http://dx.doi.org/10.1016/j.rser.2015.01.059https://linkinghub.elsevier.com/retrieve/pii/S1364032115000696.

[35] M. V. Kirthiga, S. A. Daniel, and S. Gurunathan, "A methodology for transforming an existing distribution network into a sustainable autonomous micro-grid," *IEEE Transactions on Sustainable Energy*, vol. 4, no. 1, pp. 31–41, 2013, ISSN: 19493029. DOI: 10.1109/TSTE.2012.2196771.

[36] J. Lujano-Rojas, R. Dufo-López, and J. A. Domínguez-Navarro, *Genetic Optimization Techniques for Sizing and Management of Modern Power Systems*. 2022, pp. 1–341, ISBN: 9780128238899. DOI: 10.1016/C2020-0-01018-2.

[37] D. W. Gao, *Energy Storage for Sustainable Microgrid*. 2015, pp. 1–142, ISBN: 978-0-12-803374-6. DOI: 10.1016/C2014-0-04144-5.

[38] M. A. Hannan, M Faisal, P. Jern Ker, R. A. Begum, Z. Y. Dong, and C Zhang, *Review of optimal methods and algorithms for sizing energy storage systems to achieve decarbonization in microgrid applications*, 2020. DOI: 10.1016/j.rser.2020.110022. [Online]. Available: https://linkinghub.elsevier.com/retrieve/pii/S1364032120303130.

[39] S. M. Dawoud, X. Lin, and M. I. Okba, "Hybrid renewable microgrid optimization techniques: A review," *Renewable and Sustainable Energy Reviews*, vol. 82, no. May 2017, pp. 2039–2052, 2018, ISSN: 13640321. DOI: 10.1016/j.rser.2017.08.007. [Online]. Available: https://doi.org/10.1016/j.rser.2017.08.007https://linkinghub.elsevier.com/retrieve/pii/S1364032117311383.

[40] H. Elaouni, H. Obeid, S. Le Masson, O. Foucault, and H. Gualous, "A comparative study for optimal sizing of a grid-connected hybrid system using Genetic Algorithm, Particle Swarm Optimization, and HOMER," in *IECON Proceedings (Industrial Electronics Conference)*, vol. 2021-Octob, IEEE Computer Society, 2021, ISBN: 9781665435543. DOI: 10.1109/IECON48115.2021.9589999.

[41] O Erdinc and M Uzunoglu, *Optimum design of hybrid renewable energy systems: Overview of different approaches*, 2012. DOI: 10.1016/j.rser.2011.11.011. [Online]. Available: http://dx.doi.org/10.1016/j.rser.2011.11.011https://linkinghub.elsevier.com/retrieve/pii/S1364032111005478.

[42] V. K. Soni and R. Khare, “Optimal sizing of HRES for small sized institute using HOMER,” in *Proceedings of the 2014 IEEE 2nd International Conference on Electrical Energy Systems, ICEES 2014*, IEEE, 2014, pp. 77–81, ISBN: 9781479937387. DOI: 10.1109/ICEES.2014.6924145. [Online]. Available: http://ieeexplore.ieee.org/document/6924145/.

[43] S. Bandyopadhyay, G. R. C. Mouli, Z. Qin, L. R. Elizondo, and P. Bauer, “Techno-Economical Model Based Optimal Sizing of PV-Battery Systems for Microgrids,” *IEEE Transactions on Sustainable Energy*, vol. 11, no. 3, pp. 1657–1668, 2020, ISSN: 19493037. DOI: 10.1109/TSTE.2019.2936129. [Online]. Available: https://ieeexplore.ieee.org/document/8805453/.

[44] Lingfeng Wang and C. Singh, “Multicriteria Design of Hybrid Power Generation Systems Based on a Modified Particle Swarm Optimization Algorithm,” *IEEE Transactions on Energy Conversion*, vol. 24, no. 1, pp. 163–172, 2009, ISSN: 0885-8969. DOI: 10.1109/TEC.2008.2005280. [Online]. Available: http://ieeexplore.ieee.org/document/4749288/.

[45] G. Ma, G. Xu, Y. Chen, and R. Ju, “Multi□objective optimal configuration method for a standalone wind–solar–battery hybrid power system,” *IET Renewable Power Generation*, vol. 11, no. 1, pp. 194–202, 2017, ISSN: 1752-1416. DOI: 10.1049/iet-rpg.2016.0646. [Online]. Available: https://onlinelibrary.wiley.com/doi/10.1049/iet-rpg.2016.0646.

[46] M. Sharafi and T. Y. ELMekkawy, “Multi-objective optimal design of hybrid renewable energy systems using PSO-simulation based approach,” *Renewable Energy*, vol. 68, pp. 67–79, 2014, ISSN: 09601481. DOI: 10.1016/j.renene.2014.01.011. [Online]. Available: https://linkinghub.elsevier.com/retrieve/pii/S0960148114000408.

[47] S. Vis, “A new look for residential hybrid systems,” 2021.

[48] A. A. Zaki Diab, H. M. Sultan, I. S. Mohamed, N. Kuznetsov Oleg, and T. D. Do, “Application of different optimization algorithms for optimal sizing of pv/wind/diesel/battery storage stand-alone hybrid microgrid,” *IEEE Access*, vol. 7, pp. 119 223–119 245, 2019, ISSN: 21693536. DOI: 10.1109/ACCESS.2019.2936656.

[49] Z. Javid, K. J. Li, R. Ul Hassan, and J. Chen, “Hybrid-Microgrid Planning, Sizing and Optimization for an Industrial Demand in Pakistan,” *Tehnicki vjesnik - Technical Gazette*, vol. 27, no. 3, pp. 781–792, 2020, ISSN: 13303651. DOI: 10.17559/TV-20181219042529. [Online]. Available: https://hrcak.srce.hr/239086.

[50] A. Kumar, M. Zaman, N. Goel, N. Goel, and R. Church, “In search of an optimization tool for renewable energy resources: Homer vs. in-house model,” in *2013 IEEE Electrical Power & Energy Conference*, IEEE, 2013, pp. 1–7, ISBN: 978-1-4799-0106-7. DOI: 10.1109/EPEC.2013.6802955. [Online]. Available: http://ieeexplore.ieee.org/document/6802955/.

[51] J. Lu, W. Wang, Y. Zhang, and S. Cheng, “Multi-objective optimal design of stand-alone hybrid energy system using entropy weight method based on HOMER,” *Energies*, vol. 10, no. 10, p. 1664, 2017, ISSN: 19961073. DOI: 10.3390/en10101664. [Online]. Available: http://www.mdpi.com/1996-1073/10/10/1664.

[52] S. X. Chen, H. B. Gooi, and M. Q. Wang, “Sizing of energy storage for microgrids,” *IEEE Transactions on Smart Grid*, vol. 3, no. 1, pp. 142–151, 2012, ISSN: 19493053. DOI: 10.1109/TSG.2011.2160745. [Online]. Available: http://ieeexplore.ieee.org/document/5979167/.

[53] M. Geraedts, J. Alpizar-Castillo, L. Ramirez-Elizondo, and P. Bauer, “Optimal Sizing of a Community Level Thermal Energy Storage System,” in *MELECON 2022 - IEEE Mediterranean Electrotechnical Conference, Proceedings*, IEEE, 2022, pp. 52–57, ISBN: 9781665442800. DOI: 10.1109/MELECON53508.2022.9842945. [Online]. Available: https://ieeexplore.ieee.org/document/9842945/.

[54] V. Halmschlager and R. Hofmann, “Holistic Approach for the Optimization of Industrial Hybrid Energy Hubs with MILP,” in *Computer Aided Chemical Engineering*, vol. 48, Elsevier Masson SAS, 2020, pp. 1375–1380, ISBN: 9780128233771. DOI: 10.1016/B978-0-12-823377-1.50230-5. [Online]. Available: https://doi.org/10.1016/B978-0-12-823377-1.50230-5https://linkinghub.elsevier.com/retrieve/pii/B9780128233771502305.

[55] M. Moradzadeh and M. M. A. Abdelaziz, “A New MILP Formulation for Renewables and Energy Storage Integration in Fast Charging Stations,” *IEEE Transactions on Transportation Electrification*, vol. 6, no. 1, pp. 181–198, 2020, ISSN: 23327782. DOI: 10.1109/TTE.2020.2974179.

[56] A. K. V, A. Verma, and R. Talwar, "Optimal techno-economic sizing of a multi-generation microgrid system with reduced dependency on grid for critical health-care, educational and industrial facilities," *Energy*, vol. 208, p. 118 248, 2020, ISSN: 03605442. DOI: 10.1016/j.energy.2020.118248. [Online]. Available: https://linkinghub.elsevier.com/retrieve/pii/S0360544220313554.

[57] Y. Yao, L. Ye, X. Qu, *et al.*, "Coupled model and optimal operation analysis of power hub for multi-heterogeneous energy generation power system," *Journal of Cleaner Production*, vol. 249, p. 119 432, 2020, ISSN: 09596526. DOI: 10.1016/j.jclepro.2019.119432. [Online]. Available: https://doi.org/10.1016/j.jclepro.2019.119432.

[58] L. Andreassi, M. Ciminelli, M. Feola, and S. Ubertini, "Innovative method for energy management: Modelling and optimal operation of energy systems," *Energy and Buildings*, vol. 41, no. 4, pp. 436–444, 2009, ISSN: 03787788. DOI: 10.1016/j.enbuild.2008.11.010. [Online]. Available: https://linkinghub.elsevier.com/retrieve/pii/S0378778808002442.

[59] M. Astaneh, R. Roshandel, R. Dufo-López, and J. L. Bernal-Agustín, "A novel framework for optimization of size and control strategy of lithium-ion battery based off-grid renewable energy systems," *Energy Conversion and Management*, vol. 175, no. September, pp. 99–111, 2018, ISSN: 01968904. DOI: 10.1016/j.enconman.2018.08.107. [Online]. Available: https://doi.org/10.1016/j.enconman.2018.08.107.

[60] B. Bahmani-Firouzi and R. Azizipanah-Abarghooee, "Optimal sizing of battery energy storage for micro-grid operation management using a new improved bat algorithm," *International Journal of Electrical Power and Energy Systems*, vol. 56, pp. 42–54, 2014, ISSN: 01420615. DOI: 10.1016/j.ijepes.2013.10.019. [Online]. Available: http://dx.doi.org/10.1016/j.ijepes.2013.10.019https://linkinghub.elsevier.com/retrieve/pii/S0142061513004365.

[61] J. L. Bernal-Agustín, R. Dufo-López, and D. M. Rivas-Ascaso, "Design of isolated hybrid systems minimizing costs and pollutant emissions," *Renewable Energy*, vol. 31, no. 14, pp. 2227–2244, 2006, ISSN: 09601481. DOI: 10.1016/j.renene.2005.11.002.

[62] S. T. Blake and D. T. O'Sullivan, "Optimization of Distributed Energy Resources in an Industrial Microgrid," in *Procedia CIRP*, vol. 67, The Author(s), 2018, pp. 104–109. DOI: 10.1016/j.procir.2017.12.184. [Online]. Available: http://dx.doi.org/10.1016/j.procir.2017.12.184https://linkinghub.elsevier.com/retrieve/pii/S2212827117311265.

[63] M. Bucciarelli, A. Giannitrapani, S. Paoletti, A. Vicino, and D. Zarrilli, "Sizing of energy storage systems considering uncertainty on demand and generation," in *IFAC-PapersOnLine*, vol. 50, 2017, pp. 8861–8866. DOI: 10.1016/j.ifacol.2017.08.1543. [Online]. Available: https://linkinghub.elsevier.com/retrieve/pii/S2405896317321298.

[64] A. L. Bukar, C. W. Tan, and K. Y. Lau, "Optimal sizing of an autonomous photovoltaic/wind/-battery/diesel generator microgrid using grasshopper optimization algorithm," *Solar Energy*, vol. 188, no. March, pp. 685–696, 2019, ISSN: 0038092X. DOI: 10.1016/j.solener.2019.06.050. [Online]. Available: https://linkinghub.elsevier.com/retrieve/pii/S0038092X19306243.

[65] B. Cao, W. Dong, Z. Lv, Y. Gu, S. Singh, and P. Kumar, "Hybrid Microgrid Many-Objective Sizing Optimization With Fuzzy Decision," *IEEE Transactions on Fuzzy Systems*, vol. 28, no. 11, pp. 2702–2710, 2020, ISSN: 1063-6706. DOI: 10.1109/TFUZZ.2020.3026140. [Online]. Available: https://ieeexplore.ieee.org/document/9204848/.

[66] X. Chen, Y. Si, C. Liu, *et al.*, "The value and optimal sizes of energy storage units in solar-assist cogeneration energy hubs," *Applied Sciences (Switzerland)*, vol. 10, no. 14, p. 4994, 2020, ISSN: 20763417. DOI: 10.3390/app10144994. [Online]. Available: https://www.mdpi.com/2076-3417/10/14/4994.

[67] O. Ekren and B. Y. Ekren, "Size optimization of a PV/wind hybrid energy conversion system with battery storage using simulated annealing," *Applied Energy*, vol. 87, no. 2, pp. 592–598, 2010, ISSN: 03062619. DOI: 10.1016/j.apenergy.2009.05.022. [Online]. Available: https://linkinghub.elsevier.com/retrieve/pii/S0306261909002177.

[68] A. Jafari, T. Khalili, H. G. Ganjehlou, and A. Bidram, "Optimal integration of renewable energy sources, diesel generators, and demand response program from pollution, financial, and reliability viewpoints: A multi-objective approach," *Journal of Cleaner Production*, vol. 247, p. 119 100, 2020, ISSN: 09596526. DOI: 10.1016/j.jclepro.2019.119100. [Online]. Available: https://linkinghub.elsevier.com/retrieve/pii/S0959652619339708.

[69] F. Katiraei and C. Abbey, "Diesel plant sizing and performance analysis of a remote wind-diesel microgrid," *2007 IEEE Power Engineering Society General Meeting, PES*, pp. 1–8, 2007. DOI: 10.1109/PES.2007.386275.

[70] S. P. Koko, "Optimal battery sizing for a grid-tied solar photovoltaic system supplying a residential load: A case study under South African solar irradiance," *Energy Reports*, vol. 8, pp. 410–418, 2022, ISSN: 23524847. DOI: 10.1016/j.egyr.2022.02.183. [Online]. Available: https://linkinghub.elsevier.com/retrieve/pii/S2352484722004309.

[71] J. Li, W. Wei, and J. Xiang, "A simple sizing algorithm for stand-alone PV/Wind/Battery hybrid microgrids," *Energies*, vol. 5, no. 12, pp. 5307–5323, 2012, ISSN: 19961073. DOI: 10.3390/en5125307.

[72] T Logenthiran, D. Srinivasan, A. M. Khambadkone, and T. S. Raj, "Optimal sizing of an islanded microgrid using Evolutionary Strategy," in *2010 IEEE 11th International Conference on Probabilistic Methods Applied to Power Systems, PMAPS 2010*, IEEE, 2010, pp. 12–17, ISBN: 9781424457236. DOI: 10.1109/PMAPS.2010.5528840. [Online]. Available: http://ieeexplore.ieee.org/document/5528840/.

[73] M. Ross, C. Abbey, and G. Joós, "Cost analysis for sizing energy storage systems in wind-diesel microgrids," *IEEE Power and Energy Society General Meeting*, vol. 1, pp. 1–8, 2011, ISSN: 19449925. DOI: 10.1109/PES.2011.6039595.

[74] S. Senemar, M. Rastegar, M. Dabbaghjamanesh, and N. Hatziargyriou, "Dynamic Structural Sizing of Residential Energy Hubs," *IEEE Transactions on Sustainable Energy*, vol. 11, no. 3, pp. 1236–1246, 2020, ISSN: 19493037. DOI: 10.1109/TSTE.2019.2921110.

[75] A. Sheikhi, A. M. Ranjbar, and H. Oraee, "Financial analysis and optimal size and operation for a multicarrier energy system," *Energy and Buildings*, vol. 48, pp. 71–78, 2012, ISSN: 03787788. DOI: 10.1016/j.enbuild.2012.01.011. [Online]. Available: http://dx.doi.org/10.1016/j.enbuild.2012.01.011.

[76] A. Sheikhi, M. Rayati, and A. M. Ranjbar, "Energy Hub optimal sizing in the smart grid; Machine learning approach," *2015 IEEE Power and Energy Society Innovative Smart Grid Technologies Conference, ISGT 2015*, 2015. DOI: 10.1109/ISGT.2015.7131796.

[77] S. Singh and S. C. Kaushik, "Optimal sizing of grid integrated hybrid PV-biomass energy system using artificial bee colony algorithm," *IET Renewable Power Generation*, vol. 10, no. 5, pp. 642–650, 2016, ISSN: 17521424. DOI: 10.1049/iet-rpg.2015.0298. [Online]. Available: https://onlinelibrary.wiley.com/doi/10.1049/iet-rpg.2015.0298.

[78] M. Upasani and S. Patil, "Grid connected solar photovoltaic system with battery storage for energy management," *Proceedings of the 2nd International Conference on Inventive Systems and Control, ICISC 2018*, no. Icisc, pp. 438–443, 2018. DOI: 10.1109/ICISC.2018.8399111.

[79] A. S. Wittebrood, "The economic value of combined pv-battery systems for an industrial load under different price scenarios," vol. 1, 2018.

[80] Y. Yang, H. Li, A. Aichhorn, J. Zheng, and M. Greenleaf, "Sizing strategy of distributed battery storage system with high penetration of photovoltaic for voltage regulation and peak load shaving," *IEEE Transactions on Smart Grid*, vol. 5, no. 2, pp. 982–991, 2014, ISSN: 19493053. DOI: 10.1109/TSG.2013.2282504. [Online]. Available: http://ieeexplore.ieee.org/document/6609116/.

[81] C. Coello, G. Pulido, and M. Lechuga, "Handling multiple objectives with particle swarm optimization," *IEEE Transactions on Evolutionary Computation*, vol. 8, no. 3, pp. 256–279, 2004, ISSN: 1089-778X. DOI: 10.1109/TEVC.2004.826067. [Online]. Available: http://ieeexplore.ieee.org/document/1304847/.

[82] E. A. K. Mishra, E. Y. Mohapatra, and E. A. K. Mishra, “Multi-Objective Genetic Algorithm: A Comprhensive Survey,” *Ijetae.Com*, vol. 3, no. 2, 2013. [Online]. Available: http://www.ijetae.com/files/Volume3Issue2/IJETAE_0213_13.pdf.

[83] C. Steinbrink, M. Blank-Babazadeh, A. El-Ama, *et al.*, “Cpes testing with mosaik: Co-simulation planning, execution and analysis,” *Applied Sciences*, vol. 9, no. 5, 2019, ISSN: 2076-3417. DOI: 10.3390/app9050923. [Online]. Available: https://www.mdpi.com/2076-3417/9/5/923.

[84] F. Braeuer, *Load profile data of 50 industrial plants in Germany for one year*, version 1.0, 2020. DOI: 10.5281/zenodo.3899018. [Online]. Available: https://doi.org/10.5281/zenodo.3899018.

[85] S. Barsali *et al.*, *Benchmark systems for network integration of renewable and distributed energy resources*. 2014.

[86] L. Thurner, A. Scheidler, F. Schafer, *et al.*, “Pandapower - an open-source python tool for convenient modeling, analysis, and optimization of electric power systems,” *IEEE Transactions on Power Systems*, vol. 33, pp. 6510–6521, 6 Nov. 2018, ISSN: 08858950. DOI: 10.1109/TPWRS.2018.2829021. [Online]. Available: https://ieeexplore.ieee.org/document/8344496/.

[87] [Online]. Available: https://www.weforum.org/agenda/2022/09/scope-emissions-climate-greenhouse-business/.

[88] IRENA, “Renewable power generation costs in 2021,” International Renewable Energy Agency, 2022.

[89] D. Harris and L. Figurelli, “The wacc for the dutch gas the wacc for the dutch electricity tso and electricity and gas dsos,” ACM, 2021. [Online]. Available: https://www.acm.nl/sites/default/files/documents/the-wacc-for-the-dutch-electricity-tso-and-electricity-and-gas-dsos.pdf.

[90] R. Dufo-López, T. Cortés-Arcos, J. S. Artal-Sevil, and J. L. Bernal-Agustín, “Comparison of lead-acid and li-ion batteries lifetime prediction models in stand-alone photovoltaic systems,” *Applied Sciences (Switzerland)*, vol. 11, pp. 1–16, 3 2021, ISSN: 20763417. DOI: 10.3390/app11031099.

[91] A. López-González, B. Domenech, and L. Ferrer-Martí, “Lifetime, cost and fuel efficiency in diesel projects for rural electrification in Venezuela,” *Energy Policy*, vol. 121, no. March, pp. 152–161, 2018, ISSN: 03014215. DOI: 10.1016/j.enpol.2018.06.023.

[92] C. B. voor de Statistiek, *Marktprijzen energie, 2000-2022*, 2023. [Online]. Available: https://www.cbs.nl/nl-nl/maatwerk/2023/15/marktprijzen-energie-2000-2022.

[93] 2022. [Online]. Available: https://www.co2emissiefactoren.nl/wp-content/uploads/2022/08/CO2emissiefactoren-2022-2015-dd-14-7-2022.pdf.

[94] Liander, *Tarieven voor aansluiting en transport elektriciteit*, 2022.

[95] T. Huld, R. Müller, and A. Gambardella, “A new solar radiation database for estimating PV performance in Europe and Africa,” *Solar Energy*, vol. 86, no. 6, pp. 1803–1815, 2012, ISSN: 0038092X. DOI: 10.1016/j.solener.2012.03.006. [Online]. Available: https://linkinghub.elsevier.com/retrieve/pii/S0038092X12001119https://joint-research-centre.ec.europa.eu/pvgis-online-tool/pvgis-data-download_en.

[96] Joint Research Centre, *PVGIS Online Tool Access*, 2020. [Online]. Available: https://joint-research-centre.ec.europa.eu/pvgis-online-tool_en.

[97] M. van Algemene Zaken, *Plan kabinet: Afbouw salderingsregeling zonnepanelen*, 2023. [Online]. Available: https://www.rijksoverheid.nl/onderwerpen/energie-thuis/plan-kabinet-afbouw-salderingsregeling-zonnepanelen.

[98] [Online]. Available: https://www.exchangerates.org.uk/USD-EUR-spot-exchange-rates-history-2021.html.

[99] C. B. voor de Statistiek, *Consumentenprijzen; prijsindex 1900 = 100*, 2023. [Online]. Available: https://www.cbs.nl/nl-nl/cijfers/detail/71905ned.

[100] Joint Research Centre, *PVGIS data sources & calculation methods.* 2020. [Online]. Available: https://joint-research-centre.ec.europa.eu/pvgis-online-tool/getting-started-pvgis/pvgis-data-sources-calculation-methods_enhttps://joint-research-centre.ec.europa.eu/pvgis-photovoltaic-geographical-information-system/getting-started-pvgis/pvgis-data-sou.

[101] C. S. Psomopoulos, G. C. Ioannidis, S. D. Kaminaris, K. D. Mardikis, and N. G. Katsikas, "A Comparative Evaluation of Photovoltaic Electricity Production Assessment Software (PVGIS, PVWatts and RETScreen)," *Environmental Processes*, vol. 2, no. January 2014, S175–S189, 2015, ISSN: 21987505. DOI: 10.1007/s40710-015-0092-4.

[102] [Online]. Available: https://www.wpowerproducts.com/news/types-of-industrial-generators.

[103] [Online]. Available: https://scikit-learn.org/stable/modules/generated/sklearn.linear_model.LinearRegression.html#sklearn.linear_model.LinearRegression.

[104] 2022. [Online]. Available: https://www.tln.nl/brandstofmonitor/.

[105] A.-I. Stan, M. Swierczynski, D.-I. Stroe, R. Teodorescu, and S. J. Andreasen, "Lithium ion battery chemistries from renewable energy storage to automotive and back-up power applications — An overview," in *2014 International Conference on Optimization of Electrical and Electronic Equipment (OPTIM)*, IEEE, 2014, pp. 713–720, ISBN: 978-1-4799-5183-3. DOI: 10.1109/OPTIM.2014.6850936. [Online]. Available: http://ieeexplore.ieee.org/document/6850936/.

[106] J. Alpízar-Castillo, L. Ramirez-Elizondo, and P. Bauer, "Assessing the Role of Energy Storage in Multiple Energy Carriers toward Providing Ancillary Services: A Review," *Energies*, vol. 16, no. 1, 2023, ISSN: 19961073. DOI: 10.3390/en16010379.

[107] G. Zubi, R. Dufo-López, M. Carvalho, and G. Pasaoglu, *The lithium-ion battery: State of the art and future perspectives*, 2018. DOI: 10.1016/j.rser.2018.03.002. [Online]. Available: https://linkinghub.elsevier.com/retrieve/pii/S1364032118300728.

[108] K Ralon, P., Taylor, M., Ilas, A., Diaz-Bone, H., & Kairies, *Electricity storage and renewables: Costs and markets to 2030*. 2017, p. 132, ISBN: 978-92-9260-038-9. [Online]. Available: http://irena.org/publications/2017/Oct/Electricity-storage-and-renewables-costs-and-markets%0Ahttps://www.irena.org/-/media/Files/IRENA/Agency/Publication/2017/Oct/IRENA_Electricity_Storage_Costs_2017.pdf.

[109] G. Rancilio, A. Lucas, E. Kotsakis, *et al.*, "Modeling a Large-Scale Battery Energy Storage System for Power Grid Application Analysis," *Energies*, vol. 12, no. 17, p. 3312, 2019, ISSN: 1996-1073. DOI: 10.3390/en12173312. [Online]. Available: https://www.mdpi.com/1996-1073/12/17/3312.

[110] F. B. Wu, B. Yang, and J. L. Ye, *Grid-scale Energy Storage Systems and Applications*. Elsevier, 2019, pp. 1–306, ISBN: 9780128152928. DOI: 10.1016/C2017-0-00957-6. [Online]. Available: https://linkinghub.elsevier.com/retrieve/pii/C20170009576.

[111] I. Alotaibi, M. A. Abido, M. Khalid, and A. V. Savkin, "A comprehensive review of recent advances in smart grids: A sustainable future with renewable energy resources," *Energies*, vol. 13, no. 23, pp. 1–41, 2020, ISSN: 19961073. DOI: 10.3390/en13236269.

[112] M. Hannan, A. Al-Shetwi, R. Begum, *et al.*, "The value of thermal management control strategies for battery energy storage in grid decarbonization: Issues and recommendations," *Journal of Cleaner Production*, vol. 276, p. 124 223, 2020, ISSN: 09596526. DOI: 10.1016/j.jclepro.2020.124223. [Online]. Available: https://linkinghub.elsevier.com/retrieve/pii/S0959652620342682.

[113] O. Schmidt, S. Melchior, A. Hawkes, and I. Staffell, "Projecting the Future Levelized Cost of Electricity Storage Technologies," *Joule*, vol. 3, no. 1, pp. 81–100, 2019, ISSN: 25424351. DOI: 10.1016/j.joule.2018.12.008. [Online]. Available: https://doi.org/10.1016/j.joule.2018.12.008https://linkinghub.elsevier.com/retrieve/pii/S254243511830583X.

[114] IEA, "Global EV Outlook 2023," IEA, Paris, Tech. Rep., 2023. [Online]. Available: https://www.iea.org/reports/global-ev-outlook-2023.

[115] European Association for Storage of Energy, “Lithium-ion Battery,” *European Assosiation for Storage of Energy*, pp. 8–12, 2016. [Online]. Available: http://ease-storage.eu/wp-content/uploads/2016/07/EASE_TD_Electrochemical_NaIon.pdf.

[116] A. J. Hutchinson and D. T. Gladwin, “Verification and analysis of a Battery Energy Storage System model,” *Energy Reports*, vol. 8, pp. 41–47, 2022, ISSN: 23524847. DOI: 10.1016/j.egyr.2022.05.042. [Online]. Available: https://linkinghub.elsevier.com/retrieve/pii/S2352484722008885.

[117] A. K. Rohit, K. P. Devi, and S. Rangnekar, “An overview of energy storage and its importance in Indian renewable energy sector,” *Journal of Energy Storage*, vol. 13, pp. 10–23, 2017, ISSN: 2352152X. DOI: 10.1016/j.est.2017.06.005. [Online]. Available: https://linkinghub.elsevier.com/retrieve/pii/S2352152X17300488.

[118] S. You and C. N. Rasmussen, “Generic modelling framework for economic analysis of battery systems,” *IET Conference Publications*, vol. 2011, no. 579 CP, p. 122, 2011. DOI: 10.1049/cp.2011.0147.

[119] [Online]. Available: https://www.randomizer.org/.

[120] S. Barsali *et al.*, *Benchmark systems for network integration of renewable and distributed energy resources*. 2014.

[121] [Online]. Available: https://pandapower.readthedocs.io/en/latest/networks/cigre.html.

[122] M. Braun, “Provision of ancillary services by distributed generators. Technological and economic perspective,” *Fraunhofer IWES*, J. Schmid, Ed., 2009. [Online]. Available: https://www.researchgate.net/publication/46038289_Provision_of_ancillary_services_by_distributed_generators_Technological_and_economic_perspective.

[123] G. Haines, “Power Factor Control with a Battery Energy Storage System (BESS),” pp. 3–3, 2018.

[124] G. Olson, “Impact of leading Power factor loads on energy efficiency,” Cummins, Tech. Rep., 2009. [Online]. Available: https://incal.cummins.com/www/literature/technicalpapers/PT-6001-ImpactofPowerFactorLoads-en.pdf.

[125] Y. Chang, Z. Bouzarkouna, and D. Devegowda, “Multi-objective optimization for rapid and robust optimal oilfield development under geological uncertainty,” *Computational Geosciences*, vol. 19, no. 4, pp. 933–950, 2015, ISSN: 15731499. DOI: 10.1007/s10596-015-9507-6.

[126] J. B. Chagas, J. Blank, M. Wagner, M. J. Souza, and K. Deb, “A non-dominated sorting based customized random-key genetic algorithm for the bi-objective traveling thief problem,” *Journal of Heuristics*, vol. 27, no. 3, pp. 267–301, 2021, ISSN: 15729397. DOI: 10.1007/s10732-020-09457-7. arXiv: 2002.04303.

[127] K. Deb, A. Pratap, S. Agarwal, and T. Meyarivan, “A fast and elitist multiobjective genetic algorithm: NSGA-II,” *IEEE Transactions on Evolutionary Computation*, vol. 6, no. 2, pp. 182–197, 2002, ISSN: 1089778X. DOI: 10.1109/4235.996017.

[128] K. Deb and R. B. Agrawal, “Simulated Binary Crossover for Continuous Search Space,” *Complex Systems*, vol. 9, pp. 115–148, 1994, ISSN: 08912513. [Online]. Available: citeulike-article-id:2815748%5Cnhttp://citeseerx.ist.psu.edu/viewdoc/summary?doi=10.1.1.26.8485.

[129] P. K. Muhuri, Z. Ashraf, and Q. M. Danish Lohani, “Multiobjective Reliability Redundancy Allocation Problem With Interval Type-2 Fuzzy Uncertainty,” *IEEE Transactions on Fuzzy Systems*, vol. 26, no. 3, pp. 1339–1355, 2018, ISSN: 10636706. DOI: 10.1109/TFUZZ.2017.2722422.

[130] S. Gunasekaran and M. W. Iruthayarajan, “Contour optimization of suspension insulators using real coded genetic algorithm with simulated binary crossover,” *Proceedings of the 2013 International Conference on Pattern Recognition, Informatics and Mobile Engineering, PRIME 2013*, pp. 360–364, 2013. DOI: 10.1109/ICPRIME.2013.6496501.

[131] F. Schijlen, L. Wu, and L. Mariot, “NASCTY: Neuroevolution to Attack Side-Channel Leakages Yielding Convolutional Neural Networks,” *Mathematics*, vol. 11, no. 12, p. 2616, 2023, ISSN: 22277390. DOI: 10.3390/math11122616.

[132] J. Blank and K. Deb, “Pymoo: Multi-Objective Optimization in Python,” *IEEE Access*, vol. 8, pp. 89 497–89 509, 2020, ISSN: 21693536. DOI: 10.1109/ACCESS.2020.2990567. arXiv: 2002.04504. [Online]. Available: https://ieeexplore.ieee.org/document/9078759/.

[133] 2022. [Online]. Available: https://solar-ew.nl/portfolio-item/zonnepark-moerdijk/.

[134] CAT, *Electric Power Ratings Guide - Diesel Generator Sets*, 2022. [Online]. Available: https://www.cat.com/en_US/by-industry/electric-power/Articles/White-papers/understanding-generator-set-ratings.html.

[135] A. M. G. Storage, “Https://nieuws.eneco.nl/giga-storage-en-eneco-realiseren-samen-grootste-batterij-van-nederland/ 1/2,” pp. 23–24, 2022.

[136] “Ieee recommended practice for conducting load-flow studies and analysis of industrial and commercial power systems,” *IEEE Std 3002.2-2018*, pp. 1–73, 2018. DOI: 10.1109/IEEESTD.2018.8529292.

[137] [Online]. Available: https://ev-database.org/car/1407/Tesla-Model-X-Dual-Motor#battery.

[138] S. Corsi, *Voltage Control and Protection in Electrical Power Systems* (Advances in Industrial Control). London: Springer London, 2015, ISBN: 978-1-4471-6635-1. DOI: 10.1007/978-1-4471-6636-8. [Online]. Available: https://link.springer.com/10.1007/978-1-4471-6636-8.

[139] S. Sepulveda, S. Sepulveda, A. Garces, *et al.*, “Convex optimization optimization for for the the Convex Power for the for the,” vol. 9, pp. 268–273, 2022.

[140] [Online]. Available: https://www.exchangerates.org.uk/.

[141] KPA, *Your diesel generator – what does it truly cost your business?* 2022. [Online]. Available: https://kpakpakpa.com/spotlight/diesel-generator-cost-business-nigeria/.

[142] G. I. POWER, *Total Cost of Ownership Diesel vs . Natural Gas Generators.*

[143] [Online]. Available: https://apelectric.com/cummins-c100d6-100kw-quietconnect-series-diesel-generator/.

[144] A. S. Al-Sumaiti, A. Kavousi-Fard, M. Salama, M. Pourbehzadi, S. Reddy, and M. B. Rasheed, “Economic assessment of distributed generation technologies: A feasibility study and comparison with the literature,” *Energies*, vol. 13, no. 11, 2020, ISSN: 19961073. DOI: 10.3390/en13112764.

[145] C. F. T. Matt, P. Faria, and L. Vieira, “Optimization of the Operation of Isolated Industrial Diesel Stations,” Tech. Rep. June, 2014, pp. 6–6. [Online]. Available: https://www.researchgate.net/publication/240851584.

[146] [Online]. Available: https://www.uspeglobal.com/listings/2063822-1-6-mw-2022-new-caterpillar-3516b-diesel-generator-set.

A

Python Codes

A.1. Grid

```
def step(self):
    """Perform a simulation step"""

    if self.grid_power >= 0:
        # Keep track of the kWh's that is asked of the grid
        self.grid_kWh += self.grid_power*(self.time_step/60)

    # Keep track of the maximum power [kW] that is asked of the grid
    if abs(self.grid_power) > abs(self.grid_kW_max):
        self.grid_kW_max = self.grid_power
    else:
        self.grid_kW_max = self.grid_kW_max
```

A.2. Diesel Generator

```
def step(self):
    """Perform a simulation step"""

    if self.dies_power > 0:
        # Calculate the litres of diesel used per timestep
        self.dies_litre = 0.05125128596647235*self.dies_power + 1.5621789108886397
    else:
        self.dies_litre = 0

    # Keep track of the kWh's and litres that is asked of the Diesel Generator
    self.dies_kWh += self.dies_power*(self.time_step/60)
    self.dies_litre_tot += self.dies_litre
```

A.3. BESS

```
def step(self, time):
    """Perform a simulation step by adding *batt_power* to *batt_charge*."""

    # The power [kW] is converted to [kWh] by multiplying the power by the amount of minutes
        in time_step by 60 minutes per hour.

    # Negative incoming power indicates charging, here the inputted power is "converted" to
        actual input by multiplying the input power with the charge efficiency
    if self.batt_power < 0:
        self.batt_charge1 = round(self.batt_charge - (self.time_step/60)*self.batt_power*self
            .batt_charge_eff, 6)
        self.batt_charge_kWh += (self.batt_charge - self.batt_charge1)
        self.batt_charge = self.batt_charge1

```

```
12      # Positive incoming power indicates discharging, here the outputted power is "converted"
            to actual output by dividing the output power with the discharge efficiency
13      elif self.batt_power > 0:
14          self.batt_charge1 = round(self.batt_charge - (self.time_step/60)*self.batt_power/self
                .batt_discharge_eff, 6)
15
16          # Keep track of the discharged kWh for the LCOS calculation
17          self.batt_discharge_kWh += (self.batt_charge - self.batt_charge1)
18          self.batt_charge = self.batt_charge1
19
20      # No incomping power indicates idling.
21      else:
22          self.batt_charge = round(self.batt_charge - (self.batt_self_discharge_per_time_step)*
                self.batt_charge, 6)
```

B

Diesel Generator Cost Assumptions

The assumptions made for the financial parameters of diesel generators are based on multiple sources, and an average is taken. The sources are a combination of literature and webpages containing prices for diesel generator sets. The prices are converted to Euro's if necessary and then to the 2022 value of the Euro through price histories [140]. The average normalised costs for capital and maintenance both include an outlier upwards, so these values are rounded to the nearest 50 and 5 multiple: €450 and €10 for the initial cost [€/kW] and the yearly cost [€/kW/year].

Table B.1: 2022 adjusted Diesel Generator Cost Parameters

Rating [kVA]	Capital [€]	Installation [€]	Maintenance [€/year]	Initial [€/kVA]	Maintenance [€/year/kVA]	Source
-	-	-	-	543.90	2.18	[68]
100	16500.00	-	1320.00	165.00	13.20	[141]
100	32002.10	14265	570.60	462.67	5.71	[142] [143]
1000	302500.00	81707.38	26499.00	433.96	29.93	[144]
1000	228240.00	-	5706.00	819.54	20.49	[145]
1600	382765.83	228240.00	1997.10	381.88	1.25	[142] [146]
				467.82	12.12	

C

Diesel Generator Validation RMSE Values

Because larger diesel generators introduce more volatility in terms of the ratio's between fuel consumption and power output, graphs for lower power ranges are also created. This is to put the RMSE value of 2.43 (for the whole datasheet range of diesel generators) into perspective.

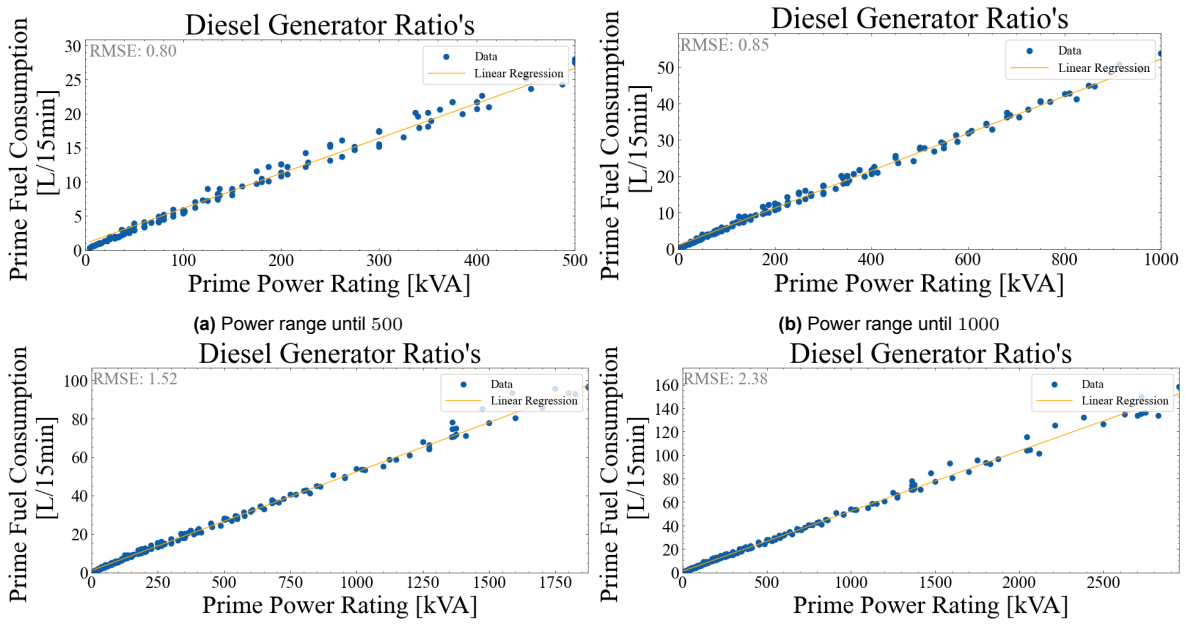

(a) Power range until 500

(b) Power range until 1000

(c) Power range until 2000

(d) Power range until 3000

Figure C.1: RMSE values for different power ranges available in the datasheets

D

Pseduo Pareto fronts of four scenarios

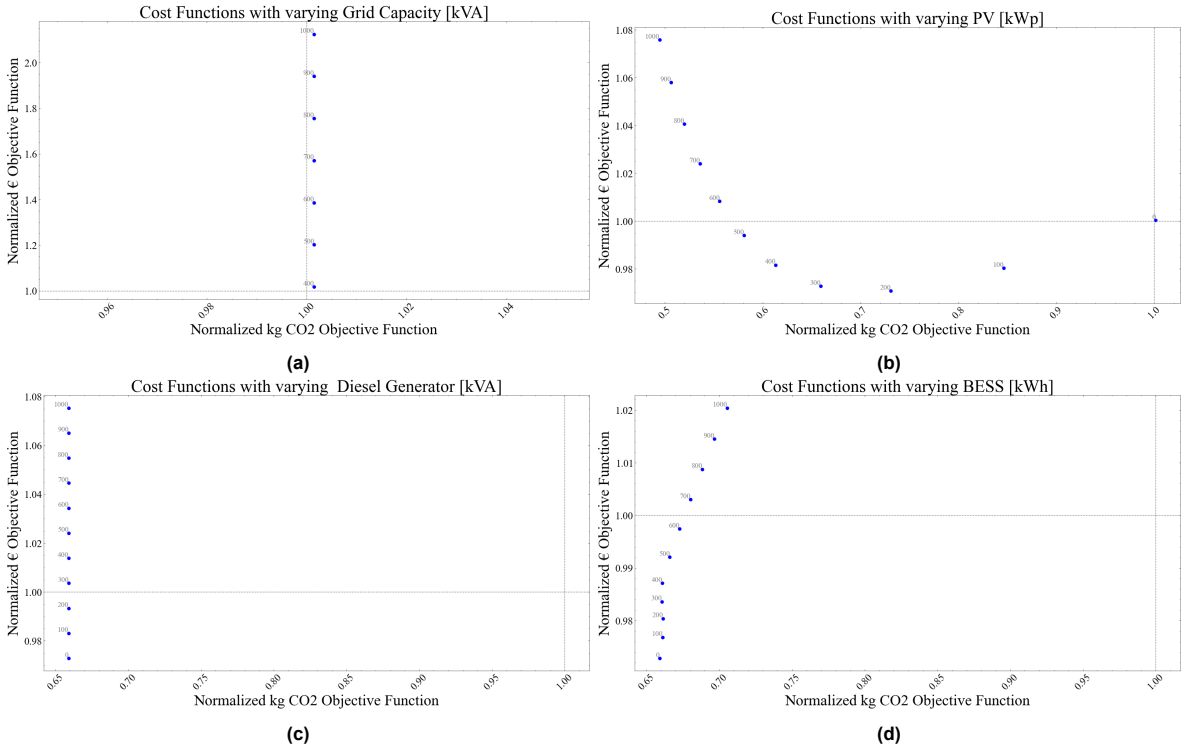

Figure D.1: "Pseudo" Pareto front created for scenario 1: a 12 hour rolling average and a static boundary of 100%

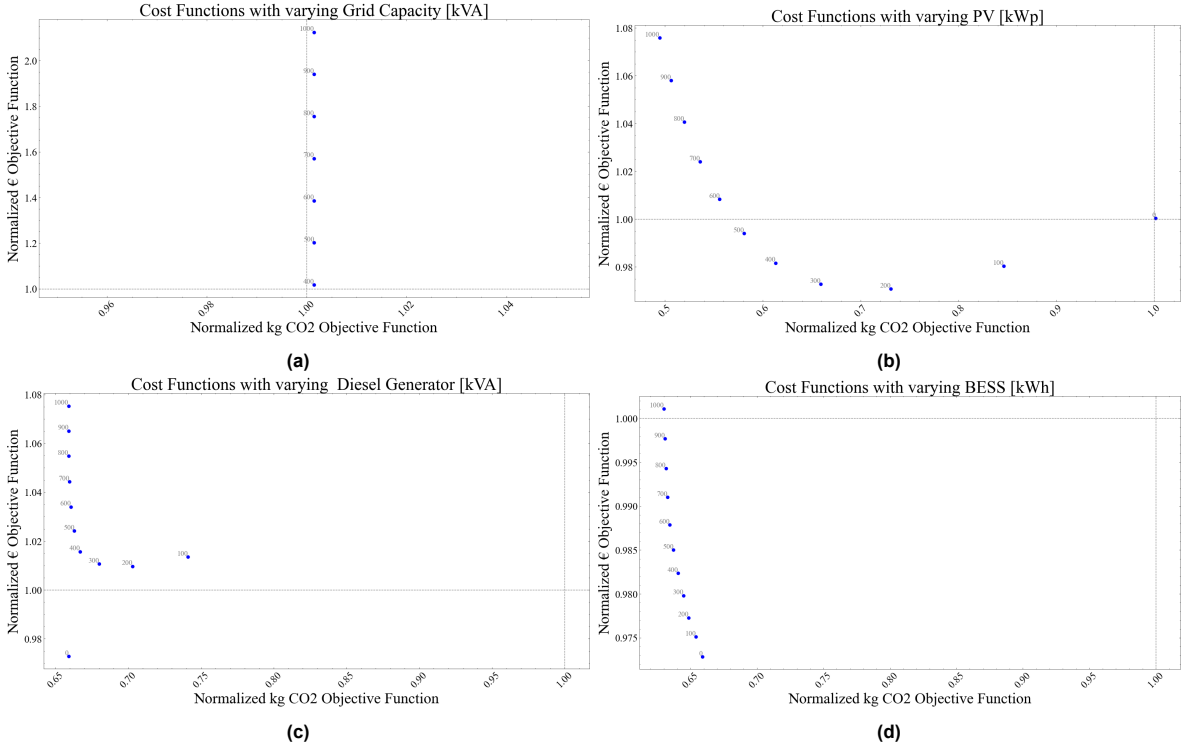

Figure D.2: ”Pseudo” Pareto front created for scenario 2: a 12 hour rolling average and a dynamic boundary of 100%

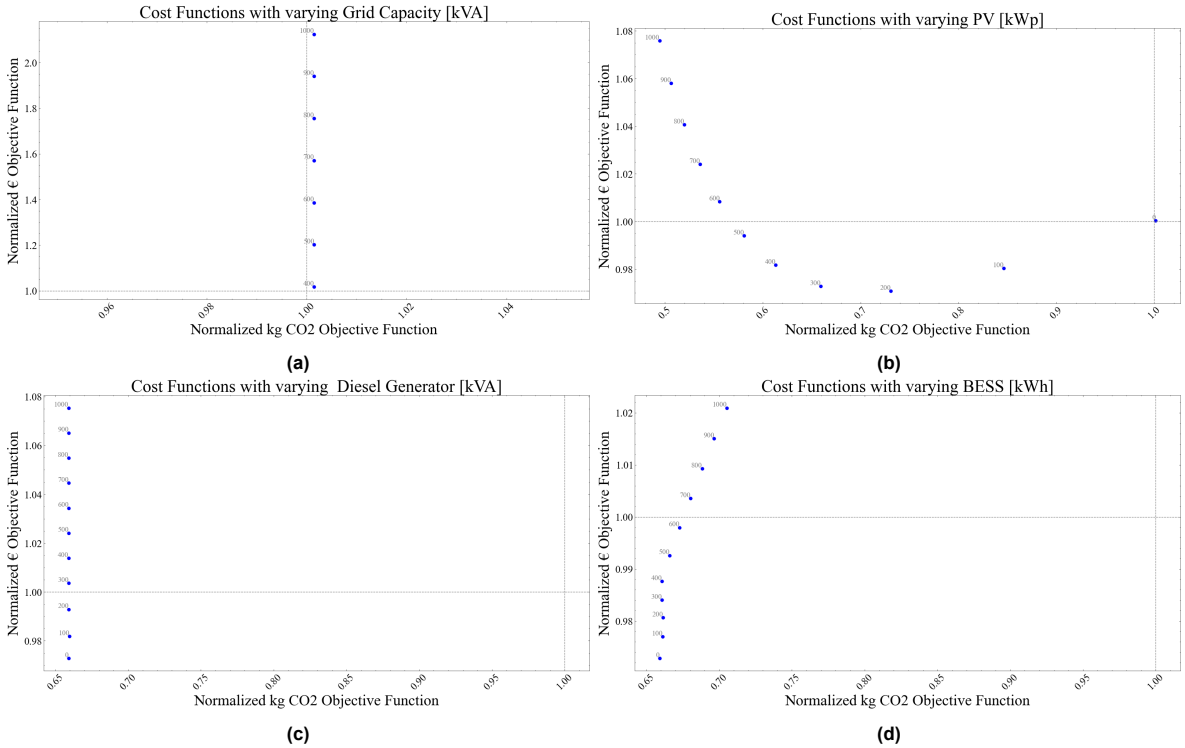

Figure D.3: ”Pseudo” Pareto front created for scenario 3: a 6 hour rolling average and a static boundary of 50%

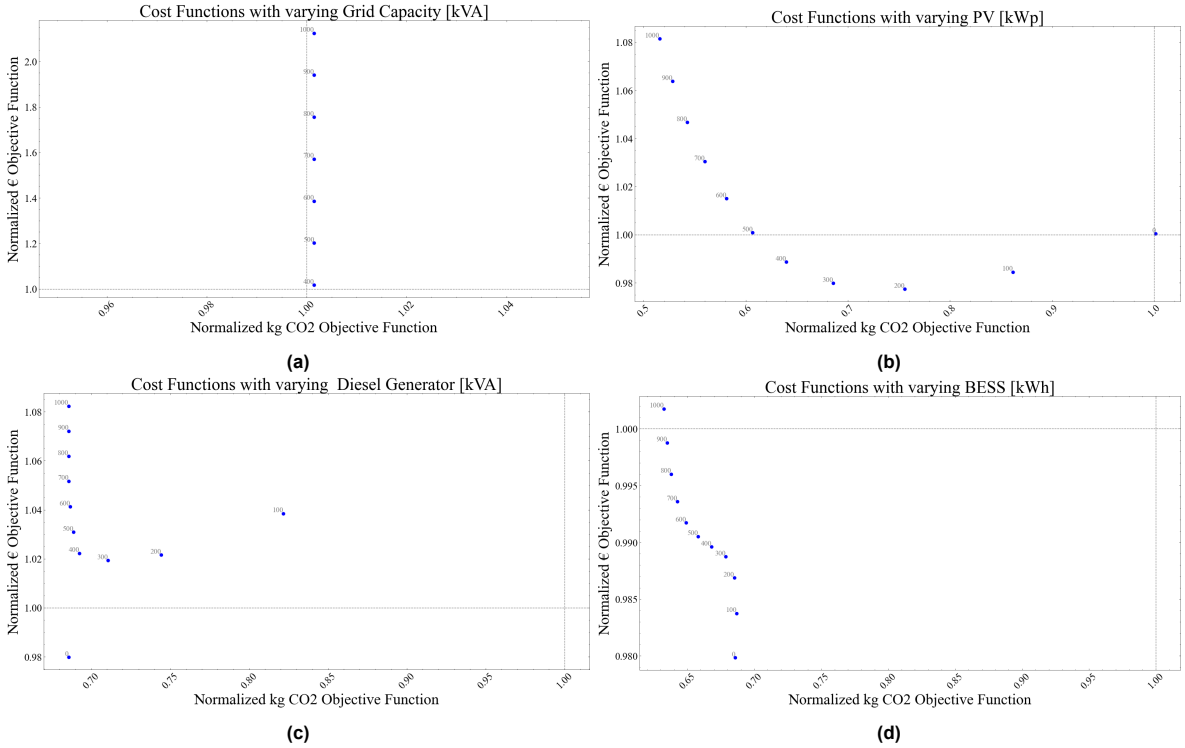

Figure D.4: ”Pseudo” Pareto front created for scenario 4: a 6 hour rolling average and a dynamic boundary of 50%

E

HPS configurations of Pareto fronts for four scenarios

The following tables present the solutions of the nondominated front of the last population for each scenario. This is the reason that the solutions sets are not the same size, as the final population is sorted with nondominted sorting to create different fronts. From these fronts the nondominated front is taken as the final Pareto front from which the optimal solution is extracted per scenario.

Table E.1: Optimization Results for Scenario 1

Objective Functions		**Sized Components**			
€	CO2	Grid Capacity [kVA]	PV Capacity [kWp]	Diesel Generator [kVA]	BESS [kWh]
5.793	0.275	1750	3500	300	1000
1.417	0.407	425	2400	0	200
5.884	0.275	1775	3500	500	1000
2.511	0.345	925	2300	1500	1200
1.190	0.462	400	1200	200	1200
2.614	0.338	975	2400	1400	1200
3.161	0.321	1000	3800	3400	1400
1.983	0.366	550	2900	2100	800
6.090	0.272	1750	3600	3000	1000
1.055	**0.514**	**375**	**800**	**100**	**1000**
4.898	0.298	1425	3200	900	1400
1.764	0.371	525	3000	0	1400
2.856	0.330	875	3600	3100	1400
5.419	0.285	1525	3600	2600	1000
4.878	0.300	1425	3100	900	1400
2.086	0.362	600	2900	2200	800
1.370	0.407	400	2400	0	200
2.557	0.343	1000	2400	300	1400
6.255	0.271	1900	3600	500	1000
1.582	0.376	450	2900	0	800
1.091	0.505	375	900	200	1200
5.725	0.282	1625	3800	2300	1400
2.215	0.359	600	2900	3400	1000
4.919	0.297	1425	3300	900	1400
1.221	0.454	425	1200	200	800
1.139	0.473	375	1200	200	1000
5.270	0.289	1550	3600	300	1400
4.195	0.307	1175	3700	0	1000
1.293	0.451	475	1100	200	800
4.143	0.319	1050	3400	3500	1000
6.433	0.268	1950	3700	600	1200
5.250	0.295	1400	3900	3600	1400
1.914	0.370	400	3800	2200	1200
2.960	0.328	925	3600	3200	1400
1.128	0.492	400	900	200	1000
6.063	0.273	1700	3900	3500	1000
1.103	0.493	375	1100	200	400
2.082	0.365	475	3800	2400	1400
2.350	0.346	925	2200	200	1000
5.259	0.289	1550	3600	200	1400
3.171	0.320	1000	3800	3500	1400
1.237	0.452	400	1200	900	600

Table E.2: Optimization Results for Scenario 2

Objective Functions		**Sized Components**			
€	CO2	Grid Capacity [kVA]	PV Capacity [kWp]	Diesel Generator [kVA]	BESS [kWh]
1.105	0.283	325	1500	100	2600
1.382	0.202	325	3100	100	1600
1.657	0.165	350	3900	300	3000
1.442	0.192	325	3400	100	1600
1.482	0.188	350	3000	300	3200
1.124	0.281	325	1500	300	2600
1.541	0.183	325	3100	100	6200
1.134	0.279	325	1500	400	2600
3.324	0.163	825	3900	600	23600
2.202	0.163	500	3900	0	11200
1.807	0.163	350	3900	300	7200
0.927	0.529	325	500	100	1600
0.913	**0.533**	**325**	**500.0**	**100**	**1200.0**
1.011	0.424	350	900	200	800
1.452	0.192	325	3400	200	1600
1.492	0.188	350	3000	400	3200
1.055	0.309	325	1400	100	1600
2.038	0.163	400	3900	800	9600
7.041	0.163	1800	3900	2600	23800
1.003	0.484	350	800	400	200
1.534	0.183	325	3100	100	6000
2.714	0.163	475	3900	1100	23200
0.941	0.529	325	500	100	2000
1.646	0.176	375	3400	100	4800
2.395	0.163	375	3900	300	21800
1.179	0.251	325	1800	300	2600
1.696	0.164	325	3900	100	6000
1.548	0.176	325	3400	200	4400
3.173	0.163	625	3900	2800	23400
2.359	0.163	425	3900	500	17800
2.522	0.163	425	3900	200	23000
0.983	0.520	350	500	300	1400

Table E.3: Optimization Results for Scenario 2

Objective Functions		**Sized Components**			
€	CO2	Grid Capacity [kVA]	PV Capacity [kWp]	Diesel Generator [kVA]	BESS [kWh]
1.657	0.330	350	2900	100	8200
1.600	0.332	350	2900	100	6600
1.152	0.520	450	800	0	0
1.267	0.505	425	1000	1000	600
1.488	0.402	350	2000	100	8200
1.143	0.537	450	700	0	200
1.244	0.508	425	1000	700	800
1.213	0.508	400	1200	100	1800
1.282	0.498	425	1300	200	1600
1.080	**0.556**	**425**	**600**	**0**	**200**
2.102	0.300	425	3900	1100	8200
1.362	0.429	400	2300	0	400
1.933	0.301	400	3800	600	6800
2.130	0.299	425	3900	400	11000
1.650	0.330	350	2900	100	8000
1.447	0.421	450	2300	0	200
1.876	0.325	425	3800	500	4000
1.338	0.460	350	2300	100	1800
1.898	0.309	400	3800	800	5200
1.526	0.359	375	2800	100	3600
2.234	0.299	425	3900	700	13000
1.143	0.552	425	800	200	200
1.815	0.329	425	3700	100	4000

Table E.4: Optimization Results for Scenario 4

Objective Functions		**Sized Components**			
€	CO2	Grid Capacity [kVA]	PV Capacity [kWp]	Diesel Generator [kVA]	BESS [kWh]
0.917	0.651	325	300	100	1600
1.063	0.302	300	1500	100	2600
1.018	0.486	350	600	100	2600
1.946	0.165	350	3800	300	11600
2.127	0.162	420	3900	1000	10200
1.877	0.166	370	3800	1000	6400
1.045	**0.312**	**300**	**1400**	**100**	**2600**
1.654	0.175	350	3700	300	4000
2.161	0.162	320	3900	100	18600
1.581	0.201	370	3200	300	3400
1.954	0.165	350	3800	300	11800
1.025	0.485	350	900	100	1000
1.467	0.248	350	3000	200	2600
1.297	0.256	350	2100	300	2800
0.926	0.580	320	400	100	1800
2.332	0.162	400	3900	500	18400
0.954	0.564	350	500	100	800
1.076	0.300	300	1600	100	2400
1.963	0.163	420	3900	100	8200
1.537	0.206	370	2900	400	3600
1.081	0.293	300	1600	100	2600
1.785	0.166	370	3800	100	6400
1.623	0.186	350	3200	300	6000

F

Load Flow results of the Cigre MV Distribution System before and after Sizing

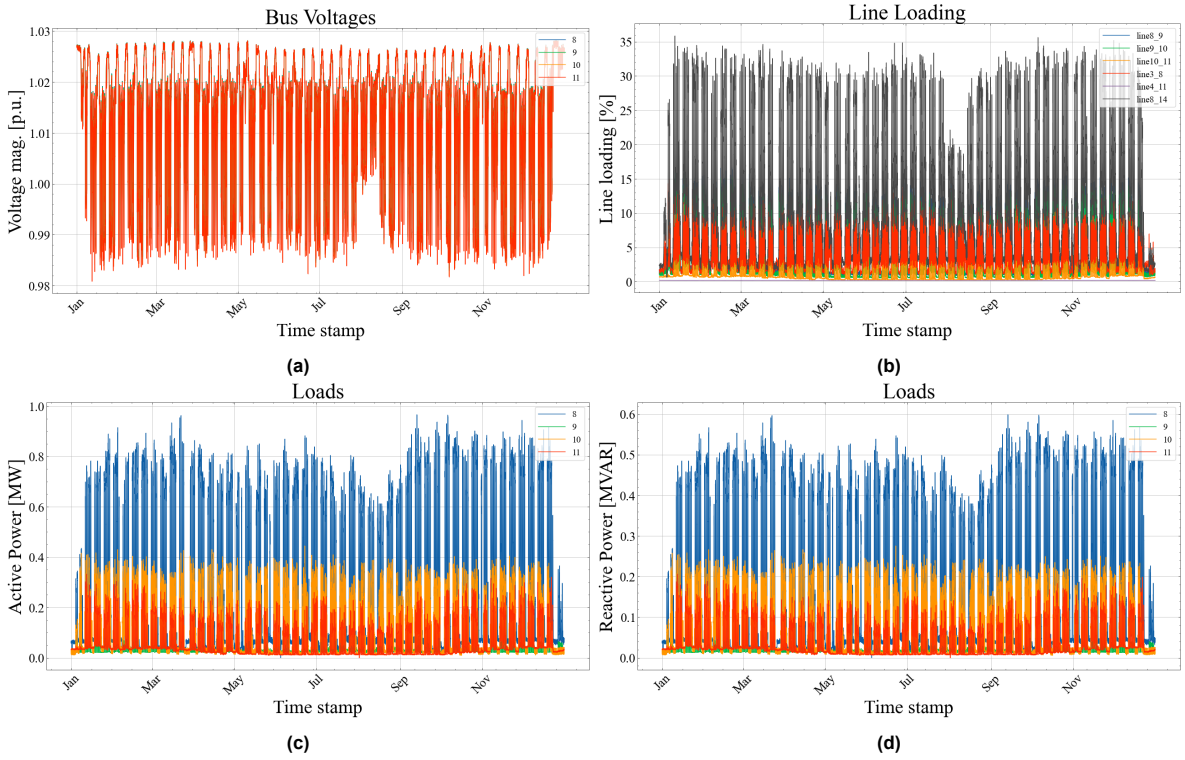

Figure F.1: Load Flow results of the CIGRE MV Distribution System before sizing

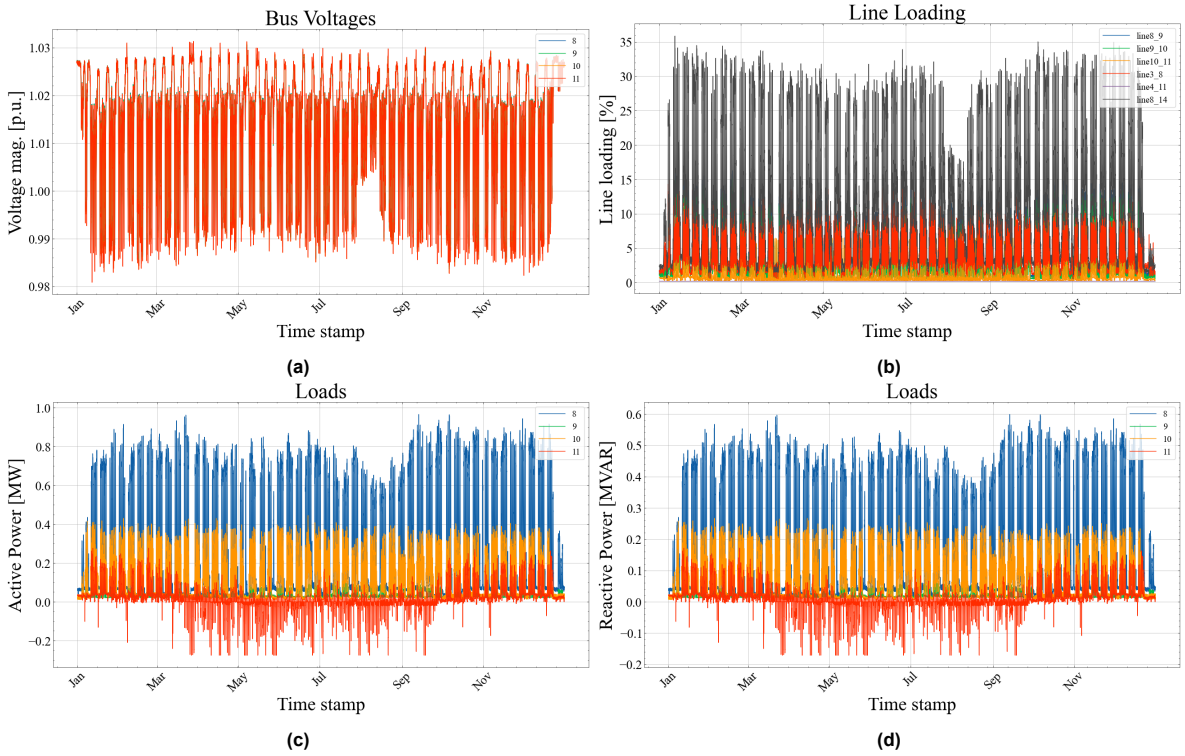

Figure F.2: Load Flow results of the CIGRE MV Distribution System after sizing

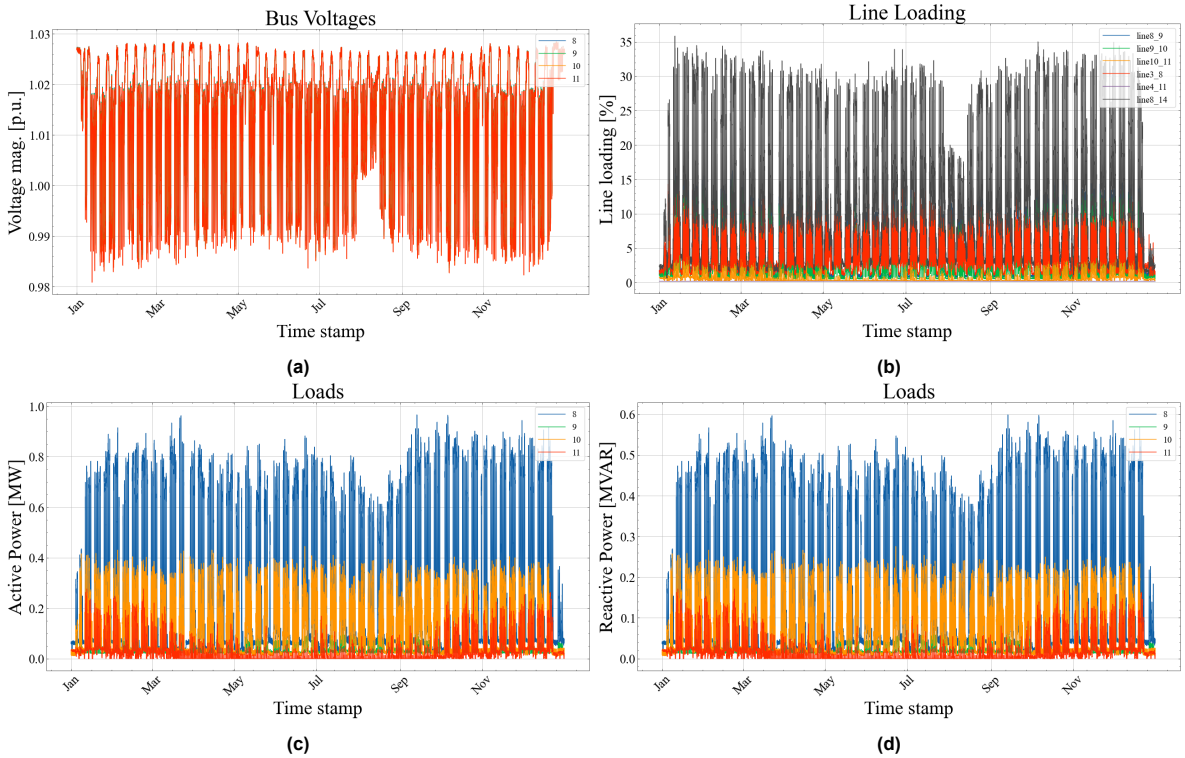

Figure F.3: Load Flow results of the CIGRE MV Distribution System after sizing but with feed-in disallowed